Machine Learning-based Detection of Compensatory Balance Responses and Environmental Fall Risks Using Wearable Sensors

by

Mina Nouredanesh

A thesis
presented to the University of Waterloo
in fulfillment of the
thesis requirement for the degree of
Master of Applied Science
in
Mechanical and Mechatronics Engineering

Waterloo, Ontario, Canada, 2016

I hereby declare that I am the sole author of this thesis. This is a true copy of the thesis, including any required final revisions, as accepted by my examiners.

I understand that my thesis may be made electronically available to the public.

Abstract

Falls are the leading cause of fatal and non-fatal injuries among seniors worldwide, with serious and costly consequences. Compensatory balance responses (CBRs) are reactions to recover stability following a loss of balance, potentially resulting in a fall if sufficient recovery mechanisms are not activated. While performance of CBRs are demonstrated risk factors for falls in seniors, the frequency, type, and underlying cause of these incidents occurring in everyday life have not been well investigated.

This study was spawned from the lack of research on development of fall risk assessment methods that can be used for continuous and long-term mobility monitoring of the geriatric population, during activities of daily living, and in their dwellings. Wearable sensor systems (WSS) offer a promising approach for continuous real-time detection of gait and balance behavior to assess the risk of falling during activities of daily living. To detect CBRs, we record movement signals (e.g. acceleration) and activity patterns of four muscles involving in maintaining balance using wearable inertial measurement units (IMUs) and surface electromyography (sEMG) sensors. To develop more robust detection methods, we investigate machine learning approaches (e.g., support vector machines, neural networks) and successfully detect lateral CBRs, during normal gait with accuracies of 92.4% and 98.1% using sEMG and IMU signals, respectively.

Moreover, to detect environmental fall-related hazards that are associated with CBRs, and affect balance control behavior of seniors, we employ an egocentric mobile vision system mounted on participants chest. Two algorithms (e.g. Gabor Barcodes and Convolutional Neural Networks) are developed. Our vision-based method detects 17 different classes of environmental risk factors (e.g., stairs, ramps, curbs) with 88.5% accuracy. To the best of the authors knowledge, this study is the first to develop and evaluate an automated vision-based method for fall hazard detection.

Acknowledgements

An special thanks to my great supervisor, Professor James Tung.

Dedication

This thesis is dedicated to my dear Mother for her enormous contribution to getting me where I am today, to my Father for supporting me all the way, to my Brother for his endless affections, and to my Love.

This thesis is also dedicated to all seniors, patients with gait and balance impairment, and the sufferers of Parkinson's disease. I hope one day, my research makes an impact on current fall risk assessment, fall prediction, and prevention methods to improve quality of life of the affected patients worldwide.

Table of Contents

List of Tables

List of Figures

Chapter 1

Introduction

Falls are an important public health problem, the leading cause of injury-related hospitalizations, and a major cause of disability and death among seniors. It is estimated that one in three persons over the age of 65 falls at least once each year [1, 2] and 50% of seniors over age 85 suffer one fall per year [4]. Falls can also lead to negative mental health outcomes such as fear of falling, loss of autonomy, isolation, and depression. These outcomes not only harm the injured individuals but also affect family, care providers and the health care system. Falls incur heavy expenses, estimated over $2 billion annually for the direct medical costs and related injuries [9], which is 3.7 times greater than fall-related expenses for younger adults [5]. In 2010, approximately 1.6 million older persons fell at least once in 2026 in Canada; and the estimated number of older persons who will fall at least once will increase to 2.8 million [10]. Moreover, the extrapolated cost of falls in older Canadians will grow from $2.4 billion[5] in 2010 to $4.1 billion in 2026[10].

Senior adults are the fastest growing segment of the population in Canada [12]. Based on a report by Statistics Canada, in 2009 Canada had 4.7 million persons aged 65 years or over, twice the number recorded in 1981. By 2036, the number of seniors is expected to be more than double, ranging between 9.9 and 10.9 million depending on the projection scenario, and in 2061, this number would range between 11.9 million and 15.0 million [13]. With the demographic shift towards an increasingly aged population, the total cost of

fall-related injury is also expected to rise dramatically over the next few decades unless effective fall prevention strategies are established. It is estimated that a 20% reduction in falls would translate to 7,500 fewer hospitalizations and 1,800 fewer permanently disabled older adults in Canada, and an overall savings of $138 million annually [7].

1.1 Motivation-Falls and consequences of falls in older adults

1.1.1 Impact on older adult

Physical consequences

Fall-related injuries are the leading cause of injury-related hospitalization for seniors in all Canadian provinces and territories. Almost 50% of seniors who fall, experience a minor injury and between 5% to 25% suffer from moderate to serious injuries. The most common reasons for fall-related hospital admission are bone fractures, head traumas, joint strains and sprains [15], soft tissue injuries, muscle contusions, cuts and abrasions [26, 21].

Analysis of the 2008/2009 Canadian hospitalization data (data from the Discharge Abstract Database (DAD [1])) for fall-related injuries among persons over age 65 years shows that in that year, 53,545 fall-related hospitalizations were observed among Canadian seniors, accounting for 85% of all injury-related hospitalizations and 7% of all hospitalizations for this group [10]. Thirty-eight percent of these fall-related hospitalizations were due to a hip fracture, 39% involved a fracture other than the hip, and 23% involved a nonfracture injury. In addition, 16,916 older Canadians were left with a partial or total permanent disability due to a fall [5].

Of all injuries from falls, hip fractures cause the greatest health problems and the greatest number of deaths. Hip fractures are serious, life-limiting and costly events for

[1]Includes fall-related hospitalization episodes and rates, length of hospital stay, injury type, place of occurrence of the fall, and differences by age group and gender for seniors aged 65 and over

older adults. About 27,000 hip fractures occur each year in Canada [16] and falls accounted for 95% of those fractures (Public Health Agency of Canada, 2005a). Four percent of hip fracture patients die in the hospital immediately following the injury [31], and over 20% of hip fracture patients die within a year of the event [17, 32]. The seniors, who sustain a low-trauma hip fracture have higher risk of death and disability [18] and those who survive, experience a substantial decline in mobility, physical activity, and functional independence [28]. Around 50% of all older adults hospitalized for hip fracture cannot return home or live independently after the fracture [29, 30].

Falls are the underlying cause of 81% of traumatic brain injuries (TBI) in adults aged 65 and older [37], and accounts for 50% of fall-related injuries among older adults [33]. In 2003, the aggregate charges for treating a principal diagnosis of TBI in patients aged 65 and older exceeded $2.2 billion [36]. The one-year survival rate for seniors after a severe TBI is as low as 20% [34, 35], and those who survive a TBI may face long-lasting effects and disabilities, including impaired memory, gait, sensation (e.g., vision or hearing), or emotional functioning (e.g., personality changes, depression) [37].

Psychological consequences

Falls that do not lead to a physical injury often begin a cycle of fear of falling [44], psychological trauma and negative mental outcomes. This post-fall syndrome includes fear of falling (FOF), loss of autonomy, isolation, confusion, immobilization, depression, and increased risk for future falls. FOF is a common consequence of falls among older people and between 25% to 55% of seniors fear falling [43]. FOF is a risk factor for future falls and decreases quality of life [24, 25] and increases the rate of physical inactivity and ability to independently perform activities of daily living [38, 39]. Between 20 to 55% of seniors who fear falling restricts their activities[43, 40]. The resulted immobility weakens the muscles and increases the risk of future falls.

1.1.2 Impact on the family and on society

The effects of a fall go beyond the individual and place a burden on family members, care providers, and governments. A fall can result in a financial obligation, and can increase the family's worry about the health, safety, and mortality of the elder family member. The increased time spent on care of the older adult and over-protectiveness may limit their activities and decision-making ability.

UK National Health Service (NHS) has reported to spend around £2 billion each year on falls [3]. Moreover, falls cost Americans about $100 billion every year [19] and result in increased use of emergency room resources and increased costs from hospital admissions. In 2000, in the United Sates of America, there were almost 10,300 fatal and 2.6 million medically treated non-fatal fall related injuries. Direct medical costs totaled $0.2 billion dollars for fatal and $19 billion dollars for non-fatal injuries. Of the non-fatal injury costs, 63% ($12 billion) were for hospitalizations, 21% ($4 billion) were for emergency department visits, and 16% ($3 billion) were for treatment in outpatient settings [8].

1.2 Risk factors for falls

Much work has been done to identify risk factors for falls, which are generally categorized into biological/intrinsic, e.g., acute or chronic illness, and environmental/extrinsic, e.g., slippery floor, and there is a complex interaction between these risk factors [6]. Falls among older adults, unlike other ages tend to occur from multifactorial etiology [60] and each older person may face a unique combination of risk factors according to his or her life circumstances. As a basis for a fall prediction and intervention program for community-dwelling elderly people, we need more specific knowledge about these risk factors [71]. There is an increased need to understand what puts each senior at the risk of falling to inform which fall prevention intervention work for whom and in what setting; however, the existing research literature on falls reveals a number of research gaps. Only a few studies have assessed hazards in the home as risk factors, with inconclusive results [102]. No studies have assessed hazards outside the home or quantified exposure to hazards (in

terms of frequency, duration, and intensity) to develop a true estimate of risk; the usual approach is simply to note the presence of hazards in the homes of subjects [61]. In addition, definitions of environmental hazards and methods for assessing them are difficult to standardize [65].

1.2.1 Intrinsic factors

Intrinsic, or patient-related, risk factors include advanced age, chronic diseases, muscle weakness, gait disorders, mental status alternations, and medications [66]. These factors can have additive effects and complicated interactions. Sarcopenia or muscle loss is thought to have direct effects on performance and leads to disabilities, increased risk for falls, and increased vulnerability to injury. There is an increased fracture risk due to greater impact forces [66]. Rawsky [67] reviewed over 100 articles published from 1979 through 1996 related to falls in the elderly population in a variety of settings (e.g., inpatient hospital, community, psychiatry facility, rehabilitation center, and long-term care facility). The following intrinsic factors were identified most often in the 21 selected studies within Rawsky's review: cognitive impairment/psychological status (16 studies), acute/chronic illness and mobility (14 studies), sensory deficits (7 studies), fall history (6 studies), and elimination (6 studies). Rawsky's review, however, did not assess the relative risk of these risk factors. Rubenstein et al. [68, 69], analyzed the 16 studies that quantitatively reported the relative risk (RR) for multiple risk factors. Their analysis summarized the mean RR associated with the risk factors and reported the following in decreasing magnitude: muscle weakness (RR 4.4), history of falls (RR 3.0), gait deficits (RR 2.9), balance deficits (RR 2.9), use of assistive devices (RR 2.6), visual deficits (RR 2.5), arthritis (RR 2.4), impaired activities of daily living (RR 2.3), depression (RR 2.2), cognitive impairments (RR 1.8), and age 80 years (RR 1.7) [14].

1.2.2 Extrinsic factors

Extrinsic factors (e.g., environmental hazards or hazardous activities that are originated outside of the body) are described as primary causes for approximately one-third to half of all falls [102, 70]. In a review of 20 articles, Connell et al., [72] found that environmental hazards (e.g., walking on slippery/rough surfaces, obstacles, inadequate light, or loose carpets) create conditions pose a particular risk for community-dwelling elderly persons who may already have multiple intrinsic risk factors for falls, and can lead to trips and slips. Additionally, the risk from hazardous activities can be aggravated by behavioral risk factors (e.g., faller was hurried or inattentive, difficulty or discomfort during a task, or moving beyond limits of stability [72]).

In independent older community-dwelling people, about 50% of falls occur within their homes and immediate home surroundings [10, 62, 63]. Most falls occur on level surfaces within commonly used rooms such as the bedroom, living room and kitchen. A high particular risk to falls was found in homes, with loose carpets on the kitchen and bathroom floors, loose electrical wires, and inconvenient doorsteps. Poor surroundings around home and irregular sidewalks to the residence, such as garden paths and walks that are cracked or slippery from rain, snow or moss are also dangerous. Entrance stairs and poor night lighting can also pose risks[73]. For example., Brodie et al., quantitatively showed that there is a strong relationship between usual stair-ascent performances (and stair negotiation) by older people during ADLs and clinical assessments and prospective falls.

Within inpatient facilities, commonly reported extrinsic factors are related to use of bed-rails, height and stability of seating (e.g., low toilets, wheelchair braking problems, portable commodes), and obstacles created by mobility aids (e.g., wheelchairs and walkers [72]). Additionally, common locations for inpatient falls are resident rooms or bathrooms, with the falls often involving problems with ambulation and transfers [72].

The remaining falls occur in public places and other people's homes. Factors related to the public environment include pavement cracks and misalignments, gutters, steps, construction works, uneven ground and slippery surfaces [64]. Even walking on a familiar route can lead to falls as a consequence of poor building design and inadequate consideration

[73].

Stalenhoef et al. [71] carried out a review on fourteen papers published between 1981 to 1994 examining risk factors and health consequences of falls among community-living elderly people, and concluded that the environmental hazards that are associated with falling have not attracted much attention among researchers. Finding an efficient way to understand the interaction between intrinsic and extrinsic risk factors and detecting the potential causes of falls for a specific community-dwelling older adult is a must to prevent future falls.

1.3 Gaps in knowledge

1.3.1 Limitations of commonly used methods for fall risk assessment

The impact of falls among older persons on Canadians and the Canadian health care system has been recognized at national, provincial, and territorial levels [10]. For each senior, there is a unique and complicated interaction between intrinsic and extrinsic risk factors, e.g., environmental hazards, medications, vision problems, and impairments in strength, gait, or balance. As a result, a multifactorial fall-risk assessment including a fall history, physical exam, gait and balance evaluation, and environmental assessment is recommended for all older adults who present with a fall or problem with gait or balance.

The adverse consequences of falls can be reduced among older Canadians with the help of fall prevention activities and cutting-edge technologies; therefore, many researchers have endeavored to develop fall risk assessment (FRA), fall prevention (FP), and fall detection (FD) tools. While many evidence-based fall prevention initiatives are well underway, there are still challenging barriers including gaps in knowledge on an optimal method for standardized reporting of falls and fall-related injuries, an incomplete understanding of the scope of fall risk factors and environmental hazards leading to falling, and inefficiency of the current FRA and FP tools.

While much effort has been devoted to the development of methods for evaluating fall risk, methods for documenting and quantification of fall risk largely depend on self-reporting, using questionnaires, fall diaries or phone calls, i.e. subjects are asked to tick each day when no falls occurs, and cross any days when a fall occurs in a fall diary [20], which are fast and easy, but also are associated with several limitations [158]. The report of fall incidents among older adults relies on the ability of the individual to accurately recall and describe the event; however, individuals are likely to misreport and underreport fall events due to recall difficulties, sustained injuries, or fear of falling, which might bias these retrospective designs [140]. As a result, improved techniques are required to detect and characterize falls in order to guide prevention and treatment strategies.

There are also several clinical FRA methods, which often involve functional or performance assessments and include evaluation of posture, balance, gait, visual acuity, sensation, vital signs in a supervised setting. These clinical assessments usually use threshold assessment scores to binarily categorize people as fallers and non-fallers [93]. These methods oversimplify geriatric fall risk, which can be more accurately by fuzzy boundaries between multiple risk categories, such as low, moderate, and high fall risk [93]. Another notable concern to all the documentation methods is the effect of subjectivity; as a result, many researchers have attempted to develop more systematic FRA methods by employing different types of sensors that measure whole body motion, ground reaction forces, and electromyographic signals to provide objective, quantitative measures for FRA. However, the associated equipment is typically located in a gait laboratory and requires a time consuming setup that is difficult to practically integrate into typical clinic schedules, limiting the testing location and frequency.

1.3.2 Need for gait and balance control assessment during activities of daily living

The research to date has tended to focus on the clinical assessment of gait and balance control behavior; however, studies on unsupervised assessment of balance control behavior are rare to find in literature. A clinical examination of balance control behavior in older adults

only evaluates the risk factors in a short period of observation, which limits understanding of the exact risk factors behind the falls for each individual and/or the interaction among the fall-related risk factors [165]; thus, more systematic methods are needed to unveil the hidden risk factors and assess the risk of falling in community-dwelling older adults.

1.4 Thesis objectives

This study was spawned from the lack of research on development of FRA methods that can be used for continuous and long-term mobility monitoring of the geriatric populations during activities of daily living and in their dwellings. To address reliability limitations in classic FRA methods, continuous monitoring of falls using wearable sensors has been proposed as an approach to measure future fall risk. A wearable system can unobtrusively and efficiently capture and analyze quantitative mobility data, which could improve fall risk assessment.

Fall rates in community-living older adults are relatively rare events (typically less than two times per year [158]); as a result, other alternatives should be investigated for development of an efficient FRA tool. An individual's risk for falls depends on how often they experience imbalance episodes, and their ability to quickly recover balance after these events. Based on this fact, an alternative approach to fall and cause of fall detection is to monitor near-falls or compensatory balance responses (CBRs), defined as stumbles or sudden loss of balance that would result in a fall if sufficient recovery mechanisms were not activated [158]. CBRs play a critical role in preventing falls [153]. The cause of imbalance is often due to complex interactions between multiple risk factors (intrinsic and extrinsic), leading to a slip, trip, or incorrect shift of body weight.

Episodes of near-falls, which are clinically relevant markers of fall risk, are common among older adults and an improved understanding of their prevalence and nature should provide a more robust estimate of fall risk and customized approaches to reducing falls. Near-fall events are particularly difficult to determine (compared to the fall events, which involve a sudden change in an individual's body acceleration and velocity), mostly because

seniors do not recognize the events themselves or do not recognize the significance of the near-fall events [165]. Considering the near-falls as predictors of potential falls, we could extract valuable information in terms of the underlying cause and frequency of CBR events, to figure out what conditions lead to losses of balance for a specific individual. This thesis was undertaken to introduce a new personalized FRA tool by detecting the CBR incidents during activities of daily living.

The long-term vision of this work is to develop wearable sensor systems (WSSs) to accurately and reliably measure balance control behaviour by detecting the cause and frequency of CBRs, in unsupervised conditions and over long periods (i.e., weeks, months). To achieve these aims, a sensor integration approach using multiple modalities (e.g., electrophysiology, machine vision) to provide information complementary to traditional movement-based WSS (i.e., inertial measurement units (IMUs) combining accelerometer, gyroscope, magnetometer sensors) will be explored.

This thesis seeks to address two main questions: 1) How can we develop a new risk of falling evaluation tool based on the monitoring of compensatory balance responses (CBRs) and identifying the frequency of CBRs, and 2) What types of contextual/environmental factors affect balance behavior and may lead to falls:

1) How can we develop a new FRA tool based on the monitoring of CBRs? Considering CBRs likely occur more frequently than falls, automatic identification and monitoring of these incidents may provide new insight into fall risk. We aim to employ several wearable sensors, i.e., inertial measurement units (IMUs), surface electromyography (sEMG), to monitor gait patterns, and integrate machine learning techniques to develop a novel, robust and reliable personalized assessment tool to evaluate the risk of falls through detection and analysis of naturally occurring compensatory balance responses (e.g. lateral CBRs including sidestep and crossover strategies), over long periods of time and in non-clinical settings. Chapter 3 describes the development of these new tools.

In section 3.3, we develop a machine-learning-based method, including feature extraction and reduction from IMU signals (overall 9 acceleration signals and 9 angular velocity signals), and apply classification algorithms, e.g., support vector machines (SVMs). Using

a combined kernel supervised principal component analysis (KSPCA) dimension reduction and SVM classification algorithm, the IMU-based detection algorithm accurately identified 92% of trials (for a 3-class problem) [45]. In section 3.4, we examine the feasibility of using wearable sEMG sensors to detect episodes of CBR. We recorded signals from 4 muscles in the right leg, (i.e., rectus femoris, biceps femoris, tibialis anterior, and gastrocnemius), to distinguish CBR events from normal walking episodes. Time domain features were extracted and the performance of three different machine learning methods, i.e., random forest, SVMs and k-nearest neighbor were evaluated. In general, testing demonstrated very good accuracy (92.35%) in distinguishing CBRs from normal walking patterns (i.e., binary classification) and good accuracy (84.60%) in distinguishing multiple classes of stepping patterns. Moreover, the impact of varying combination of muscle(s) on detecting CBRs were examined and It has been revealed that the features extracted from the thigh muscles sEMG signals outperform those extracted from shank sEMG signals in CBR detection.

The findings provide evidence that the accurate detection of CBRs is possible using wearable IMU and sEMG sensors, combined with machine learning techniques.

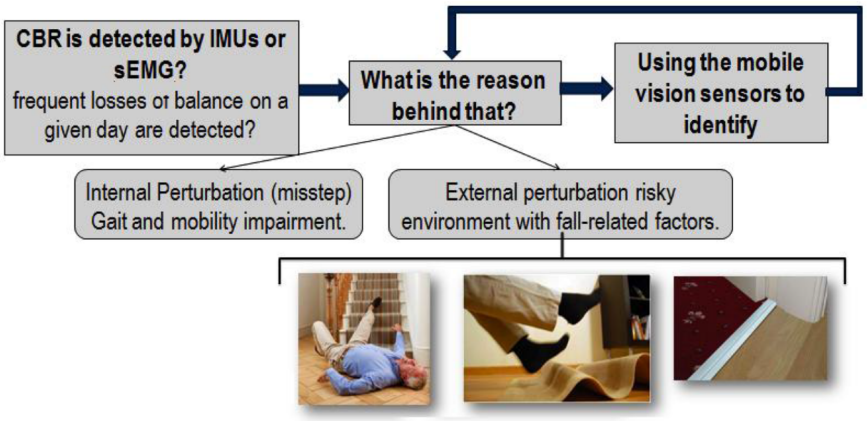

Figure 1.1: Thesis objective-Detection of cause and frequency of compensatory balance reactions

2) What types of environmental risk factors affect the balance control behavior and may lead to falls, or CBRs?

Between 25 to 75 percent of falls in older people involve an environmental component. Researchers and clinicians have recognized a number of hazards in the home and public environment that contribute to falls and related injuries. These factors interact with other risk factors, such as poor vision or balance, to compound fall-related risk for seniors [47]. The major associated challenge is a lack of techniques to extract contextual information needed to interpret ambulatory gait and balance control behavior. For example, frequent CBRs on a given day may be interpreted as gait instability or may reflect that the person is doing activities in a risky environment with fall-related factors. Without detailed information of the environment, such as the presence of other pedestrians on a crowded sidewalk, pets, obstacles, stairs, terrain changes and doorways, the ability to interpret the balance control reactions is constrained. Thus, it is of utmost importance to detect the underlying cause of CBR episodes as well (Fig. 1.1).

Advances in machine learning, and also state-of-the-art mobile vision systems and wearable egocentric cameras, i.e., GoPro, enable a new form of capturing human experience. The first-person perspective photos and videos captured by these cameras can provide rich and objective evidence of a person's everyday activities, and are expected to enable us to detect the potential contextual factors, that perturb the balance of seniors or people with gait impairment, and potentially lead to falling.

In chapter 4, the effectiveness of employing egocentric cameras along with image-processing-based (including Gabor transform for the binary feature extraction) and machine-learning- based methods (e.g. Convolutonal Neural Networks) in detection of underlying cause of the episodes of imbalances is investigated.

Chapter 2

Literature Review

2.1 Introduction and Preliminaries

Falls are a significant cause of injuries and morbidity among geriatric populations, which inflict extreme costs on seniors, families, and also governments. Due to the dramatic consequences of falls and substantial increase in the elderly populations, researchers have shown an increased interest in development of fall detection (FD) and fall preventative (FP) methods for seniors in recent years. A growing body of literature has investigated different methods for the development of fall detection (FD) methods, using cutting-edge technologies, e.g., ambient or wearable sensors, to monitor ADLs and capture fall incidents. These studies also use different strategies for detection of falls, i.e., image processing-based, signal processing-based, threshold-based, or machine learning-based techniques. While much effort has been devoted to the development of such systems, far too little attention has been paid to the development of either fall prediction methods or new FRA tools during ADLs and in seniors' dwellings.

Fall risk assessment (FRA) is the initial step for FP programs and interventions, which is performed to identify individuals at highest risk of falling. FRA plays an important role in identification of intrinsic (muscle weakness, neurological deficits, etc.) and extrinsic

(poor lighting, inappropriate footwear, etc.) risk factors and helps determine the most appropriate interventions, and ultimately reduce incidents of falls.

In this chapter, studies on different FRA methods are reviewed. We break down these studies into three main categories: 1) Supervised fall risk assessment (SFRA) methods (Section 2.2, which are required to be conducted under the supervision of a nurse or physician, in the nursing home or clinical setting, and 2) Unsupervised FRA (UFRA) (Section 2.3), which involves state-of-the-art technologies, i.e., ambient sensors, wearable sensors, instrumented shoe insoles, and smart phones, to assess risk of falling within the home environment or community setting, with no need for a physician to conduct experiments, and 3) Studies that are concerned with the assessment of compensatory balance reactions either in a supervised or unsupervised fashion (Section 2.4).

2.2 Supervised fall risk assessment

2.2.1 Classic fall risk assessment measures

In the past decades, numerous studies have attempted to propose efficient supervised FRA methods. Clinical FRA methods often involve questionnaires or functional assessments of posture, gait, cognition, and other fall risk factors. These clinical assessments are subjective, qualitative, and use threshold assessment scores to binarily categorize people as fallers and non-fallers. This binary categorization oversimplifies geriatric fall risk, which is more accurately modeled with fuzzy boundaries between multiple risk categories, such as low, moderate, and high fall risk [93].

Perell et al. [14] proposed three main categories for the different types of falls and mobility assessments, on the basis of setting or specific discipline factors: 1) Comprehensive medical assessments, 2) nursing fall risk assessments, and 3) functional mobility assessments completed by physical therapists or physicians in an outpatient setting.

The first approach (comprehensive assessment) is generally performed by a geriatrician or nurse practitioner in a clinical setting or a nursing home [48] to evaluate the risk of

future falls and/or treat the patients who have recently fallen. This type of assessment entails detailed medical assessment of previous falls history, cognition, balance control behavior, gait, muscle strength, chronic diseases, mobility, nutrition, and medications [49]. Such assessment is time-consuming [50] and often involves a team of clinicians [51]; and it typically focuses on identifying intrinsic risk factors that can be treated to reduce the likelihood of a fall [48].

The "nursing assessment" of a patient's risk of falling is typically based on specific screening instruments or forms, and has been widely employed in hospitals or nursing home settings for several decades. Similar to the first approach, the nursing assessment aims to identify the likelihood of a senior's future falls on the basis of intrinsic or medical characteristics of the patient (e.g., psychological status, mobility dysfunction, fall history, dependence, acute or chronic illnesses, and sensory deficits). Such type of FRA assessment includes Morse Fall Scale [52], STRATIFY [53], Resident Assessment Instrument (RAI) [54], Hendrich Fall Risk Model [55], High Risk for Falls Assessment Form [56], and Royal Melbourne Hospital Risk Assessment Tool [57]. These instruments are commonly used by nurses upon admission to a hospital or long-term care facility and are periodically updated (e.g., per shift, daily, or weekly) depending on the acuity level of the patients [14]. Because of the frequency of use, these tools tend to be short and do not require intensive assessment of the patient. Poor scores tend to trigger either further assessment or anticipatory nursing interventions (e.g., staff routinely provides assistance with toileting or out of bed activities).

Balance control and postural sway are typically assessed in a clinical setting using functional performance scales [59]. The older adult performs a series of tasks, which require steady state or anticipatory postural control. The patient's ability to complete these tasks is subjectively scored by a clinician. Such functional performance scales include Tinetti Performance Oriented Mobility Assessment (POMA)[58], Berg Balance Test [74], Functional Reach [77], or Dynamic Gait Index [78] and have been reviewed by Berg and Norman [75]. Only some of these scales have specifically tested the ability to predict falls, but all provide standardized measures of functional limitations and disability. The interpretation of patient's scores is restricted by a lack of data describing the range of performance among people without disabilities [82].

More information about different classic FRA measures is provided in Appendix (6).

2.2.2 Limitations

The classic FRA methods and clinical scales are inexpensive, easy-to-use, non-invasive, and relatively fast. However, such measures are characterized by subjectivity and might be inadequate and inefficient when used outside the place of development, even in very similar clinical settings and case. For example, staff using the tool might interpret the same observation differently [83]. This problem leads to a dispute about the reliability and validity of the clinical FRA scales, and heightened the need for new FRA tools, which are able to provide more objective, systematic, and precise gait, balance, and function evaluation in elderly.

Additionally, despite many available FRA tools in the literature, there often is a lack of awareness of existing scales and uncertainty regarding how to choose an appropriate FRA scale for their patient population, among clinicians [14]. Hospital or long-term care facilities often develop their specific FRA scale on the basis of intrinsic risk factors from the literature or retrospective chart reviews of their own patient falls. As a result, FRA scales and the associated thresholds used to categorize fallers and non-fallers are not standardized.

FRA measures usually assess only gait and balance as intrinsic factors and typically ignore the multifactorial nature of falls. These functional-FRA methods appear to lack responsiveness and discriminative ability in relatively healthy populations [140]. Laessoe et al. (2007) [85] studied the effectiveness of different FRA scales in an active elderly population of ninety-four males and females (aged between 70-80 years) in a one year follow-up study. A battery of nine functional tests were selected to cover different aspects of physical performance related to fall risk including standing balance "FICSIT-4 scale" + one leg eyes closed, Four Square Step Test (FSST), and "Timed Up and Go" (TUG) [81]. They found that there was not a considerable difference between the scores of fallers and non-fallers (except in one test, "balance in standing position"). The authors emphasized that falling is a complex phenomenon of multifactorial origin and fall risk cannot be predicted in a healthy and active elderly population by solely assessing intrinsic factors and physical

performance. So, we need more systematic methods for FRA encompassing the wide range of factors including extrinsic conditions (e.g. terrain).

2.2.3 Instrument-based methods for risk of falling assessment in clinical setting

The limitations associated with the classic fall risk-assessment tools stimulate the need for the development of more systematic FRA methods. Sensors that are able to capture information related to gait and balance control behavior, body motion, muscle activities, and ground reaction forces, provide objective, quantitative measures for FRA [93].

In clinical and research settings, gait performance is widely accepted as a general measure of functional ability among individuals. Many researchers have attempted to develop specific FRA tools by recording movement data and analysis of gait patterns. The gait pattern is a cyclic process consisting of repetitive gait cycles, which is equivalent to a stride and describes the motion from initial heel strike (with the stance phase), proceeding through a swing phase and ending with the next heel strike (successive initial contacts (ICs) and toe-offs (TOs)). Comparing individual's successive strides and extraction of gait parameters, allow the determination of gait variability and asymmetry (differences in left and right leg movement, steps). The parameters include walking speed, stride frequency, stride-to-stride variability, index of harmonicity, harmonic ratios, and entropy. It has been shown that increased gait variability relates to fall risk [84]; and researchers have shown that several gait characteristics are significantly associated with prospective falls [140], e.g., gait velocity is a predictor of disability and can quantitatively estimate risk of future hospitalization, [106].

Although motion capture systems provide reliable and objective measurement of gait, they are impractical for large subject groups as they are laboratory based, time consuming, complex and expensive. These systems are therefore mainly used for research purposes.

Posturography

Patients may be referred for posturography, which is a general term that covers all the techniques used to quantify postural control in upright stance in either static or dynamic conditions. Computerized dynamic posturography (CDP) or test of balance (TOB), is a non-invasive specialized clinical assessment technique, used to objectively identify abnormalities by challenging and quantifying the central nervous system adaptive mechanisms (visual, vestibular, somatosensory) that are involved in the control of posture and balance. The EquiTest system is the first commercially available CDP system that was launched by NeuroCom International, Inc. (NeuroCom EquiTest 2010) [1] (Fig. 2.1). Complex and bulky equipment is required for posturography, including a movable force place (refer to 2.2.3), variable stimuli, and a tethering harness and frame for safety. The other commercially available instrument for the assessment of balance control behavior is Metitur Good Balance System (Metitur Ltd, Jyvskyl, Finland) [2], which is a triangular force platform used to measure postural control in different static and dynamic testing conditions and uses visual and auditory biofeedback to aid rehabilitation of balance and asymmetric posture [76].

Posturography is considered too expensive, cumbersome, and time consuming for all but the most detailed balance evaluation or research environments.

Pressure sensitive floor mats, force plates, and pressure shoe insoles

Pressure sensitive floor mats, such as the GaitRite M2 [3] (CIR Systems Inc), Tekscan Sway Analysis Module and Sensors (2010)(www.tekscan.com), and NovelPedar (2010) (www.novel.de), measure pressure distribution under the feet and deviations in center-of-pressure, while the person performs a series of tasks (ground reaction force). Some companies, such as Biodex (www.biodex.com), have developed specialized fall-risk screening tools (e.g. the Biodex Falls Screening and Conditioning Program 2010) that are used in association with their existing balance-measuring sensors.

[1] www.resourcesonbalance.com
[2] www.Metitur.com
[3] www.gaitrite.com

Figure 2.1: NeuroCom Balance Manager Systems' advanced computerized assessment tools that allow assessment, treatment and documentation of patient progress.[90]

Force-plates (AMTI Force Platforms 2010) are costly but highly accurate instruments that measure three-dimensional ground reaction forces generated by a body standing on or moving across them. Force plates enable researchers to calculate several gait- and balance-parameters in clinical settings, including location of the center-of-pressure (COP) under the feet, the whole body center-of-mass (COM), acceleration, and velocity.

Gait mats, e.g., the GaitMat II (E.Q., Inc., Chalfont, PA) system, can be used in

a laboratory or fall clinic for gait analysis. The GaitMat II consists of a 4-meter-long walkway and a computer system that analyzes the data it receives. As an individual walks on the walkway, opening and closing of pressure sensitive switches will be represented on the computer screen as footprints. Brach et al. [130] used such a system to calculate gait speed and variability of step length, step width, and stance time of 379 older adults (mean age=79 years).

Instrumented treadmills are an option as a repeatable and sensitive method to analyze common spatiotemporal gait parameters and vertical ground reaction forces. Feasel et al. [133] utilized an instrumented treadmill for a rehabilitation of asymmetric gait purposes (integrated virtual environment rehabilitation treadmill (IVERT)), which intended to provide real-time feedback regarding gait speed and asymmetry during gait training. In [132] a comparison of four different methods for calculation of symmetry of spatial-temporal parameters of gait was provided using an instrumented treadmill (FDM-THM-S, Zebris Medical GmbH).

The aforementioned equipment must be installed in a customized environment (e.g. laboratory) and requires experts to administer the motion analysis tests and interpret the results. Such systems are typically too costly for use in standard clinics, but fall clinics may refer patients for in-depth evaluation if they observe balance impairment that warrants a comprehensive assessment.

In an effort to extend the usability of pressure sensitive sensors to real-life situations and unsupervised settings instrumented insoles (or in-shoe pressure sensors) are introduced. Similar to force plates in action, these systems are able to capture dynamic and force information to measure the interaction between foot and footwear. For instance, The F-Scan system (Tekscan, Boston, MA) [4] provides dynamic pressure, force and timing information for foot function and gait analysis. Recently, researchers have shown an increased interest in these insoles, [120, 134, 138, 136, 137], mostly due to the capability of these sensors in gait analysis on every step and in more typical daily life environments outside clinics [135].

In sections 2.2.3 and 2.3.2, some studies that have utilized the pressure shoe insoles in

[4] www.tekscan.com

conjunction with a smart phone or IMUs, to assess risk of falling in natural and daily life situations are discussed.

Table 2.1: sensor-based studies for gait and risk of falling assessment

Sensor	**Description**
Force Plate	Measures the ground reaction forces generated by a body standing on or moving across them.
Gait Walkway	Long (35 meter) pressure sensitive walkway that measures static and dynamic pressure and force measurements over several steps using a low profile floor walkway
Gait Mat	Short and low-profile floor mat that captures dynamic pressure as person walks over it
Instrumented treadmill	Are able to gather large amounts of step data, but are limited by their controlled environment and prescribed walking pattern
Pressure Shoe Insoles	Are similar to force plates in action, and are able to capture dynamic and force information to measure the interaction between foot and footwear.

Optical motion capture systems and stereophotogrammetry

In laboratory settings, advanced motion capture systems like 3D optical motion capture systems allow the derivation of spatio-temporal gait variables (e.g. cadence, stride length, gait velocity), kinematic (concerning joint movements, e.g. joint angle) and kinetic (concerning the forces that produce the movement, e.g. muscle activity) gait parameters from

a few steps. Stereophotogrammetry is a popular approach for gait analysis, which can be based on either conventional photography, video or optoelectronic sensors and image processing systems [59]. Systems such Vicon (Vicon Ind., Oxford, UK) and CODA have gained popularity for Gait Analysis. This system relies on the observation of reflective markers by IR cameras. Some studies [92] employ the Cartesian Optoelectronic Dynamic Anthropometer (CODA) optical systems from Codamotion (Charnwood Dynamics Ltd.)[5], which consist of body worn markers with embedded infra-red LEDs. These marker-based motion capture units track (reflective) markers attached to the patient's body to compute the underlying motion of different body parts during gait. The markers are tracked by tripod-mounted motion capture units and the captured data are sent to a data acquisition unit. Afterward, the data is sent to a PC where the measurement information can be displayed in real-time and variables, such as joint angles, moments and powers, are calculated.

Although some motion capture systems (first two rows in Table 2.2), can provide accurate body sway and gait information, such systems require individuals to wear markers on specific parts of their bodies, and the test can be performed in the lab or clinical environment.

Table 2.2: Types of motion capture systems [91]

Sensor	**Description**
Optical-Passive	This technique uses retroreflective markers attached to subjects that are tracked by infrared cameras. It is the most flexible and common method used in the industry e.g., Vicon [1] and OptiTrack[2]
Optical-Active	This technique uses LED markers connected by wires to the motion capture suit. A battery or charger pack must also be worn by the subject.

Continued on next page

[5]www.codamotion.com
[5]http://www.vicon.com/
[5]www.optitrack.com/

Table 2.2 – continued from previous page

Sensor	Description
Video/Markerless.	This technique does not require markers to be worn and instead relies on software to track the subjects' movement. Varying tracking methods yield different results, but real-time and final data error ranges tend to be larger than marker-based solutions.

Wearable sensors

Despite the undeniable potential of wearable sensors in recording the physiological/motion signals during daily life activities, their primary use in FRA is to instrument the classic tests performed in the clinical settings.

Instrumenting the traditional clinical tests such as the TUG test (as depicted in Table 6.1) with wearable sensors, e.g., IMUs, provides a more systematic way of gait and balance analysis, which has been extensively investigated by many researchers over the past decade for the development of fall risk assessment methods. Such systems include accelerometers, gyros, magnetometers, tilt sensors and/ or barometric pressure sensors. IMUs are non-invasive, relatively inexpensive, and easy-to-use, and are able to collect and stream kinematic signals during different activities.

Howcroft et al. [93] provided an exhaustive, methodical review of forty studies that employed accelerometers to develop FRA methods in geriatric populations. Most of these papers proposed FRA methods by gait analysis and estimation of spatio-temporal gait parameters (e.g. walking speed), and variability and stability-related parameters (e.g. variability in gait rhythm, root mean square), that were extracted from acceleration signals. Various activities were used for inertial-sensor-based FRA. The most frequently assessed activities were 1) level ground walking, 2) TUG, 3) sit-to-stand transitions (STS), 4) standing postural sway, 5) left-right Alternating Step Test (AST) on level ground, and

6) uneven-ground walking, and 7) a combination of activities. All of these studies were conducted in a clinical setting; however, they differ from each other in terms of the set-up and sensor placement, e.g., lower lumbar spine, chest, leg, and the employed pattern recognition approach, threshold-based or machine learning-based. Typically these studies aimed to categorize the subjects into fallers and nonfallers and lack validation for use in daily life activities.

Menz et al. [95, 96], examined the gait of 100 community-dwelling elderly subjects, aged 75 to 93, using temporo-spatial gait parameters and acceleration patterns at the head and pelvis were measured while subjects walked on a flat corridor and an unpredictably irregular walkway. Harmonic ratios of head and pelvis accelerations in each plane were calculated to provide an indicator of stability. Gait features between young and elder subjects have been compared by investigating accelerometry data. They concluded that root mean square values of accelerations obtained from the pelvis and head of senior subjects are smaller compared to those obtained from young subjects. Elder subjects showed slower velocity, shorter step length, and larger step timing variability during both walking on level and irregular surfaces from the temporal-spatial gait parameters between young and elder subjects.

Marschollek et al. (2011) [94] recruited 119 geriatric inpatients and asked them to wear an accelerometer on their waist during a 20 m walk and a TUG test. In a one-year follow-up study, fifty patients were included and their fall events and average physical activity scores (at home) were recorded by telephone-interviews. The sensor data were processed to extract gait and dynamic balance parameters, from which four fall risk models, including two classification trees and two logistic regression models, were computed: models CT_1 and SL_1 that employed accelerometer data only, models CT_2 and SL_2 that included the physical activity score. The risk models were evaluated in a 10-fold cross-validation. They found that both classification trees show a fair to good performance (accuracy 80% and 78% for models CT_1 and CT_2, respectively) and these models outperformed logistic regression models. While the authors suggested that accelerometer data may be used to predict falls in an unsupervised setting, the generalizability of their method remains unexplored.

Although there are numerous studies that have attempted to develop accelerometry-based methods for FRA, just a few papers have examined the possibility of using wearable surface electromyography sensors to assess FRA in the elderly, in a clinical setting. In one study by Wong et al. [97], electromyography sensors were used to record the activity patterns of bilateral tibialis anterior and gastrocnemius muscles in twenty-three volunteers (mean age 73 years), for a series of five static balance challenges (Romberg eyes open/closed, Sharpened Romberg eyes open/closed, and Single Leg Standing). Participants then were categorized as 'at-risk' or 'not-at-risk'. They concluded that Increased fall risk is associated with elevated co-contraction about the ankle during static balance challenges in older adults.

Rouhani et al. (2011) [138], presented an ambulatory system, comprised of plantar pressure insoles and IMUs (mounted on the shank and foot), for kinematics and kinetics assessment of ankle and foot joints during long-term gait, by measuring the spatio-temporal parameters of gait, 3D joint angles, joint moments, joint power, ground reaction force, and plantar pressure distribution. Twenty-two subjects (age: 58 ± 13 years, 12 patients with ankle osteoarth, and 10 healthy adults) were recruited and walked two 50 m trials in a hospital corridor. The results show a high level of accuracy compared to those obtained by an optoelectronic motion capture system and a force-plate in a gait laboratory. Although their method was not developed for the purpose of FRA, (for distinguishing populations with foot and ankle pathologies from healthy population and assessing the improvements in the patients' gait after surgical treatments), their results are promising for future studies.

Recently Howcroft et al. (2016) [120], proposed a wearable-sensor-based classification model of faller status in older adults. One hundred older individuals (age: 75.5 ± 6.7 years; 76 non-fallers, 24 fallers based on 6 month retrospective fall occurrence) were recruited and asked to wear pressure-sensing insoles and tri-axial accelerometers at the head, pelvis, and left and right shanks, while walking (7.62 m) under single-task and dual-task conditions. Fall risk classification models were assessed for all sensor combinations after feature extraction from signals, e.g. temporal features and Fast Fourier Transform (FFT)-based features. Afterward, they developed three machine-learning model types, including multi-layer perceptron neural network, nave Bayesian, and support vector machine to classify fall

occurrence. For all models, 75% of participant data (18 fallers, 57 non-fallers) were used for training and 25% were used for testing (6 fallers, 19 non-fallers) which will represent the generalizability of the model. The best performance was achieved from a multi-layer perceptron neural network with input parameters from pressure-sensing insoles and head, pelvis, and left shank accelerometers (accuracy = 84%). The older adults who participated in this study walked under the researchers' supervision and only for a short period of time, which completely differs from real-life situations that older adults may deal with. However, due to the use of shoe pressure insoles, the results are promising and have the potential to be extended to real-life situations.

The aforementioned studies are still based on measurements of mobility performed under supervision in a controlled setting and do not afford a detailed analysis of patterns of mobility behavior in the home and community. Patients also often make their best effort in front of a clinician and thus the resulting observations are not representative of the patients' typical movements.

2.3 Efforts for the development of unsupervised FRA methods

Realizing the gap in the extant literature, more research is needed to develop methods for unsupervised assessment of balance control behavior over long periods of time. There are only a few studies in the literature that has examined risk of falling assessment strategies by monitoring balance control behavior during daily living and over long periods of time.

Virtual reality (VR) systems aim to simulate complex environmental conditions [86, 87, 88, 89]; however, a considerable difference in balance control behavior is observed in natural every day settings. The recent explosion of ambient sensors, smart-phones, and wearable sensor technologies has advanced the possibility of these sensors, specifically WSSs, to examine balance control in natural environments. One advantage of such systems over VR approaches is the potential for long-term monitoring to examine trends and detect

significant motor changes arising from typical daily activities in a natural environment. By automatic fall risk assessment using diverse types of sensors, e.g., WSSs or environmentally placed sensors in the homes of elders, fall risk can be measured in everyday living activities. In that way, seniors can be notified when fall risk increases, so that they can take steps to improve physical function to avoid devastating falls (in an unsupervised fashion).

Although most of the reviewed studies were conducted in a clinical setting and employed healthy young subjects; the long-term goal of these studies is to extend the findings into real-life situations and develop an unsupervised FRA tool. We also provide a brief description of some studies that attempted to monitor posture and balance control behavior during activities of daily living; however, most of them do not directly assess the risk of falling.

In this section, we classify the current trends in the development of unsupervised FRA tools into two main parts: 1) Ambient sensor-based methods, and 2) WSS-based methods.

2.3.1 Ambient sensors

Ambient FRA and fall detection (FD) systems are considered to be passive systems since, once installed, they do not rely on daily decisions by the user to utilize the device. Such systems include video cameras, e.g., Microsoft Kinect and web cameras, infrared cameras, acoustic sensors mounted on the wall or ceiling, and pressure sensors or vibration sensors embedded in the floor or furniture. Ambient sensors allow seniors to live independently and safely in their own homes, reduce the need for expensive care facilities, and also enable caregivers detect not only adverse events such as falls, but also continuously assess and monitor the risk of such events. The main advantage of such systems is that the users do not need to wear any special device, e.g., sensors, and markers on their bodies. Several groups have examined the capability of camera-based fall detection systems to automatically detect falls, however, fewer studies focus on the risk of falling assessment [114].

Ranasinghe et al. [110] employed a battery-free RFID (Radio Frequency Identification)

tag that can be attached on clothing to continuously and automatically monitor ADLs of frail patients at acute hospitals or the seniors in residential care facilities. Ten healthy adults age from 23 to 30 years overall performed 197 tasks, including standing-to-sitting, sitting-to-standing, sitting-to-lying, lying-to-sitting. They obtained accuracy of about 94%; however, no machine learning techniques were employed. Instead, postural transitions were detected based on the threshold values that were obtained for the displacement of θ (inclination angle between the trunk and vertical axis).

Markerless vision based motion capture systems, e.g, Microsoft Kinect, which consists of an infrared depth sensor and an RGB image sensor for capturing video in 3-D, provide a potential alternative for affordable capture of human motion in a wide range of settings, and has received a great deal of attention from the computer vision and biomechanics community [98]. Most of the related studies integrate a markerless image processing algorithm to estimate the trajectory of the center of mass (COM) from video sequences obtained from commercially available systems. Moreover, measurement of joint kinematics, e.g., knee flexion-extension or ankle angle, is possible using a markerless motion capture system [98].

Researchers at the University of Missouri [100, 101, 108, 103, 105] aim to use gait measurements from everyday living environments to estimate the risk of falling and enable improved interventions. [100] proposed a method to measure walking speed, stride time and length based on the depth data from a Kinect camera. Moreover, Rantz et al. [103] placed a pulse-Doppler radar system (deployed in a decorative wooden box), a Microsoft Kinect, and 2 orthogonal web cameras in the apartments of 19 older adults (mean age = 87 years) at a senior living facility for two years. They tested the mentioned sensor system for the FD and FRA tasks with the data collected from the GaitRite mat. The FRAs included six measures: 1) Habitual Gait Speed (HGS) (Bohannon, 1997; Fransen, Crosbie, and Edmonds 1997), 2) TUG, 3) Multidimensional Functional Reach (FR) (Newton 2001), 4) Short Performance Physical Battery (SPPB) (Guralnik 1994), 5) the Berg Balance Scale (BBS-SF) (Berg et al. 1992), and 6) the single leg stance (SLS) (Vellas 1997). They showed that all FRAs that were completed by the GaitRite mat were highly correlated ($\rho < .01$) with the Kinect derived fall risk scores of gait velocity and stride length. Moreover, the

calculated velocity from the radar system was correlated ($\rho < .05$) to all the FRAs and highly correlated ($\rho < .01$) to most of them. Their system is also able to send real-time alerts to clinicians in case of actual falls and urgent situations.

Furthermore, Yardibi et al. [105] employed pulse-Doppler range control radar to obtain gait characterization, track mean gait velocity, mean stride duration and stride duration variability. In another study (Gabel et al. [107]) Microsoft Kinect was used to capture information needed for measuring arm kinematics and strides. lower and upper body gait parameters, i.e., stride information and arm kinematics, were extracted from the skeletal data and a machine learning approach was developed to simulate feature signals similar to those that are obtained from gyroscopes. The measured mean difference to the wearable sensors was less than 1%.

Staranowicz et al. [99], proposed a robotic-based gait monitoring method, in which an autonomous robot, equipped with a Microsoft Kinect, follows the person (at a safe distance) in a desired environment, e.g., at his/her home. The method evaluates three different metrics in order to perform the fall prediction: 1) stride length, 2) stride duration, and 3) Motion of the center of mass (COM). Twenty subjects were asked to walk back and forth for a total length of 8 meters and an extensive comparison to a commercial marker-based motion capture system, e.g., Vicon, was carried out. Being inexpensive, easy-to-use, and being able to capture unlimited volume of data are the most important advantages of this system.

Hagler et al. [106] utilized passive infrared (PIR) motion detectors in order to measure gait velocity. In another study, Kaye et al. [109] used PIR motion sensors to measure walking speeds and the variance, median number of walks for 76 men and women (mean age= 86).

Wang et al. [113] developed an inexpensive method to capture silhouettes, extract parameters of body sway in the anterior-posterior and lateral directions during standing and walking from two calibrated web cameras and a three-dimensional voxel reconstruction. The results were validated with a Vicon motion capture system. potential capability of measuring body sway in daily living environment for elderly people, and can be used as

part of a balance, stability and fall risk assessment tool.

Limitations

While ambient sensors have provided valuable information on mechanisms of human movement in at-home settings, the generalizability of these findings to everyday behavior in other environments, e.g., streets, shopping centers, and garden remains impossible. Moreover, installation, calibration and maintenance of the ambient sensors in nursing home cares, hospitals and dwellings of seniors, is a time consuming and expensive process and limits the testing location and frequency just to a specific place (not generalizable).

Some vision based systems such as Kinect systems can detect motion within their fields of view, therefore, it might face challenges due to occlusions (e.g. furniture) may obstruct the sensor's field of view so that it may not be able to collect proper data [103].

Risk of loss of privacy is another important barrier for the acceptance of camera-based ambient assisted living [114]. Moreover, while some types of ambient sensors, e.g., PIR sensors, do not raise privacy concerns among older adults, due to the coarse nature of the PIR sensors, they usually do not produce measurements of the necessary details for the FRA, specifically, spatio- temporal gait parameters beyond walking speed (e.g., step time, step length, gait symmetry), timed up and go (TUG) time, sit to stand time, etc [100].

2.3.2 Wearable sensors

WSSs have advantages over ambient sensors in terms of ease of installation, coverage area, and privacy [115]. As it is discussed in section 2.2.3, a WSS that can efficiently capture and analyze quantitative mobility data could improve the accuracy of the classic fall risk assessment methods in the clinical settings by reducing the subjectivity, and have the potential to provide a more accurate reflection of gait in the home and other unsupervised environments during habitual behaviours. Emerging research suggests that measurement of gait in uncontrolled settings using WSSs is feasible but this has not been investigated in depth [121]. A traditional barrier to the adoption of WSS has been the size and weight

of the sensors, which has limited their suitability for long-term monitoring. However, recent advances in the miniaturization of sensor hardware has enhanced the feasibility of these systems **to track human activity and movement in and outside of the laboratory.** This section presents an comprehensive review on the most recent studies that employ WSSs for ambulatory monitoring of elderly in unsupervised settings, including accelerometers and pressure shoe insoles.

IMU-based methods

There are numerous studies in the literature that have attempted to employ WSSs to perform balance and gait analysis; however, very few studies have examined the performance of WSSs for monitoring of ADLs in an uncontrolled and unsupervised setting. Del Din et al. [121] and Brodie et al. [123] quantitatively reveal that there is a remarkable difference between FRA in clinical and non-clinical settings. Some studies evaluate gait characteristics by recording durations that range from two days to eight weeks [128, 127, 125, 126, 123].

Weiss et al., [125, 126] addressed the association between accelerometer-based gait characteristics obtained in daily life and prospective falls and showed that there is a significant difference in spectral characteristics of trunk accelerations measured in daily life between older fallers and nonfallers. Seventy-one community-living older adults were recruited in their study and their walking abilities were quantified using performance-based tests of mobility (eg, TUG). Afterward, subjects wore a triaxial accelerometer on their lower back for 3 consecutive days, and acceleration-based parameters, e.g., total activity duration, number of steps taken, and the amplitude and width at the dominant frequency in the power spectral density were extracted. To explore the predictive values, self-report of falls was collected for 6 months. Subjects were classified as fallers or nonfallers based on a history of 2 or more falls. The authors revealed that during the 3 days, step-to-step consistency was lower in the fallers in the vertical axis ($\rho = .008$); in the mediolateral axis, step-to-step consistency was higher in the fallers ($\rho = .014$). The 3-day measures improved the identification of past and future falls status ($\rho \leq .005$), compared to performance-based tests.

Schooten et al. [140] recruited 169 older adults (mean age=75 years) and collected data from a tri-axial accelerometer (DynaPort MoveMonitor), worn at the level of L5, for overall 7 days. The participants wore the accelerometer at all times, except during aquatic activities. The data obtained during this period was used to estimate gait parameters and duration of physical activity (or inactivity). The gait characteristics includes walking speed, stride time, stride length, gait intensity, symmetry, smoothness, complexity and variability. All characteristics were determined for each of the three directions of acceleration, that is, anteroposterior (AP), medi-olateral (ML), and vertical. The activities were detected using the manufacturer's algorithm, which includes periods of nonwearing, locomotion, sitting, lying, and standing. Afterward, in a six-month follow-up, fall incidence was obtained retrospectively by recall and prospectively by fall diaries and monthly telephone contact, and during this period 35.5% of the participants had a history of falling and 34.9% experienced falls. Twenty-eight out of 169 participants experienced multiple falls during follow-up. The authors used a univariate logistic regressions to identify parameters that were associated with either or both retrospective or prospective falls and had a $\rho < .05$. They revealed that having a history of falls was significantly associated with the inability to use public transportation, a lower grip strength, a higher FOF, a higher depression score, having a walking aid, a lower number of strides per day, a lower total duration of daily locomotion, and a higher power in the dominant frequency in ML. The authors showed that daily-life accelerometry can identify the fallers with a good accuracy.

Culhane et al. showed that ambulatory activity monitoring using accelerometers is a reliable technique, providing continuous, unsupervised, objective, monitoring of mobility [116]. Five older adults, with varying degrees of mobility, resident in a rehabilitation clinic, participated in their experiment for over four days. Two Analog 2-axis accelerometers (50 Hz) were employed, one on the trunk and another on the leg. They found that these 2 accelerameters were sufficient to distinguish between sitting, standing, lying and movement, with activity detection accuracy of 92%, using a threshold-based method [117].

Najafi et al. [118] found that a single device on the trunk comprising an accelerometer and a gyroscope is capable of accurately detecting posture change and walking in older adults.

Aziz et al. [119] (2014) indicated the utility of a three-node accelerometer array, placed on left ankle, right ankle, and sternum, for distinguishing the cause of falls, e.g., slips. Sixteen young adults were recruited in an experiment involving falls due to slips, trips, and other causes of imbalance. Three-dimensional acceleration data acquired during the falling trials were input to a linear discriminant analysis (LDA) technique. This routine achieved 96% sensitivity and 98% specificity in distinguishing the causes of a falls using acceleration data from three markers. In contrast, a single marker provided 54% sensitivity and two markers provided 89% sensitivity.

The study of Del Din et al. (2016) [121], provides encouraging results to support the use of a single Accelerometer-based body worn monitors (BWMs) for free-living gait evaluation in people with PD with potential for research and clinical application. Fourteen clinically relevant gait characteristics organized in five domains (pace, variability, rhythm, asymmetry, postural control) were quantified using laboratory based. Free-living data collected over 7 days using a BWM placed on the lower back in 47 PD participants and 50 controls. Free-living data showed that both groups walked with decreased pace and increased variability, rhythm and asymmetry compared to walking in the laboratory setting.

Brodie et al. (2015) [122] employed a freely worn small pendant device (housing a triaxial accelerometer and pressure sensor) to investigate the relationship between usual stair-ascent performances (and stair negotiation) by older people during ADLs (free-living experiment) and clinical assessments and prospective falls. Fifty-two healthy community-dwelling older people (83±4 years) were participated in their study and for each participant ADLs were recorded for 30 min, using the pendant device. Sensor-derived stair-ascent features (comprising intensity, variability, and stability) were investigated and classification accuracy was assessed using annotated videos and four-fold cross validation. Accurate identification of stair events (99.8%) was possible in both frail and athletic participants by scaling the barometer threshold to stair cadences. Moreover, they showed that cautious double-stepping strategy could be detected remotely and also argued that reduced functional performance and altered strategies for undertaking ADLs could soon be routinely tracked to augment health care. Although the results are promising, the data was collected in a short period of time (30 minutes per adult) which might not be enough and also the

authors did not indicate the types of the recorded ADLs, which might not be challenging,

In another tudy, Brodie et al. (2015) [124] collected 1085 days of walking data from eighteen independent-living older people (mean age 83 years) using a freely worn pendant sensor. They showed that using a freely worn device and wavelet-based analysis tools allow long-term monitoring of walks greater than or equal to three steps and one week's monitoring is sufficient to reliably assess the long-term propensity for falling. Statistical distributions from several accelerometer-derived gait features (encompassing quantity, exposure, intensity, and quality) were compared for those with and without a history of falling. They concluded that in older people, short walks constitute a large proportion of exposure to falls. Statistical distributions of gait performances provide a reference for future wearable device development and research into the complex relationships between daily-life walking patterns, morbidity, and falls.

Smart phone-based and pressure shoe insole-based methods

Recent improvements in smartphone (SP) technology, the widespread adoption and the high market penetration of them even among older adults, enable implementation of new forms of FD and FP systems. These systems take advantage of the array of embedded smartphone sensors, e.g., triaxial accelerometer, gyroscope, magnetometer, digital compass, GPS, microphone, and camera, and use Bluetooth and Wireless Fidelity (Wi-Fi) technologies for communication purposes and real-time data streaming.

In SP-based fall detection systems (SPFD), upon detecting a fall incident and identifying the location of a faller, the SP application sends a message, e.g., via SMS or email, to a caregiver. SP-based fall prevention (SPFP) and fall risk assessment (SPFRA) tools are comparatively less explored with respect to SPFD methods in the literature[149]. Most of these proposed solutions were based on standard FRA tests, e.g., TUG, instead of active fall prevention [149].

Majumder et al. (2013) [151] proposed a SPFP system-Smart Prediction- by integrating the sensor data recorded by a SP (iPhone) embedded accelerometer and gyroscope (3

signals), along with a smart shoe that contains four pressure sensors and a Wi-Fi communication module to enable collecting data and evaluating normal and abnormal walking patterns in any environment. The SP can be either in pocket or hand. They simulated two abnormal walking patterns that are due to two common abnormalities in most elderly, 1) peg leg (simulated by walking with a straight ended left knee), and 2) leg length discrepancy (simulated by taking one shoe off and wearing an extra heel on top of the regular heel on the left shoe), which lead to a huge number of falls among them. The system can generate an alert message to warn the user about the high-risk gait patterns and potentially save them from an imminent fall. They generate 4 tilt-invariant signals and extracted 3 quantitative features and validated the approach using a decision tree with 10-fold cross validation. They found a high classification accuracy $\simeq 97\%$ in gait abnormality detection when the training data was collected only from the same subject, however, they observed a remarkably lower accuracy $\simeq 71\%$ when attempting to classify one subject's gait based on the other subjects'. The problem with single subject data is that it requires the subject to train the system by simulating abnormalities which raises a generalizability concern.

Mellone et al. [145] developed the uFall and uTUG Android applications for the purposes of fall detection and fall assessment respectively. The applications utilize the data from SP in-built accelerameter and gyroscope and require that subjects wear the SP by means of a waist belt, for monitoring the user's motor activities at home. The uTUG is an application for instrumenting the TUG test, which is capable of recording the trial and also real-time data processing and displaying the results [145]. The authors do not declare the performance/accuracy of their system, because such the articles present very preliminary investigations on SP-based fall prevention systems [149].

Guimares et al. [147] propose a SP-based method for measuring 1) One Leg Standing, 2) Sit to Stand and 3) Falls Efficacy Scale. Experimental results of this system support the feasibility of a reliable phone-based fall predictor, which constitutes an alternative to evaluate fall risk factors in aging. The same authors in another paper [146] examine the possibility of SP-based measurement of 1) ankle flexibility, 2) gait and 3) voluntary stepping. Their results show a good correlation with force platforms or cameras measurements.

SP-based FD and FP methods offer a clear advantage in usability over stand-alone wearable sensor systems. However, the performance and usability of such systems still remain limited because of the relatively lower quality and resolution of the embedded sensors. For example, most of the SP pre-built accelerometers have a limited measurement range (e.g,. +/-2 g) that may too small for accurately detection of fall and compensatory balance reaction incidents from other activities of daily living such as sitting down or bumping against an object [152]. Most of the SP-based solutions in the literature employ additional systems, e.g., shoe insoles, which may improve the accuracy and resolve these issues, but this reduces the attractiveness of SPs as a stand-alone tool for FD and FRA. The other barrier is the need to wear the SP in a fixed position, usually on sternum or belt. Users usually do not carry SPs on their bodies, so those methods are not suitable for home environments.

2.3.3 Studies to achieve context-awareness

To date, there is a lack of methods to investigate balance control behavior in complex, real-world environments. Falls have a multifactorial nature and are not originated from one intrinsic or extrinsic cause. This fact necessitates the need to develop methods for detection of associated risk factors. Most of the FRA tools neglect the extrinsic fall risks, which might explain why current clinical prediction models provide only poor to fair predictive ability [140]. The exposure to environmental hazards, such as curbs, carpets and pets, can only be investigated in daily life. Therefore, achieving contextual awareness during daily life activities may offer more promising estimates of fall risk.

Robinovich et al [111] installed digital video cameras in common areas (dining rooms, lounges, hallways) of two long-term care facilities in British Columbia, Canada and captured 227 falls from 130 individuals (mean age = 78 years, SD 10). The authors did observational study between April 2007, and June 2010. When a fall occurred, facility staff completed an incident report and contacted them so that we could collect video footage. A team reviewed each fall video with a validated questionnaire that probed the cause of imbalance and activity at the time of falling. They found that the most frequent

cause of falling was incorrect weight shifting, which accounted for 41% (93 of 227) of falls, followed by trip or stumble (48, 21.41%), hit or bump (25, 11.41%), loss of support (25, 11.41%), and collapse (24, 11.41%). Slipping accounted for only 3.41% (six) of falls. The three activities associated with the highest proportion of falls were forward walking (54 of 227 falls, 24.41%), standing quietly (29 falls, 13.41%), and sitting down (28 falls, 12.41%). Compared with previous reports from the long-term care setting, they identified a higher occurrence of falls during standing and transferring, a lower occurrence during walking, and a larger proportion due to centr-of-mass perturbations than base-of-support perturbations.

The only SP-based context-aware system that we found in the literature is proposed by Menelas [139]. The authors employ a smartshoe to track the movement of patients and categorize the fall risk status of the environment, and then broad-cast this in real-time to a smart-phone application which focuses solely on reducing extrinsic risk factors. It considers the environmental conditions in which older adults function and notifies them of potential risks. The environment is scanned for slippery surfaces and steep slope by means of a smart shoe with built-in sensors. No vision-based sensor was employed in their research.

Advances in mobile vision systems and wearable egocentric cameras, i.e., GoPro and Autographer wearable cameras, enabling a new form of capturing human experience. The first-person perspective photos and videos captured by these cameras can provide rich and objective evidence of a person's everyday activities that (in contrast to other motion capture systems) can be worn to capture contextual information in environments other that senior's dwellings.

The results of the recent research (2015) [141, 142, 143] supported by Fujisto Laboratories, Japan, indicate that the external environment has a significant impact on the quality of gait metrics; s a result. They emphasized that context of external walking environment is an important consideration when analyzing ambulatory gait metrics from the unsupervised home and community setting. The intention of their research is to understand the relationship between mobility metrics obtained outside of the clinic or laboratory and the context of the external environment.

Taylor et al. (2015) [143] employed three sensors to collect gait and environmental context information. Participants (N =12, age 70.9 ± 6.63 years) were recruited from the community and a falls clinic, including a control group with no history of falling and individuals who had fallen at least once in the past 6 month. The participants were studied during their daily lives for seven days. Two Shimmer3 9-dof inertial sensors(Shimmer Research Ltd, Dublin, Ireland) were attached via custom made semi elastic Velcro straps above the ankle to obtain gait information. An Autographer wearable camera (Autographer, Cambridge, UK) was worn around the participants' neck used to determine what type of environment was being walked in (images being recorded every 15 seconds) Gait metrics for each gait event were found, and for each identified gait event, the Autographer images corresponding to the same time period were manually reviewed to obtain contextual information. The most common annotations that were found in most of the participants were outdoors on pavement, indoors on carpet, and indoors on polished or hardwood. The results showed that both groups spent relatively little time walking in challenging environmental conditions, and that the fallers spent significantly less time walking under regular conditions (no effect on gait) and outdoors. Analysis of gait metrics showed that the fallers were slightly slower in general, and more noticeable differences were observed when the participants were regrouped according to mobility levels determined from baseline assessments using traditional methods.

Patterson et al. [141], used the same three-sensor system that was implemented in [143] and asked 10 healthy subjects (age 29.4 ± 4.7 years) to wear the inertial sensor on their both shanks and a wearable camera around their neck. Participants were asked to walk for thirty minute in five different conditions: 1) normal path, 2) busy hallway, 3) rough ground, 4) blind folded, and 5) on a hill. Several gait parameters such as stride time, stride time variability, stance time, and peak shank rotation rate during swing were calculated. A researcher walked alongside the participants to tell them where to go and noted the times. The authors pointed out that the algorithm that was presented by Greene et al. [148] did not work properly in detection of ICs and TOs in a gait cycle (from the sagittal plane gyroscope signal), mainly because the algorithm was developed for straight line walking; so they needed to modify the algorithm in order to detect ICs and TOs under

those five different conditions in a more natural environment. They found that stride time was considerably different between several of the conditions. Moreover, the "peak shank rotation rate" during swing was calculated (because it is a useful variable in detecting abnormal gait patterns), which was lower in the busy, blind and hill walking conditions.

Although the aforementioned studies have attempted to detect gait abnormalities and characteristics in different environments, none of them have proposed an automated vision-based way for detection of fall-related environmental risk factors. While these research groups have recorded videos, either with egocentric cameras or ambient cameras in the seniors' dwellings, to laboriously identify environmental circumstances manually, the present thesis is the first to develop and evaluate an automated method to the author's knowledge. In section 4.2 more related studies to our approach for the detection of environmental risk factors (discussed in chapter 4) that integrated computer vision techniques to achieve context-awareness, specifically in robotics, are discussed.

2.3.4 Limitation of the proposed UFRA methods

Despite exhibiting high classification accuracy in laboratory experiments, inertial sensor based fall detection systems have yet to achieve high market penetration. One barrier to the acceptance is the lack of evidence of their effectiveness in real-world falling scenarios in older adults. The accuracy of various systems has been measured in laboratory experiments, involving young adults falling onto gymnasium mats, and undertaking various activities of daily living (ADLs). Clearly, additional field studies, incorporating longer durations and larger number of falls, are required to measure and refine the real-life performance of FRA algorithms based on the wearable sensors.

Different functional performance in non-clinical settings

The gait strategies and patterns during the fall may have been different from those during the assessment, because the participants could have adjusted their walking and mobility patterns to be more conservative, stable, and safe.

A number of assessment tools are readily available to identify adults' fall risk factors. The major associated challenge is a lack of techniques to extract contextual information needed to interpret ambulatory gait and balance control behavior. For example, frequent losses of balance on a given day may be interpreted as gait instability or may reflect that the person is doing activities in a risky environment with fall-related factors. Without detailed information of environment, such as the presence of other pedestrians on a crowded sidewalk, pets, obstacles, stairs, terrain changes and doorways, the ability to interpret the balance control reactions is constrained.

2.4 Studies on compensatory balance reactions

The previous technology-based FRA tools have primarily concentrated on the gait and balance parameters. These parameters have the potential to quantitatively estimate the risk of future falls and hospitalization; however, they are mostly carried out in a controlled setting and are still lacking context-awareness. Although gait- and balance-related parameters such as asymmetry and variability in gait are markers of fall risks [93], it is possible to find other reliable markers of impaired gait that indicate and predict the future risk of falling in older adults.

Missteps or near falls are stumbles or sudden loss of balance that would result in a fall if compensatory reactions or sufficient recovery mechanisms were not activated [158]. Near-falls are also more frequent than falls and play a critical role in preventing falls [153]. These compensatory reactions are much more rapid than volitional limb movements and can be very effective in decelerating the centre-of-mass motion induced by sudden unpredictable balance perturbation. Age-related deterioration in the neural, sensory and/or musculoskeletal systems may affect the ability to execute these reactions properly [154]. Evidence support the view that impaired ability to execute compensatory stepping reactions is an important contributor to the unsteadiness, loss of balance confidence, and risk of falling that is associated with aging and age-related pathology [155].

There were some research about CBRs, including those representing the effect of

perturbation-based balance training and stimulation of CBRs on reducing fall risks [153], or those investigating the changes in center of pressure or center of mass of participants after stimulating a near-fall by perturbing their balance; however, there are just few studies focused on the detection of near-fall or CBRs [159].

Mansfield et al. [153] studied the impacts of a perturbation-based balance training program on compensatory stepping and grasping reactions in older adults. They found their method as an effective intervention to improve the ability of older adults to prevent themselves from falling when they lose their balance and concluded that perturbation-based training may reduce fall risk in daily life [153]. However, they count the reactions manually and their method is a supervised way of FRA.

Maki et al. [154] showed that fallers required 0.5 more steps to recover balance, compared to nonfallers, suggesting that it is important for clinicians to assess compensatory stepping, in order to identify the individuals who are at a higher risk of falling and to pinpoint specific control problems to target for balance or strength training or other intervention.

The only CBR-related study that employed sEMG sensors is by Hof et al. [156]. The authors studied the EMG patterns of human hip abductor and showed that the foot placement actions, which effectively assure balance in walking after lateral perturbations, are caused by activations in gluteus medius with various latencies.

Automatic identification of CBRs should provide quantification of fall risk over a shorter time interval and can potentially be used as an estimator of fall risk [159]; however, the detection of CBRs is not an easy task. It is not complicated to distinguish falls from usual walking but it would be more challenging to distinguish near-falls from usual walking [158].

Weiss et al. [159] employed a tri-axial accelerometer on the participants' pelvis as they walked on a treadmill. Near falls were induced by placing obstacles on the treadmill. They develop a threshold based method to distinguish 21 near-falls and 668 non-near-falls. The best single method was based on the maximum peak-to-peak vertical acceleration derivative, with detection rates better than 85% sensitivity and specificity. rule-based approaches that rely on simple thresholding of the sensor outputs and definitely have

several limitations in proper detection by changing conditions

More related to the methods that were used in the present thesis, is the experiment conducted by Aziz et al. [163], who conducted laboratory experiments to determine how the number and location of wearable inertial sensors affect the accuracy of a machine learning algorithm in distinguishing near-falls from ADLs. They employed seven inertial sensors with the sampling rate of 128 Hz. The researchers recruited 10 healthy young adults, and asked the participants to wear the sensors bilaterally on their ankles and thighs, and at the waist (sternum). Near-falls included five different scenarios: 1) slips, 2) trips, 3) incorrect transfer while rising from sitting to standing, 4) misstep while walking, and 5) hit and bump by another person. ADLs included eight scenarios: 1) walking, 2) standing quietly, 3) rising from sitting, descending from, 4) standing to sitting, 5) standing to lying, 6) picking up an object from the ground, 7) ascending and 8) descending stairs. The participants performed three trials in each category. The authors performed binary classification with 150 near-falls and 240 ADL trials. The authors found that SVMs with RBF Kernel showed a good sensitivity and specificity in distinguishing near-falls from ADLs with various sensor combinations. With a single sensor, the sensitivity and specificity of the system was at least 88% except for the waist sensor (which had 80% sensitivity). With two sensors, the least number of false positives (FP) and false negatives (FN) was provided by the left ankle + right ankle combination, which distinguished near-falls and ADLs with 96% sensitivity and 98% specificity. With three sensors, the highest sensitivity and specificity was provided by a) left foot + right foot + sternum and b) left foot + right foot + waist. Both combinations showed 100% sensitivity and 99% specificity. The best overall performance was observed with the five sensor combination of left foot + right foot + right thigh + waist + head, which did not result in any false positive or false negative, and provided 100% sensitivity and specificity in distinguishing near-falls and ADLs. Although this study provided promising results for every-day-measurement of mobility, the study has been conducted in laboratory and involved young adults falling onto gymnasium mats, and undertaking various ADLs. Clearly, additional field studies, incorporating longer durations and larger number of falls, are required to measure and refine the real-life performance of FRA algorithms based on the wearable sensors. Although the results of this study

are promising, the authors did not consider the impacts of environmental hazards that may lead to falling and also no attempt was done to explore the automatic detection of environmental risk factors.

It appears from the aforementioned investigations that most attention has been paid on supervised assessment of CBRs. So it is necessary to do deep research on the detection of CBRs and their associated environmental causes, which has motivated the present thesis. In this study, we are trying to integrate machine learning algorithms and develop a classifier to automatically distinguish near-falls episodes from regular stepping patterns and we propose a video-processing based method to automatically detect the associated environmental risk factors.

Chapter 3

Automated Detection of Compensatory Balance Reactions Using Machine Learning Techniques and Wearable Sensors

3.1 Introduction

Due to the fact that a fall is associated with serious physical and psychological consequences in geriatric populations, fall prevention has a high priority in health promotion for senior adults. As an alternative to the FRA methods that are based on gait analysis, automatic identification of CBRs should provide quantification of fall risk over a short time interval; and can be potentially used as an estimator of fall risk [159]. This chapter presents a machine learning based method that automatically distinguishes CBR episodes from regular stepping patterns, using wearable inertial measurement units and sEMG sensors.

CBRs can happen in different directions; i.e., forward, backward, and medial-lateral (M-L). In contrast to forward stability, lateral balance requires active control [161]; and

there is accumulating evidence that proves aging effects on balance control behavior may be impaired in lateral direction, e.g., hip fractures in seniors frequently happen in association with falls in lateral direction [160]. Moreover, researchers indicate that measures of medial-lateral sway in older individuals have been associated with both past falls and future risk of falls [160]; however, the mechanisms for the lateral vulnerability and the underlying associated circumstances remain unclear [160].

Considering the aforementioned facts, we initially focus on the development of a machine-learning based method to automatically detect CBRs in lateral direction during normal walking (NW). Lateral CBRs include: 1) the side step (SS) (or Lateral CBR type 1), and 2) crossover step (CO) strategy (or the Lateral CBR type 2) (Fig. 3.1).

This chapter consists of two main parts: 1) Automated (machine learning based) detection of CBRs based on the movement data captured from wearable IMUs, and 2) Automated (machine learning based) detection of CBRs based on surface electromyography signals. Results from an initial evaluation in young, healthy adults are reported and discussed with the aim of advancing methods of detecting CBR events in everyday behavior.

3.2 Participants and Equipment

The wearable sensor equipment used to collect movement data is the SHIMMER (Sensing Health with Intelligence, Modularity, Mobility, and Experimental Reusability, Shimmer, Ireland) wireless system. Each SHIMMER sensor comprises of: microprocessor, Bluetooth radio, 3-axis accelerometer, 3- axis gyroscope, 3-axis magnetometer, 2 channels of ExG (i.e., ECG, EMG), and MicroSD card. Five healthy young participants aged between 18 and 40 (1 woman and 4 men), were recruited in this study. Three SHIMMER sensors were mounted on the subjects' 1) right shank, 2) right thigh, and 3) sternum, and secured by straps. Although sacrum is closer to subject's center of mass, we decided to place the sensor on sternum. To avoid discomfort when sitting with the device attached. Sensors placement on participants' body is depicted in Fig. 3.2.

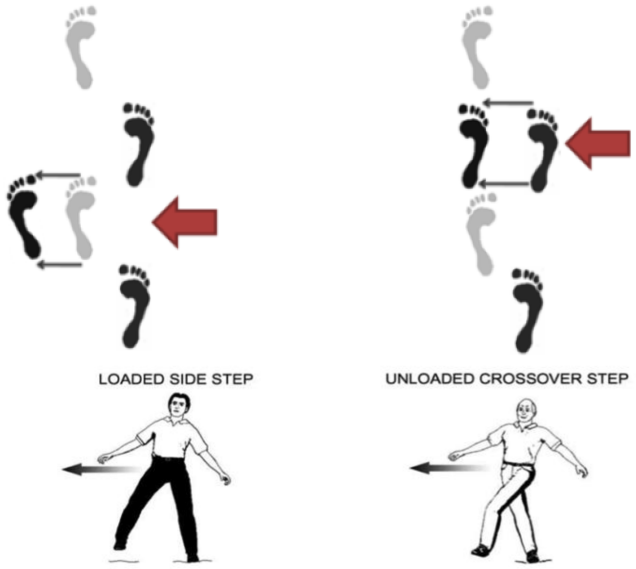

Figure 3.1: Types of compensatory balance responses (CBR) to lateral perturbation: left panel - right foot loaded at perturbation (arrow), eliciting a left foot side step (SS), right panel -left foot loaded at perturbation (arrow), eliciting right foot crossover (CO) step

In addition to IMU signals (e.g., 3D acceleration, angular velocity, and magnetometer signals), the sEMG signals were acquired synchronously from 4 muscles in right leg: 1) Rectus femoris, 2) Biceps femoris, 3) Tibialis anterior, and 4) Gastrocnemius (Table 3.1). These muscles were selected because they play an important role in maintaining balance and stabilization. The subjects' skin was prepared by shaving the area, gentle local abrasion using abrasive paste, cleaned with alcohol wipes, and dried prior to attachment of the surface electrodes, in accordance with the SENIAM (www.seniam.org) recommendations for skin preparation [170]. The sensors and wires were affixed to the skin using hypoallergenic medical adhesive tape in order to minimize sliding.

In the current study, each participant walked over a 10 meter walking path at their preferred speed for 100 trials. In $\approx$ 66% of the trials (randomly), each participant was perturbed by lateral pushes to his/her right shoulder by a researcher walking alongside. Perturbation magnitude was calibrated to consistently elicit a compensatory balance response (CBR) by slowly increasing push magnitude over a series of 5-10 training trials.

Perturbation trials were labeled as CBR events in which subjects recovered their balance (and prevented a fall). Half of the perturbation trials ($\approx 33\%$ of total) were timed to be delivered during left leg swing to elicit a sidestep strategy or CBR type 1 (see Fig. 3.1, left panel). The remaining perturbation trials were delivered during right swing eliciting a crossover strategy or CBR type 2 (see Fig. 3.1, right panel).

Three acceleration and sEMG signals captured from one subject, for 10 successive trials are depicted in Fig. 3.3.1 and Fig. 3.7 respectively. All data were processed using Matlab (R2011b, MathWorks Inc, USA). All IMU and sEMG signals were recorded synchronously with a sampling rate of 512 Hz and were streamed wirelessly via Bluetooth to an Android mobile device (Nexus 7, Google Inc.).

The study has received ethics clearance and was reviewed and approved by the Office of Research Ethics (ORE), University of Waterloo.

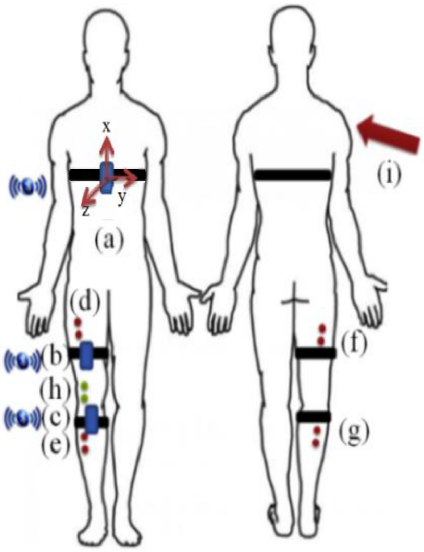

Figure 3.2: (a), (b), and (c) indicate SHIMMER sensors on sternum, thigh, and shank. sEMG electrode placement for d) rectus femoris, e) tibialis anterior, f) biceps femoris, and g) gastrocnemius. Electrodes on the h) patella were selected as the reference. Arrow indicates location of perturbation.

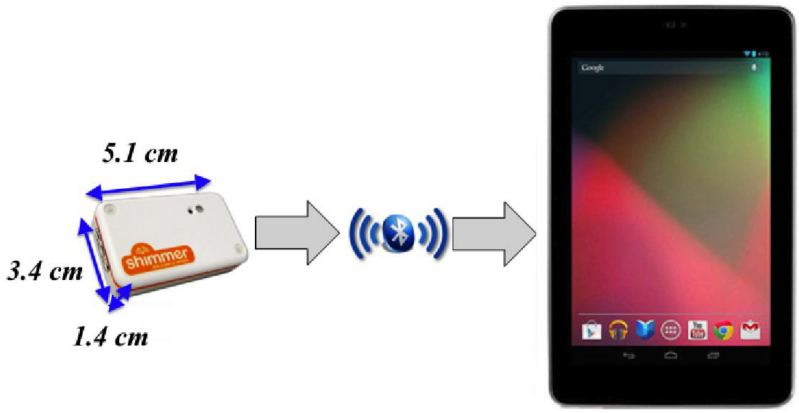

Figure 3.3: All signals are recorded simultaneously and streamed to a Google Nexus 7 tablet via Bluetooth

3.3 Detection of compensatory balance reactions using inertial measurement units

3.3.1 Data segmentation

Segmentation refers to identifying a reference time to form a window, or segment, which features are calculated. Eighteen kinematic signals, including 9 acceleration and 9 angular velocity signals were collected (3 sensors $\times$ 3 axes). We first segment all 18 signals acquired in each trial corresponding to the most likely time window for a CBR event. Upon visual inspection of all recorded IMU signals, the maximum of signal vector magnitude recorded by the sternum IMU ($A_{T-sternum}$), was the best representative of the onset of the perturbation and elicited compensatory reaction. The signal vector magnitude was calculated by 3.1 where Ax, Ay, and Az are the accelerations along the x, y, and z axes, respectively (y is approximately lateral, x is approximately vertical, and z is approximately anteroposterior).

$$A_{T-Sternum} = \sqrt{A_x^2 + A_y^2 + A_z^2} \tag{3.1}$$

In each trial, the time index corresponding to the maximum A_T value was identified. For all acceleration signals (9 signals), we used 256 samples before and after of this point, corresponding to time window of 513 samples (256+A_T+256), and ignored the rest of the data. A similar strategy for data segmentation was adopted in [167] for detection of fall incidents. For the angular velocity signals (9 signals from 3 gyroscopes in x, y and z directions), the time windows were selected empirically by identifying the sample time index corresponding to the maximum value of the angular velocity in x direction captured from the sternum IMU. Similar to the acceleration signals, 256 samples before and after of this point were used to calculate the features and the rest of the data in the trial were not used. The time domain features (in total 138) for each of these time segments were extracted as described below (section 3.3.2).

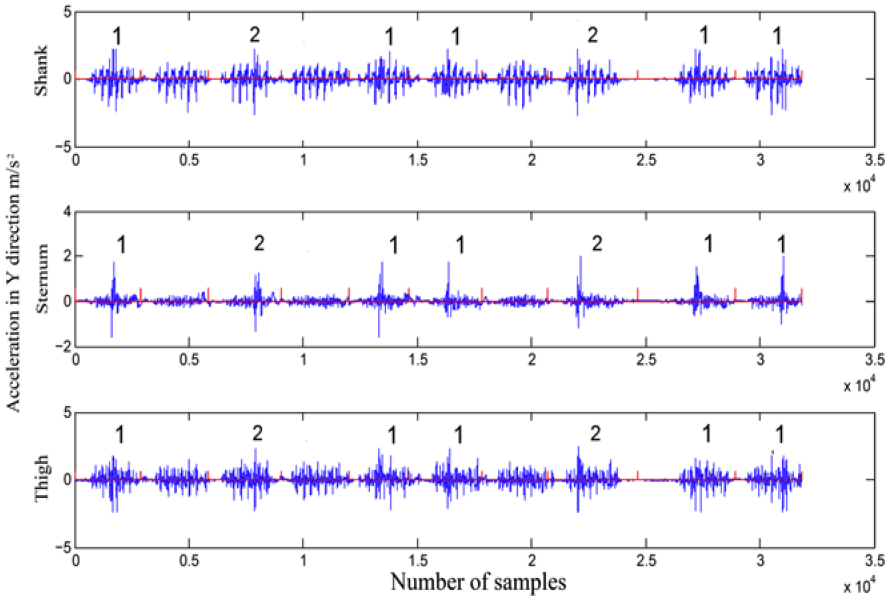

Figure 3.4: Sample acceleration signals in the y direction for 10 successive trials from shank, sternum and thigh IMUs. Numbers 1 and 2 indicate elicited sidestep and crossover stepping strategies, respectively.

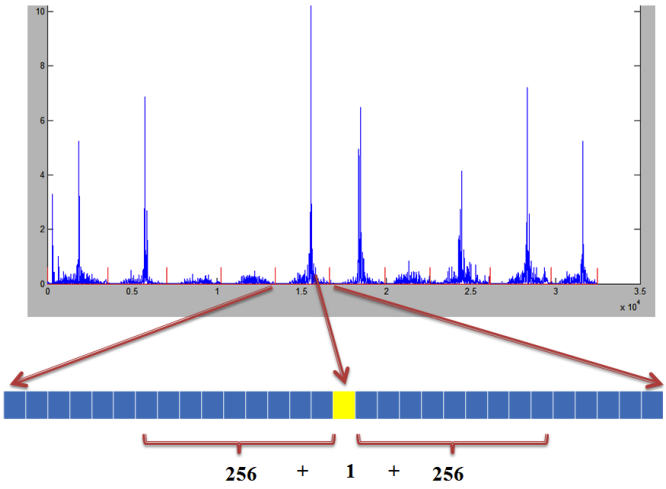

Figure 3.5: Signal segmentation using maximum SVA

3.3.2 Feature extraction

Extraction of discriminative features from acquired IMU signals is an important step in our machine learning based method for recognition of CBR patterns, and is of utmost importance in generating an appropriate training data set. A list of the extracted IMU-based features, e.g., acceleration and angular velocity features, is provided as below.

Acceleration features

The following features of acceleration signals were extracted for each time window of 9 (3 sensors $\times$3 axes) captured signals: 1) root mean square (RMS) value of the acceleration signal which shows the acceleration intensity, 2) absolute value of the signal mean, an indicator of the orientation of body segment, 3) variance of the acceleration signal, which depicts the signals variation, 4) range of the acceleration signal, calculated as the maximum peak-to-peak signal value (large values of range indicate high activity with significant movement of a body segment), 5) the skewness and 6) kurtosis features to determine the shape and dynamics of the acceleration signal, 7) the maximum absolute value of the acceleration signal, 8) mean of the acceleration derivative, 9) variance of the acceleration

derivative, 10) total acceleration (A_T) of shank, thigh and sternum sensors over full period of time for each trial. Appendix 2 (6) shows the full list of the acceleration features.

Angular velocity features

The following features for each of the nine angular velocity signals (i.e., 3 sensors × 3 axes) were extracted from each time window: 1) mean absolute value, 2) variance, 3) maximum of absolute value, 4) maximum of the absolute value of the signal derivative, 5) mean of the absolute value of the signal derivative, 6) variance of the signal derivative. Appendix 2 shows the full list of the angular velocity features (6).

Criteria for finding the best indicators of CBRs

Among the 138 extracted features, the best indicators of CBR incidents can be obtained by calculating the correlation of the features and labels from (2), where $X = \{x_1, x_2, , x_n\}$ is the normalized data matrix (all values are between -1 and 1) and n is the number of samples, X^j is a row vector which includes j^th feature of all samples so $j = \{1, , 138\}$, and Y is the vector of labels. This provides a convenient ranking of the features for CBRs detection to indicate the most relevant features.

$$\begin{aligned} A_j &= |X^j \times Y| \\ Sort(A = \{A_j\}_{j=1}^{138}) \end{aligned} \tag{3.2}$$

3.4 Detection of CBRs Using Surface electromyography signals

This section investigates the possibility of using wearable surface electromyography (sEMG) sensors, combined with machine learning algorithms to discriminate between 3 stepping patterns (i.e., SS, CO, and NS).

The objectives of this section were to examine the effects of: 1) filtering characteristics, 2) different segmentation methods, and 3) varying muscle combinations on the accuracy of CBR classification using sEMG signals and machine learning techniques (e.g. k-nearest neighbors, SVMs, and random forests). Results from an initial evaluation in young, healthy adults are reported and discussed. The findings from this study will contribute to the continued advancement of WSS capable of tracking the frequency and type of naturally-occurring CBR incidents in daily activities, with the long-term goal of developing new personalized fall risk assessment tools.

Table 3.1: The lower exterimity muscles that are studied in this thesis, and their function in maintaining balance

Muscle	**Function**
Biceps femoris	Flexion and lateral rotation of the knee joint.The long head also extends and assists in lateral rotation of the hip joint.
Gastrocnemius	Flexion of the ankle joint and assist in flexion of the knee joint.
Tibialis anterior	Dorsiflexion of the ankle joint and assistance in inversion of the foot.
Rectus femoris	Extension of the knee joint and flexion of the hip joint.

3.4.1 Preprocessing

Filtering and normalization

Filtering sEMG signals plays a key role in extraction of discriminative features, and consequently detection of CBRs. While a corner frequency of 20 Hz is recommended for preprocessing of sEMG signals to remove typical artifact sources [171], we considered alternate corner frequencies ($f_c >= 20$) to distinguish postural muscle activity associated

with CBRs. A 5th order digital Butterworth filter was employed to filter each sEMG signal, after full-wave rectification, and removing the expected value (mean) from the signal. Several highpass (20, 40, 50, 80 Hz) and lowpass (100 and 200 Hz) corner frequencies were examined to determine the optimal frequency range to extract the most discriminative features to detect CBRs.

After filtering 3.6, the sEMG signals were normalized to allow comparisons across subjects, and compensate for individual differences in strength, muscle tone, body fat, muscle geometry, etc. sEMG signals were normalized by dividing signal amplitudes by the root mean square (RMS) value of the filtered signal, recorded for each participant separately.

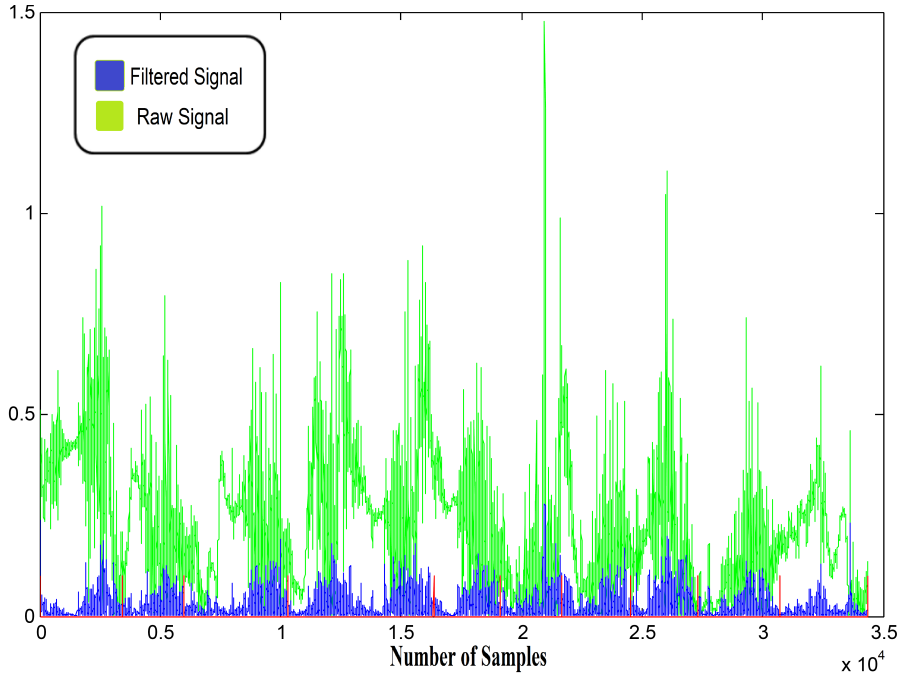

Figure 3.6: Captured thigh-sEMG signal before and after filtering

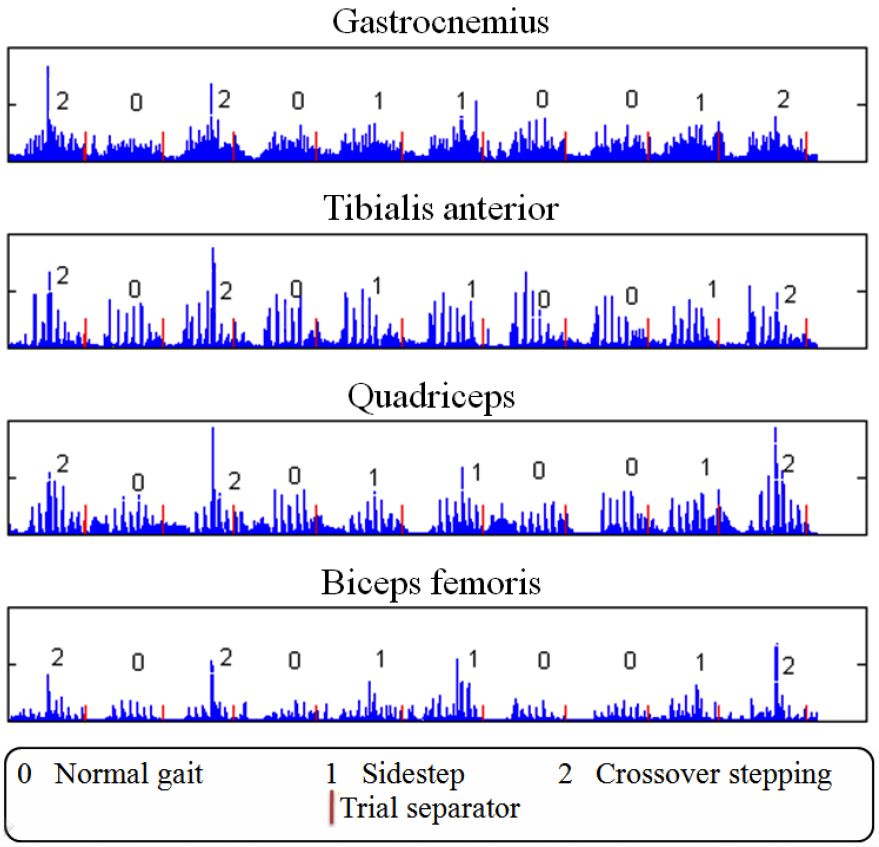

Figure 3.7: Representative sEMG signals (rectified, filtered at 50-200Hz) for 10 successive trials from four muscles. Numbers 0, 1, and 2 indicate normal walking (NW), elicited sidestep (SS) and crossover (CO) stepping trials, respectively.

3.4.2 Segmentation of signals

We investigated three approaches for segmentation of each trial by estimating the: 1) maximum peak sEMG, 2) maximum total acceleration of the sternum ($A_{T-Sternum}$) and 3) maximum total sEMG (EMG_T). The time indexes corresponding to each of these three points were identified as the segmentation point. To extract features, we used 256 samples before and after of these points, corresponding to a time window of 513 samples.

Maximum Peak sEMG

After signal preprocessing, the maximum amplitude of each sEMG signal (e.g. from biceps femoris) in each trial, i.e., normal gait or CBR, was identified.

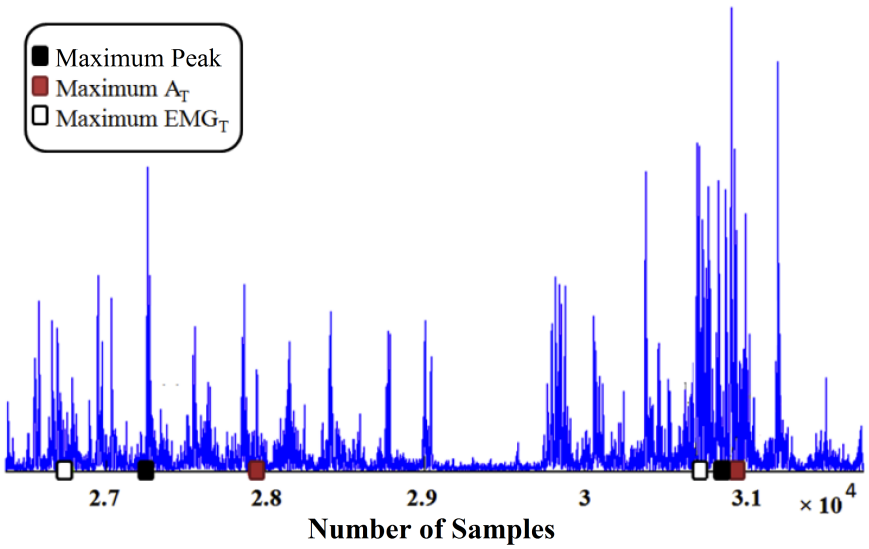

Figure 3.8: Two successive trials of biceps femoris sEMG data (rectified, filtered 50-200Hz). The data points corresponding to maximum A_T, maximum EMG_T, and maximum peak are depicted in each trial. 256 samples before and after of these points were used for feature extraction.

Maximum total acceleration of sternum

In this approach, the SHIMMER sensor positioned at the sternum was employed to capture acceleration data. In [45], it was shown that the maximum value of the total acceleration at the sternum $IMU_{A_{T-Sternum}}$, is a reliable measure for the onset of a perturbation and compensatory reaction which can be estimated as in 3.1, where A_x, A_y, and A_z are the accelerations along the x, y, and z axes, respectively. The maximum $A_{T-Sternum}$ point in each trial was used as the segmentation point.

Maximum total EMG

Similar to the second approach, we calculated the total EMG (EMG_T) as given in Eq. 3.3. EMG_{TA}, EMG_G, EMG_{RFM}, and EMG_{BF} denote the amplitudes of the normalized, filtered sEMG signals captured from tibialis anterior, gastrocnemius, rectus femoris, and biceps femoris, respectively. The maximum EMG_T in the trial was chosen as the segmentation point.

$$EMG_T = \sqrt{EMG_{TA}^2 + EMG_G^2 + EMG_{RFM}^2 + EMG_{BF}^2} \tag{3.3}$$

3.4.3 Feature extraction

For all 100 trials, features were extracted using the time window estimated by the proposed segmentation points. The following time domain features (except entropy) are described by Phinyomark et al. [169] for sEMG pattern recognition: 1) maximum peak, 2) root mean square (signal power), 3) square integral, 4) integrated sEMG, 5) waveform length, 6) mean absolute value (MAV), 7) modified mean absolute value, 8) variance, 9) zero crossing (ZC), 10) slope sign changes, 11) V-order, 12) log-Detector (logDetect) and 13) (Shannon) entropy. Slope sign changes and ZC features were obtained from filtered signal, prior to rectification. Entropy was calculated using the wentropy function in Matlab. Overall, we extracted 4×13 (number of muscles $\times$ number of features) to form a 52 dimensional feature space representing properties of muscle activities during regular or CBR stepping. The obtained features were normalized (mean=0) and divided by maximum absolute value (i.e., final features are $\in [-1, 1]$) before applying classification algorithms.

Table 3.2: sEMG-based features (N denotes the length of the signal and x_n represents the sEMG signal in a segment. [169])

Feature	**Description**
Integrated EMG (IEMG)	$\text{IEMG} = \sum_{n=1}^{N} \lvert x_n \rvert$
Mean Absolute Value(MAV)	$\text{MAV} = \frac{1}{N} \sum_{n=1}^{N} \lvert x_n \rvert$
Modified Mean Absolute Value 1 (MMAV1)	$\text{MMAV1} = \frac{1}{N} \sum_{n=1}^{N} W_n \lvert x_n \rvert$ $W_n = \begin{cases} 1 & \text{if} \quad 0.25N < n < 0.75N \\ 0.5 & \text{otherwise} \end{cases}$
Modified Mean Absolute Value 2 (MMAV2)	$\text{MMAV2} = \frac{1}{N} \sum_{n=1}^{N} W_n \lvert x_n \rvert$ $W_n = \begin{cases} 1, & \text{if} \quad 0.25N < n < 0.75N \\ \frac{4n}{N}, & \text{if} \quad n < 0.25N \\ \frac{4(n-N)}{N}, & \text{if} \quad 0.75N < n \end{cases}$
Simple Square Integral (SSI)	$\text{SSI} = \frac{1}{N} \sum_{n=1}^{N} \lvert x_n \rvert^2$
Variance	$\text{V} = \frac{1}{N-1} \sum_{n=1}^{N} x_n^2$
Root mean square (RMS)	$\text{RMS} = \sqrt{\frac{1}{N} \sum_{n=1}^{N} x_n^2}$
Waveform Length (WL)	$\text{WL} = \sum_{n=1}^{N} \lvert x_{n+1} - x_n \rvert$
Slope sign changes (SSC)	$\text{SSC} = \sum_{n=2}^{N-1} f((x_n - x_{n-1}) \times (x_n - x_{n+1}))$, $f(x) = \begin{cases} 1, & \text{if} \quad x > \text{threshold} \\ 0, & \text{otherwise} \end{cases}$

Continued on next page

Table 3.2 – continued from previous page

Feature	Description
Zero crossings (ZC)	if $x_k > 0 and x_{k+1} < 0$ or $x_k < 0 and x_{k+1} > 0$ and $\lvert x_k - x_{k+1}\rvert > \epsilon$
V-order	$\sqrt[v]{E(x_k)^v}$
Log-detector	$e^{\frac{1}{N}\sum_{k=1}^{N} log(\lvert x_k\rvert)}$

An alternative to the FFT based calculations is the simple counting of crossings through the zero line of the EMG signal. This Zero Crossing rate is highly correlated to the FFT based mean/median frequency and can be used as an alternative to FFT calculations which is more computationally complicated. Moreover, slope-sign-change parameter is related to the EMG signal frequency and is defined as the number of times that the sign of the EMG waveform slope changes within an analysis window. To avoid signal crossing counts and slope-sign-changes due to low-level noise, a threshold ϵ is included ($\epsilon = 0.015V$) in the related equations [169]. $V-order$ and $log-detect$ features provide estimate of the exerted muscle force.

The E is the expectation operator applied on the samples in one analysis window. The best value for v is equal to 2, which leads to the variance feature [169].

3.5 Machine learning techniques

The machine learning based design is described in three main phases: feature extraction (which is discussed in sections 3.3.2 and 3.4.3), feature reduction (e.g., PCA, SPCA, and KSPCA (section 3.5.1)), and classification (or supervised learning).

In this chapter we apply three important classification methods: 1) $k-$nearest neighbor, 2) Support vector machines (SVM), and 3) Random forest (RF). In chapter 4, we employ

other machine learning methods, e.g., convolutional neural networks and artificial neural networks (multi-layer perceptron), for vision-based detection of environmental hazards.

The training data points are as (x_i^p, y_i), where $x_i \in \mathbb{R}^p$ (p is the number of features/principal components selected after the feature reduction step), and the class labels are $y_i \in \{1,1\}$ for the binary classification problem (1 for all CBRs and -1 for the normal walking episodes). In order to distinguish between the episodes of CBR type 1 (sidestep) and 2 (crossover stepping), we also define a three-class classifier ($y_i \in \{0, 1, 2\}$).

3.5.1 Feature reduction methods (employed for IMU-based features)

Because the initial set of IMU-based features was quite large (138 IMU-based features compared to 52 sEMG-based features), and not all of the feadtures were equally useful in discriminating between CBRs and regular stepping, also to increase the generalizability of the classifier results towards a robust real-time predictor, we reduced the number of features through feature reduction algorithms (i.e. principal component analysis (PCA), supervised PCA (SPCA) and kernel SPCA (KSPCA) [168]).

In feature reduction applications, principal component analysis (PCA) is a widely used and well-known transformation that finds the linear combinations of the features to identify which components account for the largest possible data variance. Supervised principal component analysis (SPCA) and kernel supervised PCA (KSPCA) algorithms are extensions of PCA that are effective for regression and classification problems with high-dimensional input data. SPCA is a supervised version of PCA in which the bases of low dimensional space has maximum dependency to the label matrix. The dependency measure used in this study is Hilbert-Schmidt independence criterion (HSIC). KSPCA is another variation of PCA which not only uses the label matrix to build the bases of the lower dimension space, but can also capture some nonlinearity of the input data. Further information regarding the SPCA and KSPCA methods can be found in [168]. Obtained features were normalized (mean=0) before applying the feature selection algorithms. In this thesis radial basis

function (RBF) kernel was selected for the KSPCA method.

Assume we have a set of n data points $\{x_i\}_{i=1}^n$ each consisting of p features, stacked in the $p \times n$ matrix X. In addition, assume that Y is the $l \times n$ matrix of outcome measurements. We would like to find a transformation, denoted by the matrix U, which maps the data points into a d-dimensional subspace. Three different method are used in my work which are described as the following.

PCA

PCA is a transformation that finds the optimal linear combinations of the features, in the sense that they represent the data with the highest variance in a feature subspace, without taking the intra-class and inter-class variances into consideration separately. PCA is useful when there is data on a large number of variables, and (possibly) there is some redundancy in those variables. In this case, redundancy means that some of the variables are correlated with one another. And because of this redundancy, PCA can be used to reduce the observed variables redundancy. The objective function of PCA is:

$$\begin{gathered} \arg\max (U^T X)(U^T X)^T \\ \text{subject to } U^T U = I \end{gathered} \tag{3.4}$$

SPCA

We address the problem of finding the subspace $U^T X$ such that the dependency between the projected data $U^T X$ and the outcome Y is maximized. In order to measure the dependence between $U^T X$ and the output variable Y, we use the Hilbert-Schmidt Independence Criterion. We need to maximize $tr(HKHL)$ where K is a kernel of $U^T X$ (e.g. $X^T U U^T X$), L is a kernel of Y (e.g. $Y^T Y$), and $H = I - n^{-1} e e^T$ (I is the identity matrix and e is a vector with all entries equal to 1). This objective can be formulated as

$$tr(HKHL) = tr(HX^T U U^T X H L) = tr(U^T X H L H X^T U) \tag{3.5}$$

We are looking for an orthogonal transformation matrix U which maps data points to a space where the features are uncorrelated. Besides, without any constraint this objective function can be unbound. Thus, our optimization problem is constrained and becomes:

$$\text{argmax } tr(U^T XHLHX^T U) \text{ subject to } U^T U = I \tag{3.6}$$

It is obvious this optimization problem can be solved in closed-form. If the symmetric and real matrix $Q = XHLHX^T$ has eigenvalues $\lambda_1 \leq ... \leq \lambda_p$ and corresponding eigenvectors $v_1, ..., v_p$, then, the maximum value of the cost function satisfying the constraint is $\lambda_p + \lambda_{p-1} + ... + \lambda_{p-d+1}$ and the optimal solution is $U = \{v_p, v_{p-1}, ..., v_{p-d+1}\}$. Here, d denotes the dimension of the output space S. The Supervised PCA procedure is depicted in 1, where: Input is the training data matrix (X), the testing data example (x), the kernel matrix of the target variable (L), and the training data size (n). Output: Dimension reduced training and testing data, Z and z.

Algorithm 1 Supervised PCA

1: $H \leftarrow I - n^{-1} ee^T$
2: $Q \leftarrow XHLHX^T$
3: Compute basis $U \leftarrow$ eigenvector of Q corresponding to the top d eigenvalues.
4: Encode training data:$Z \leftarrow U^T X$
5: Encode test data: $z \leftarrow U^T x$

KPCA

In many cases, nonlinear transformations of the data are required to successfully apply learning algorithms. One efficient method for doing this is to use a kernel that computes the similarity between any two data points. In this section, we show how to perform Supervised Principal Component Analysis in the feature space implied by a kernel, which allows our method to be extended to nonlinear mappings of the data. Kernel Supervised PCA can be formulated directly, without use of the dual formulation. The key idea is to express the transformation matrix U as a linear combination of the projected data points,

$U = \phi(x)\beta$, via representation theory. Thus we can rewrite the objective function as:

$$\begin{aligned} tr(U^T\phi(X)HLHphi(X)^TU) &= tr(\beta^T\phi(X)^T\phi(X)HLH\phi(X)^T\phi(X)\beta) \\ &= tr(\beta^T KHLHK\beta) \\ \textit{with the constraint: } U^TU &= \beta^T\phi(X)^T\phi(X)\beta = \beta^T K\beta \end{aligned} \tag{3.7}$$

where K is a kernel function. We have now expressed the objective function and the constraint in terms of inner products between data points, which can be computed via the kernel. The new optimization problem has the following form:

$$\begin{aligned} &\arg\max tr(\beta^T KHLHK\beta) \\ &\textit{subject to: } \beta^T K\beta = I \end{aligned} \tag{3.8}$$

This is a generalized eigenvector problem. β can be computed as the top d generalized eigenvectors of $(KHLHK, K)$. The Kernel Supervised PCA procedure is summarized in algorithm 2 where Input: Kernel matrix of training data, K, kernel matrix of testing data, K_{test}, kernel matrix of target variable, L, testing data example, x, training data size, n. Output: Dimension reduced training and testing data, Z and z.

The experiments suggest that both variations of Kernel Supervised PCA produce very similar results in practice. However, the direct formulation has slightly less computational complexity, as there is no need to decompose the kernel matrix L and compute the matrix Δ. In this thesis, all experiments with Kernel Supervised PCA are reported using this algorithm.

Algorithm 2 Kernel Supervised PCA

1: $H \leftarrow I - n^{-1}ee^T$
2: $Q \leftarrow KHLHK$
3: Compute basis $\beta \leftarrow$ generalized eigenvectors of (Q, K) corresponding to the top d eigenvalues.
4: Encode training data:$Z \leftarrow \beta^T[\phi(X)^T\phi(X)] = \beta^T K$
5: Encode test example: $z \leftarrow \beta^T[\phi(X)^T\phi(X)] = \beta^T K_{test}$

3.5.2 Supervised learning methods

This work explored the application of three supervised learning methods, $k-$nearest neighbor ($k - NN$), support vector machines (SVMs), and random forest (RF) classification approaches.

$k-$nearest neighbor

The $k-$NN classifier is a representative of the 'lazy classifiers' group, which requires a large set of training examples to give satisfying results. The k-NN classifier chooses the k closest points to a sample using a predefined metric, specifically Euclidean distance in this work, and the output label is the mode of the labels for the k data points.

Support vector machines

The support vector machine (SVM) method constructs an optimal separating hyper-plane (or a set of hyper-planes) with the largest margin in a high dimensional space. The initial set of coefficients and kernel parameters considerably affect the classification outcome of SVMs. Kernel functions are a measure of similarity (generalization of dot products). In this study, a Radial Basis Function (RBF) kernel (or Gaussian) (Eq. 3.9) is employed to map the data to a higher dimension space and gain linear separation, and then construct a separating hyperplane with maximized margin around that. The width σ^2 is specified a priori.

$$K(x, x_j) = e^{\frac{-||xx_j||^2}{2\sigma^2}} \tag{3.9}$$

Random forest

Random forests are a powerful classification method, which uses an ensemble learning method by constructing a collection of randomly trained decision trees. RF_N denotes a random forest, containing N decision trees. An advantage of tree ensembles over standard

classifiers is reduction in dependence on linear features and higher generalization power. Additionally, tree ensembles are capable of processing large training sets well and very rapidly, which is appropriate for our final goal of to a real-time classification algorithm. The structure of Random Forest trees is shown in Fig. 3.9.

The training for Random Forest begins with identifying a random subset of the dataset, at sequential nodes the data is repeatedly divided into two subsets using a random threshold applied with a splitting function shown below [173] . In the training procedure, the random

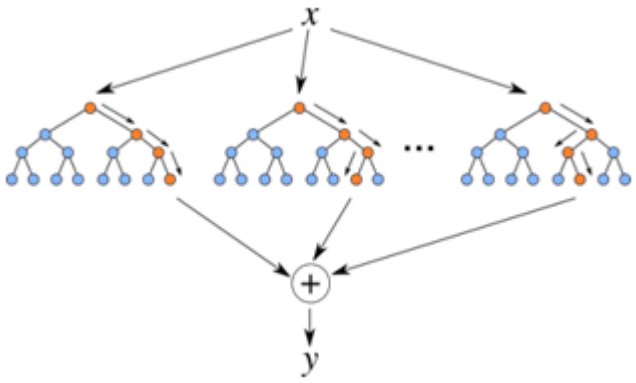

Figure 3.9: Algorithm of the random forest classification method

forest starts by choosing a random subset I' from the training data, I. At the node n, the training data I_n is iteratively split into left and right subsets I_l and I_r by using the threshold, t, and split function, $f(v_i)$, for the feature vector, v, using Eq. 3.10. The threshold, t, is randomly chosen by the split function, $f(v_i)$, in the range $t \in (minf(v_i), max(f(v_i))$.

$$\begin{aligned} l_t &= \{i \in I_n | f(v_i) < t\} \\ I_r &= \tfrac{I_n}{I_l} \end{aligned} \tag{3.10}$$

Then, several candidates are randomly created by the split function and threshold at the split node. Among those, the candidate that maximizes the information gain about the corresponding node is selected. The information gain (ΔE) is easily calculated by entropy

estimation, according to Eq. 3.11.

$$\Delta E = -E(I_l) - \frac{|I_r|}{|I_n|} - E(I_r) \tag{3.11}$$

Eq. 3.11 is used in chapter 4, where E(I) is the Shannon entropy of the classes in the set of training I [173].

3.6 Results

3.6.1 IMU-based results

The training data points are as (x_i^p, y_i), where $x_i \in \mathbb{R}^p$ (p is the number of principal components selected after the feature reduction step) and the class labels are $y_i \in \{1, 1\}$ for the binary classification (1 for all CBRs and -1 for the normal walking episodes). In order to distinguish between the episodes of CBR type 1 (sidestep) and 2 (crossover stepping), we developed a three-class classifier, using the one-vs-all technique. Following training, evaluation was performed using a leave-one-out cross-validation procedure.

Based on (Eq 3.2), the best two indicators (features) of CBRs were: 1) the peak value of the acceleration signal in y direction captured from the thigh sensor, 2) the peak value of the acceleration signal in z direction captured from the shank sensor. After excluding the maximum peak features, the three most robust indicators were: 1) mean value of the acceleration signal in y direction captured from the sternum sensor, 2) RMS value of the acceleration signal in y direction captured from the sternum sensor, and 3) skewness of the acceleration signal in z direction captured from the thigh sensor. After reducing the dimensionality of the data points with three different algorithms, i.e., PCA, SPCA, and KSPCA, we used $k-$NN and SVMs methods to distinguish between CBRs situations and normal walking episodes. Considering the $k-$NN algorithm is sensitive to the local data structure, there is no standard value for k. We conducted a search across k and found that k=7 produced the optimal classification accuracy for our purposes. Moreover, for SVM

classification, we used a radial basis function (RBF) kernel to map the data to a higher dimensional space and form a linearly separable data.

Generally, a large set of features (or principal components) for a two-class problem is highly likely to produce a linearly separable solution. However, the linear separator is also likely to give a poor generalization. In this study, the results of applying 2, 5 and 10 principal components (p) for detection of CBRs were high ($\approx 98\%$ for $p = 10$) in the binary classification problem. Overall, the highest accuracies for the problems with two and three classes were 98.07% and 92.02%, using KSPCA feature reduction method ($p = 10$) and SVM classifier, respectively. Table 3.3 and 3.4 show the results of each combination of the feature reduction and classification methods, for the two and three class approaches respectively.

Table 3.3: **Leave-one-out cross-validation results for the binary classification (CBRs) and normal walking trials) using PCA, SPCA and KSPCA dimension reduction methods, p refers to the number of principal components**

	PCA		SPCA		KPCA	
P	SVM	kNN (K =7)	SVM	kNN (K =7)	SVM	kNN (K =7)
2	92.53	92.36	94.88	94.70	95.45	94.30
5	94.32	93.83	95.80	95.22	96.98	96.62
10	95.07	95.66	96.88	96.09	98.07	97.61

Table 3.4: **Leave-one-out cross-validation results for multi-class classification Normal gait, CBR type 1, and CBR type 2), using PCA, SPCA, and KSPCA dimension reduction methods, P refers to the number of principal components**

	PCA		SPCA		KPCA	
P	SVM	kNN (K =7)	SVM	kNN (K =7)	SVM	kNN (K =7)
2	80.85	80.47	85.39	81.88	86.83	85.97
5	89.53	83.91	90.36	85.59	91.12	86.63
10	90.51	85.89	90.12	88.76	92.02	89.98

Conclusion and discussion

In this section, we successfully distinguished incidents of compensatory balance reactions from normal walking episodes by using wearable IMU sensors. We performed both binary (detection of all CBRs from normal walking) and three-class (distinguishing between CBR type 1 and 2) classifications. Based on our initial evaluation in 5 young adults, the highest classification accuracies for the two and multi-class problems were 98.07% and 92.02% respectively.

Each of these approaches would provide valuable information on the quality and quantity of the balance control behavior, i.e., the frequency and likelihood of the occurrence of CBRs (sidestep or crossover) in young or older adults. Obtaining the accuracy above the 98% in our first approach indicates the reliability and robustness of our method for detection of CBRs. In total, 138 features were extracted from 18 acceleration and angular velocity signals. Considering the large number of features imposes a computational burden on the process of CBRs detection, different feature reduction techniques were investigated to choose appropriate feature set. Our evaluation of several methods demonstrated, that KSPCA outperformed the PCA and SPCA, likely due to the innate ability of KSPCA method to capture nonlinearity in data. We focused on SVMs and $k-$NN machine learning techniques and compared the classifiers' performance based on the cross-validation methods (leave-one-out).

As described earlier, the sensors were placed on the right shank and right thigh of the subjects. In the CBR type 1 (Sidestep), since the lateral perturbation was applied during the stance phase of the right foot, the CBRs were performed predominantly using of the left foot (Fig.3.1). Hence, the movement signals recorded on the right leg were significantly smaller than CBR type 2 (crossover) and increased the likelihood of misclassification. Conversely, clearer changes were observed in signals during the crossover stepping strategy performed predominantly with the right leg leading to better detection of CBR Type 2 (Fig. 3.1, right panel). Based on our evaluations, the signal patterns of CBRs type 1 is very similar to the signal patterns of normal walking. These are the reasons behind the lower accuracy of the three-class classifier (the highest is 92.02%) in comparison to the binary

classifier (the highest is 98.07%). While the successful CBR detection results of the current study are promising, methods through the next phases of our project accommodate the long-term goal of our studies towards developing a personalized fall risk assessment tool in non-clinical settings. As a case in point, we may explore alternative strategies for selecting an appropriate time window for segmentation, the placement and number of sensors, and examine the potential for EMG-based features.

3.6.2 sEMG-based results

While the results were promising, there were difficulties in distinguishing SS responses from NW, largely attributable to the lack of motion in the instrumented leg providing postural support only. A potential approach to enhance detection is to employ surface electromyography (sEMG) signals to capture muscle activity associated with postural muscle responses. In this section, we examine alternative segmentation, filtering, sensor sites, and machine learning techniques. The key measure is average accuracy after employing 100 times classification with 10-fold cross validation (10% of data points for testing and 90% for training), for each combination of segmentation approach, frequency range, and classification methods. To evaluate relative contributions of the muscles, the combination of muscle inputs to the classification were varied systematically. Table 3.5 shows the accuracy results for binary classification distinguishing both types of CBRs ($n_{CBR} = 334$) from normal walking trials ($n_{NW} = 166$), tabulated by segmentation method, frequency range, and classification method. The most accurate method achieved 92.35% using RF_{20} method, $A_{T-Sternum}$ for segmentation, and in 50-200 Hz range. In binary classification, RF_{20} and k-NN showed similar performance to each other (RF_{20}) provided a slightly higher performance), and both outperformed SVM. Considering the relatively lower accuracy using the SVM method, this technique was not included in the 3-class analysis.

Table 3.6 indicates the accuracy results for three-class classification defining sidestep (SS, $n_{side-step} = 117$ trials), crossover (CO, $n_{crossover} = 117$ trials), normal walking (NW, $n_{NW} = 166$) trials by segmentation method, frequency range, and classification technique. For three-class classification, the maximum mean accuracy of 84.60% was observed using

RF_{30} and the same conditions ($A_{T-Sternum}$, 50-200 Hz) for the greatest accuracy for binary classification.

In Table 3.7, the impact of varying combination of muscle(s) on detecting CBRs are shown. We applied the same procedure ($A_{T-Sternum}$, 50-200 Hz) to examine the use of sEMG signal recorded from single muscles, two muscles in right shank (gastrocnemius (G) and tibialis anterior (TA)), or in right thigh (rectus femoris muscle (RFM) and biceps femoris (BF)). The SVM approach to detect CBRs was superior when using data from one (87.52% using RFM data) and two (89.80% using RFM+BF) muscles for binary class classification. For the 3-class problem, the thigh muscle signals (RFM+BF) produced the greatest accuracy (79.13%) using the RF_{30} classification technique.

Table 3.5: **Accuracy of binary classification using $A_{T-Sternum}$, Maximum peak sEMG signal, and maximum EMG_T**

	Maximum $A_{Tsternum}$			Maximum peak sEMG			Maximum EMG_T		
Frequency range	KNN11	SVM	RF20	KNN11	SVM	RF20	KNN11	SVM	RF20
20-100	86.83	75.88	89.00	85.02	74.50	86.95	82.77	70.75	82.55
20-200	88.12	82.27	89.82	87.70	71.23	88.80	83.80	75.55	84.33
40-100	89.10	68.40	91.13	86.85	69.23	88.70	82.77	69.35	82.63
40-200	89.82	84.22	91.45	87.98	71.50	90.15	84.85	74.55	85.53
50-200	90.83	85.68	92.35	89.08	77.58	90.25	84.65	69.17	85.73
80-200	89.85	77.85	91.55	88.05	69.00	89.82	83.23	67.85	83.98

Table 3.6: **Accuracies of three-class classification by segmentation method and frequency range**

	Maximum $A_{Tsternum}$		Maximum peak sEMG		Maximum EMG_T	
Frequency range	KNN11	RF20	KNN11	RF20	KNN11	RF20
20-100	76.52	78.45	72.55	75.25	70.88	72.64
20-200	78.73	80.73	76.05	79.33	72.43	74.43
40-100	78.25	82.57	76.55	80.00	72.05	72.48
40-200	80.65	83.47	76.57	80.30	75.15	75.62
50-200	81.33	84.60	78.05	81.43	75.02	76.88
80-200	79.83	82.82	77.25	81.15	75.12	76.42

Table 3.7: **Accuracy by classification method and muscle group**

	Binary Classification			Three-class classification	
Frequency range	KNN11	SVM	RF_{20}	KNN11	RF_{30}
G	78.08	78.33	78.85	31.33	53.37
TA	75.62	72.45	75.35	30.00	64.40
RFM	83.73	87.52	86.28	53.23	72.32
BF	85.65	87.35	86.36	46.05	69.83
G+TA	74.78	76.40	80.15	30.40	65.7
RFM+BF	87.45	89.80	89.00	63.35	79.13

Conclusion and discussion

In this section, a method to distinguish CBR events from normal walking episodes using wearable sEMG sensors from 4 muscles in the right leg, (i.e., rectus femoris, biceps femoris, tibialis anterior, and gastrocnemius) was developed and evaluated. In general, testing demonstrated very good accuracy (92.35%) in distinguishing CBRs from normal walking patterns (i.e., binary classification) and good accuracy (84.60%) in distinguishing multiple classes of stepping patterns.

In comparison, the results from the current sEMG-based method are lower than IMU-based method evaluated previously. For binary and 3-class classification, respectively, the optimal IMU-based method (98.07% and 92.02%) outperformed the best sEMG-based method (92.35% and 84.60%). Considering the dataset and classification methods were similar for both studies, we reject the hypothesis that sEMG features are superior to IMU signals for detection of CBRs associated with lateral perturbations.The impact of three segmentation methods and filter cut-off frequencies were examined. Based on our experimental results, total acceleration of the sternum ($A_{T-Sternum}$) marginally demonstrated the best performance for segmentation, with a mean accuracy of 92.35% for the binary classification, compared to peak EMG (90.25%) and EMG_T (85.73%). Considering mean accuracy of the methods $A_{T-Sternum}$ and peak EMG are similar, using an additional sternum sensor for segmentation may be unnecessary. The 50-200 Hz band consistently provided the highest classification accuracies. These results suggest that content between

the recommended 20 Hz corner frequency and 50 Hz does not contain strong discriminative information for the detection of lateral CBRs. It should be noted the 200 Hz is relatively close to the Nyquist rate of 256 Hz, which may bias the informational content and limits the interpretation of these results.

In the assessment of relative contribution of the muscles, the features extracted from the sEMG signals of right thigh muscles (i.e., rectus femoris, biceps femoris) were more discriminative compared to the features obtained from shank muscles (i.e., tibialis anterior, gastrocnemius) in detecting lateral CBRs. The experimental results illustrate that it is possible to detect lateral CBRs using only one SHIMMER sensor, mounted on the thigh, with an accuracy of 79.13% for detection of both CO and SS strategies during normal walking (3-class classification) and accuracy of 89.80% for the detection of CBRs during normal walking (two-class classification). In general, the random forest (RF) method outperformed both SVM and k-NN classifiers in binary classification, and outperformed k-NN in 3-class classification.

This study contributes towards development of wearable sensor systems to accurately monitor gait balance control behavior by detecting CBRs in an ambulatory fashion. While the results indicate the proposed sEMG-based method is not as accurate as previously reported IMU-based approaches, the potential for a combined approach at a single site (i.e., thigh) appears promising. Future work will focus on extending to multidirectional (i.e., lateral and sagittal plane) perturbations and towards capturing a wider range of CBRs.

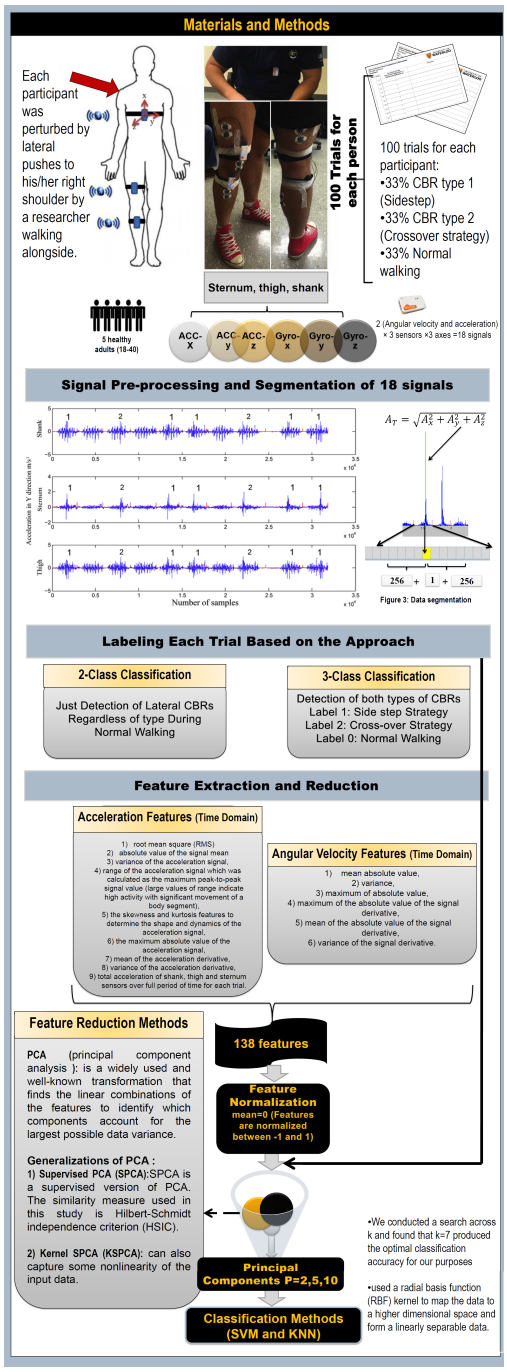

Figure 3.10: Diagram of the proposed method for detection of lateral CBRs.

Chapter 4

Wearable Vision Detection of Environmental Fall Risks using Machine Learning Techniques

4.1 Introduction

One of the biggest challenges for development of a fall prediction and prevention method is a lack of techniques to extract contextual information needed to interpret ambulatory gait and postural behaviour. For example, a specific pattern in IMU signals or sEMG signals can be interpreted as gait instability or a compensatory balance reaction, or may reflect anticipatory adjustments to avoid collisions on a crowded sidewalk. Without detailed information of the mobility context, such as the presence of other pedestrians, terrain characteristics, and obstacles, the ability to interpret ambulatory gait data is constrained.

This chapter examines the potential for wearable egocentric cameras, combined with image processing techniques (e.g. Gabor Barcodes) and machine learning techniques (e.g., convolutional neural networks, random forest), to automatically detect fall risk hazards. Other techniques using egocentric cameras rely on manual identification of environmental

circumstances, which are inefficient and impractical for real-time use [141, 142, 143]. To the best of the authors' knowledge, this study is the first to develop and evaluate an automated method for fall hazard detection.

In this chapter, a mobile vision camera (GoPro Hero 4 Session) is employed to complement the CBR detection methods (discussed in chapter 3), by automated detection of associated risk factors. The details of a computer vision method that can handle a diverse set of obstacles/objects (e.g., stairs) and subtle features (e.g., ground textures) are provided. In sections 4.4.1 and 4.4.2 the process of automated terrain feature detection based on the extraction of Gabor Barcodes and Covolutional neural networks (CNN) are discussed respectively.

4.2 Studies on detection of environmental risk factors (Terrain and obstacles)

4.2.1 Trrain and environmental hazard detection

Automatic terrain type detection is a challenging problem that has attracted attention of researchers in different areas of research, especially robotics for precise velocity control, gait adaption of legged robots, and safe navigation. Moreover, terrain detection has applications in teleoperation during critical missions, such as urban search and rescue and bomb disposal [197, 198, 199, 200].

In [197] authors employed a monocular camera and used bag-of-words (BoW) features for detection of eight types of terrains (i.e. grass, asphalt, gravel, mud, pavement, sand, floor, and fine gravel). They used image processing based methods for feature extraction, i.e., SIFT (Scale-invariant feature transform) and SURF (speed up robust features) and applied support vector machines (SVMs) for classification. They observed up to 90% accuracy; however, their method requires huge computational power, making their algorithm inefficient for real-time detection of terrains (e.g. their classifier requires 5 seconds with SIFT features).

In another study [200], Lu et al. presented an algorithm to detect and localize curbs and stairs for the task of obstacle avoidance and navigation of autonomous robots, using an stereo camera. They combined information from range data and images, using image processing-based techniques, e.g., edge points extraction, Hough transform, which are computationally complicate. Moreover, their results indicate that using stereo range data solely would not produce acceptable detection results in general.

In [201] a framework to detect and recognize stairs, pedestrian crosswalks, and traffic signals based on RGB-D (Red, Green, Blue, and Depth) images, were developed. Since both stairs and pedestrian crosswalks are featured by a group of parallel lines, the authors applied Hough transform to extract the parallel lines based on the RGB channels. Then, the Depth channel was employed to recognize pedestrian crosswalks and stairs. The detected stairs are further identified as stairs going up (upstairs) and stairs going down (downstairs). However, their method is computationally complicated and is developed based on a limited and controlled set of images, which may affect the generalizability of their system.

One of the biggest challenges associated with our study and similar works is the presence of unwanted/dynamic objects in real images or videos. Such objects considerably affect the accuracy of the classifier, and also increase the need for development of a classifier with a high generalizability power. However, none of the mentioned papers has focused on this challenge and mostly used completely controlled images. Moreover, computational complexity of an algorithm for terrain or environmental hazard detection plays an important role in efficiency of a real-time detection system. These papers mostly employed image processing based methods, e.g. Hough transform, SIFT and SURF for feature extraction, which require high computational time.

4.3 Data acquisition and pre-processing

The equipment that has been used in this study is the GoPro Hero 4 session camera, which is the smallest, lightest GoPro yet. The camera can record high resolution 1080p60 videos, 12MP photos up to 30 frames per second and is waterproof to 40m. The HERO4 Session

(Figure 4.3) features built-in Wi-Fi and Bluetooth, allowing us to connect to the GoPro App for mobile and Smart Remote. The GoPro App allows a phone or tablet to be used to view live video remotely.

Figure 4.1: The GoPro Hero Session Camera and its chest harness. The camera is facing down to capture terrain features.

Healthy young participants were asked to walk around the University of Waterloo campus. The initial videos (three videos) were recorded in different times, and overall, 22001 (6742, 10430, and 4829 frames) video frames were collected, using a GoPro Hero4 camera attached on participants' chest, while the camera was facing downward 4.3. The frames were manually annotated with the following labels: 1: crosswalk, 2: curbs, 3: ramp, 4:stairs (ascending), 5: stairs (descending), 6: gravel, 7:grass, 8: concrete, 9: tiles, 10: bricks, 11: carpets, 12: dirt, 13: water, 14: snow, 15: slush, 16: ice, 17: rocks.

Afterward, each frame was: 1) converted to a grayscale image, 2) resized into 128 $\times$ 128 images (Fig. 4.3-the 2nd image), and 3) cropped by a 64 $\times$ 64 rectangular window (Algorithm 3) (Fig. 4.3-the 3rd image). Cropping frames is useful to remove participants' feet and other unnecessary objects (far from the participants), appearing in the camera's field of view. The feet are captured in the frames since the camera is inclined to the ground (Fig. 4.3). The parameters in the Algorithm 3 were achieved empirically upon visual inspection of different numbers' effect on classification results. The number of data points in each class is provided in Tables 4.3 and 4.3. Number of data points in the class "concrete (pavement)" and brick were reduced (from $\approx$ 7200) to alleviate the effect of

Algorithm 3 The steps for resizing and cropping the frames)

1: Initialize $a = b \leftarrow 128$
2: $I_{gray} \leftarrow I_{rgb}$
3: $I = \text{Normalize}(I_{gray}, a, b)$
4: Initialize $x_{min} \leftarrow 32, y_{min} \leftarrow 0, W_x = W_y \leftarrow 64$
5: $I = \text{Crop}(I, [x_{min}, y_{min}, W_x, W_y])$

imbalanced data on the classification performance. For the first approach (CNN), we used the video with 10430 frames, and for the second approach (Gabor barcodes), we first used a subset of data with a fewer number of classes (video1 with 12 classes of environmental characteristics, Table 4.1) for feature extraction and training, and then concatenated all of the frames together in one single matrix with 12382 data points and reduce the number of samples in some classes, e.g., "concrete" (we randomly removed some data points from classes with high number of samples to achieve more reasonable/balanced distribution of data points).

Table 4.1: **number of frames extracted for each 12 classes (video$_1$)**

Crosswalk	Curb	Ramp	Stairs(asc)	Stairs(dec)	Gravel	Concrete	Tile	Brick
103	78	436	81	208	253	499	96	991
Carpet	Water	Rock						
736	25	63						

Table 4.2: **Total number of data points in 17 classes after concatenating all of the captured videos**

Crosswalk	Curb	Ramp	Stairs1	Stairs2	Gravel	Grass	Concrete	Tile
103	78	436	254	208	253	910	10118(initial)	952
Brick	Carpet		Dirt	Water	Snow	Slush	Ice	Rock
4782	2369		189	142	746	315	83	63

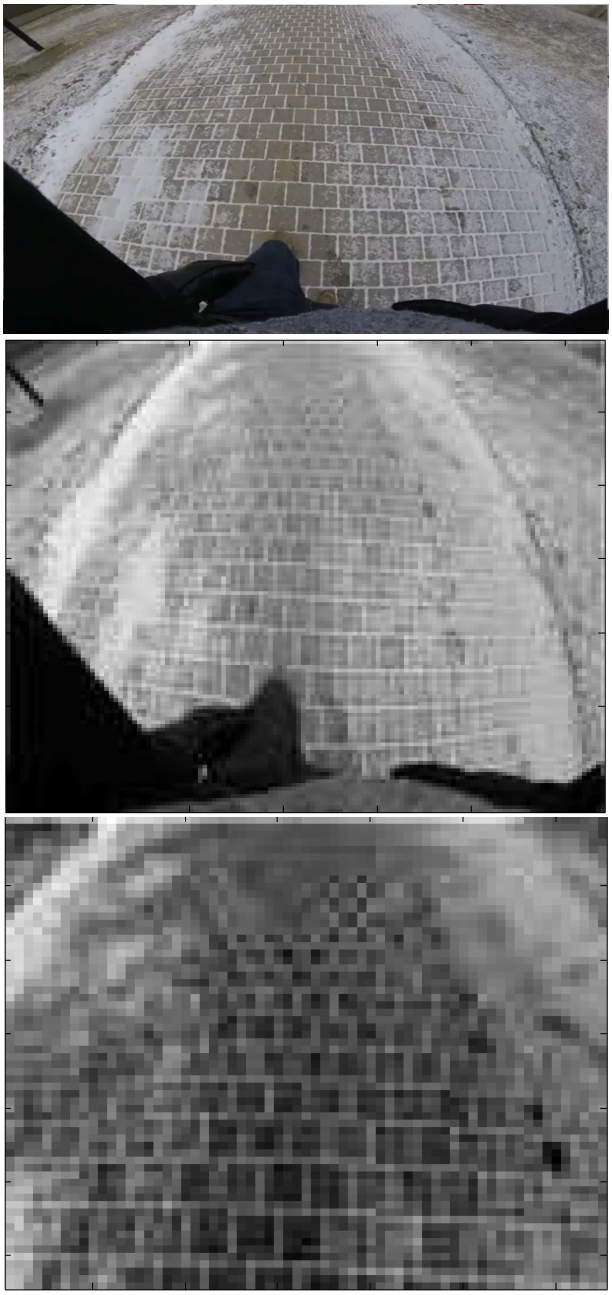

Figure 4.2: The captured frames by a GoPro Hero Silver camera and their associated Gabor Barcode, when the participant was perturbed on a crosswalk.

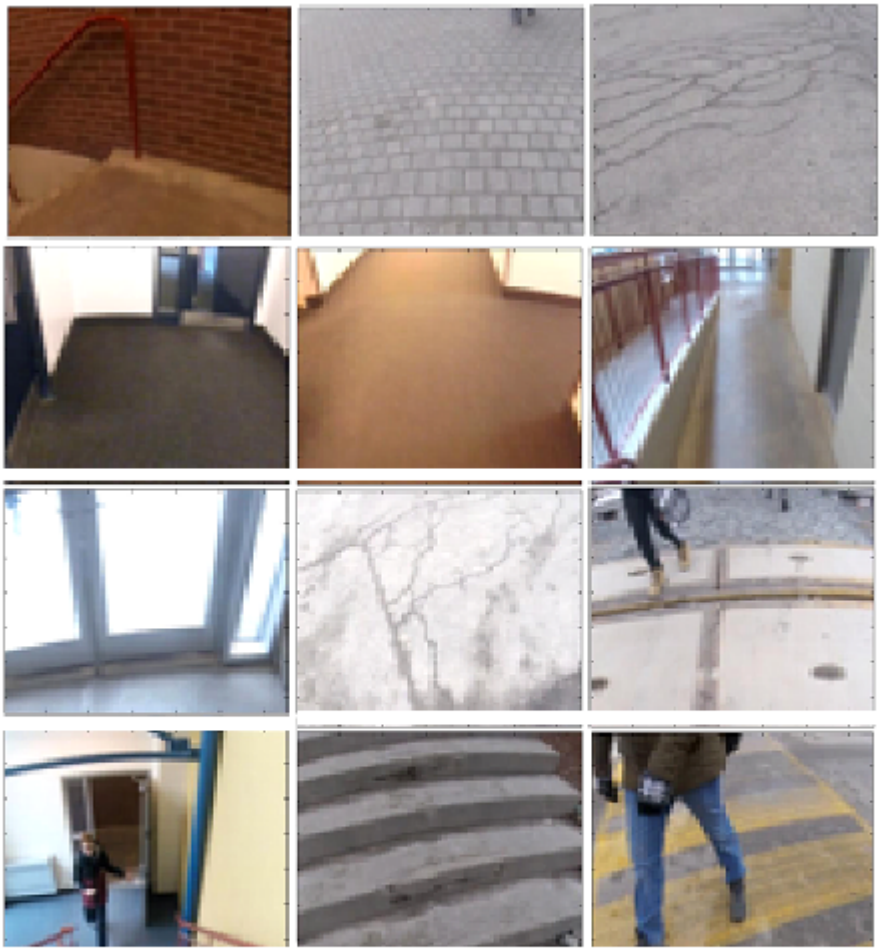

Figure 4.3: Sample resized and cropped frames that were captured by a GoPro Session camera during walking around the University of Waterloo campus. While the gray images were used for feature extraction, for a better visualization the color (RGB) frames are shown.

4.4 Machine learning techniques for detection of environmental risk factors

4.4.1 Gabor Barcodes for detection of fall-related hazards

Due to the specific characteristics of our images, specifically for the brick, tiles, rocks, and carpet classes, texture seems to be an appropriate feature for describing the contents of them [173]. Texture analysis has been an active research and numerous algorithms has been proposed based on different models, e.g., grey-level co-occurrence (GLC) matrices and Markov random field (MRF) model [173, 174]. In recent works, wavelets have become very popular due to their capacity to provide multi-resolution analysis of the images. Among different kinds of wavelet transform, the Gabor transform has some interesting mathematical and biological properties (resembling the characteristics of human visual cortical cells) and has been widely used to extract texture features from images for either segmentation tasks [177, 178], object detection and biometric identification [183, 184], and image retrieval [179, 180, 181, 182]. In [175], the authors have compared the effectiveness of various texture analysis and classification methods such as dyadic wavelet, wavelet frame, Gabor wavelet, and steerable pyramids, and have observed that the Gabor-based methods outperform the others on textured images. Moreover, the performance of Gabor wavelet features for texture analysis is investigated, and compared with other features, i.e., tree-structured wavelet transform, showing that Gabor features provide the best pattern retrieval accuracy compared to other multiresolution texture features on the Brodatz texture database [176].

The most important property of Gabor features is their robustness against rotation, scale, and translation. Furthermore, they are robust against photometric disturbances, such as illumination changes and noise. These properties are mainly due to the fact that the parameters of Gabor filters enable us to establish invariance in this regard [185].

In recent years, some studies have attempted to develop fast feature extraction methods from images or develop query search systems, using binary features, e.g., binary hashing. The important strengths of the binary features (compared to the other commonly used

techniques e.g. SIFT) are their efficiency in terms of detection speed (due to the possibility of using Hamming distance (Eq.4.3)) and lower requirements toward storage space.

Recently, the concept of barcode annotation has been proposed. Tizhoosh introduced the notion of using Radon transform to generate a content-based barcode [172]. Inspired by Radon Barcodes, we further develop the idea of barcodes from a different point of view and generate texture-based barcodes for the task of content-based medical image retrieval. We have recently introduced the notion of Gabor Barcodes (GBCs) in [188] and tested the GBC performance for content based medical x-ray image classification and retrieval using IRMA (The Image Retrieval in Medical Application) database [1] with 193 classes [2]. A total error score as low as $\approx 80\%$ accuracy for the first hit) was achieved.

Considering the effectiveness of GBCs in texture identification, in the present chapter, we aim to employ this method on real-life images, captured by an egocentric camera (Fig. 4.3) and aim to investigate the capability of Gabor Barcodes (binary features) in detection of fall-related environmental risk factors that may affect seniors' balance control behavior during ADLs. In the next sections, more details will be provided on our strategy for generation of memory-efficient, and discriminative texture-based Gabor-Barcodes.

Generating Gabor Barcodes

In the spatial domain, a two-dimensional Gabor filter is a Gaussian function, modulated by a exponential or complex sinusoidal plane wave, defined as:

$$G(x,y) = \frac{f^2}{\pi\gamma\eta} \exp\left(-\frac{x'^2 + \gamma y'^2}{2\sigma^2}\right) \exp\left(j2\pi f x' + \phi\right) \tag{4.1}$$

where $x' = x\cos\theta + y\sin\theta$, $y' = -x\sin\theta + y\cos\theta$, f is the frequency of the sinusoid (modulation frequency), θ represents the orientation of the normal to the parallel stripes of a Gabor function, ϕ is the phase offset, σ is the standard deviation of the Gaussian

[1] The images were randomly collected from daily routine work at the Department of Diagnostic Radiology of the RWTH Aachen University, from different ages, genders, view positions, and pathologies

[2] Comprising of 12,677 x-ray images for training, and 1,733 x-rays images for testing

envelope, and γ is the spatial aspect ratio which specifies the ellipticity of the support of the Gabor function [184]. Given an image $I(x, y)$, the response of Gabor filter is the convolution of Gabor window with image I given by

$$\psi_{u,v}(x, y) = \sum_{s} \sum_{t} I(x - s, y - t) * G_{u,v}(s, t) \tag{4.2}$$

where s and t are the window/mask size of the Gabor filter, u is the number of scales and v is the number of orientations that are used in the Gabor filter bank (GFB(u, v, s, t)). The $\psi_{u,v}(x, y)$ forms complex valued function including real and imaginary parts. In this study, in order to obtain Gabor features, the magnitudes of the $\psi_{u,v}$ values ($\psi_{ABS-u,v}$) are calculated. There have been several studies in the literature reporting the optimal values for the parameters of the Gabor filter bank (i.e., spatial frequencies and number of orientations) in such a way that it can mimic human visual system as much as possible [186].

Based on the algorithm that we proposed in [188], in order to obtain the Gabor feature vectors with the same-length, images should be resized into $R_N \times C_N$ images, i.e., $R_N = C_N = 2^n \in \mathbb{N}^+$ (in this study 32×32 images). To generate the Gabor Barcode (GBC$_m$) for the query image I_m, after obtaining the magnitude of each filtered responses ($\psi_{ABS-u,v}(x, y)$), for every u and v in the Gabor filter bank, the 2-D matrices of $\psi_{ABS-u,v}(x, y)$, are first downsampled with the coefficient factor of 4, and transformed to the row vectors of real-value Gabor feature (Gabor-ABS$_{u,v,m}$). For each (Gabor-ABS$_{u,v,m}$ vector, the median ($T_{u,v,m}$) is calculated and employed as a threshold to binarize the corresponding feature vector and obtain $B_{u,v,m}$ (same approach to binarize Radon barcodes in [172]). The final GBC$_m$ extracted for I_m is obtained by concatenating all $u \times v$ binary vectors (Fig. 4.4). Employing a GFB with N_g Gabor filters ($N_g = u \times v$), the dimension of the feature vector before downsampling is $M \times N \times N_g$ (e.g., for $N_g = 40$ and $M = N = 32$, the dimension of the feature vector is 40960). Since the adjacent pixels in an image are usually highly correlated, it is possible to reduce this redundancy by downsampling the feature images. The features were downsampled by a factor of $d1$ and $d2$ for the column and row, respectively, in which $d1 = d2 = 4$ (the downsampled feature vector will have

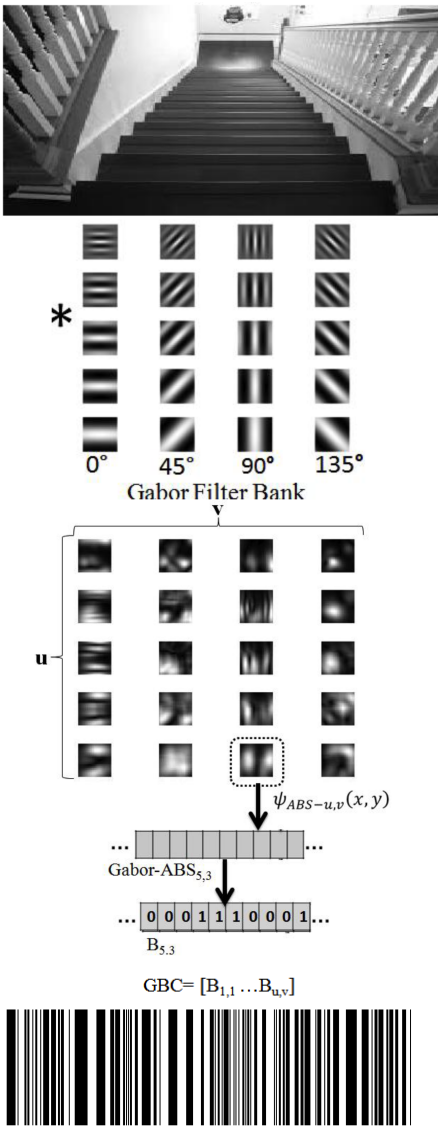

Figure 4.4: Generation Of Gabor Barcodes By Binarizing And Appending The Gabor Feature Vectors, Median Values Are Selected As The Binarization Threshold

a size of $\frac{40960}{4\times4} = 2560$ for forty Gabor filters). Generally, the Gabor feature vector of a $M \times N$ image is a column vector with length $(M \times N \times u \times v)/(d1 \times d2)$ [184]. The steps of the approach are described in Algorithm 4.

Algorithm 4 Generation of Gabor Barcodes (inspired by [172])

Initialize Gabor Barcode for image I_m: $\text{GBC}_m \leftarrow \emptyset$
Initialize $R_N = C_N \leftarrow 32$
$I = \text{Normalize}(I, R_N, C_N)$
Apply Gabor filters with u scales v orientations
for all u and v **do**
    Calculate the magnitude of $\psi_{u,v}(x, y)$:
    $\psi_{ABS-u,v}(x, y) = |\psi_{u,v}(x, y)|$
    Downsample each $\psi_{ABS-u,v}(x, y)$ with factor of 4
    Generate row feature vectors $\text{Gabor-ABS}_{u,v,m}$
    $\text{Typical}_{u,v,m} \leftarrow \text{median}(\text{Gabor-ABS}_{u,v,m})$
    $B_{u,v,m} \leftarrow \text{Gabor-ABS}_{u,v,m} \geq \text{Typical}_{u,v,m}$
    $\text{GBC}_m \leftarrow \text{append}(\text{GBC}_m, \text{B}_{u,v,m})$
end for

Developing a machine-learning model using GBCs

GBCs are similar to the features that we extracted from IMU and sEMG signals in chapter 3; as a result to complete the procedure for automatic identification of fall-related environmental hazards, we need to apply a machine learning technique, e.g. $k-$NN, RF, and artificial neural networks (that are previously discussed in section 3.5.

Moreover, since GBCs are binary features, it is easily possible to calculate the Hamming distance between the data points (similar to $k-$NN ($k = 1$) but the Euclidean distance is replaced with Hamming distance). For each of the test images complete search is performed to find the most similar image and the similarity of an input image I_i^{query} annotated with the corresponding barcode $\text{B}_i^{\text{query}}$ is calculated based on Hamming distance to any other image I_j with its annotated barcode B_j:

$$\max_{j=1,2,3,\ldots,N_{test};j\neq i} \left(1 - \frac{|\text{XOR}(\text{B}_i^{\text{query}}, \text{B}_j)|}{\text{B}_i^{\text{query}}}\right), \tag{4.3}$$

where 'B' can be GBC.

In section 4.5.1, the complete procedure for GBC-based training is provided.

4.4.2 Convolutional Neural Networks

One of the most promising approaches for automated detection and classification of objects is Convolutional Nural Networks (CNN), which roughly mimic the human visual system. The CNN method originally proposed by LeCun [195], which is a neural network model (biologically-inspired variants of ANN-MLPs) with three key architectural ideas (Fig. 4.5): local receptive fields, weight sharing, and sub-sampling (i.e. max pooling). The input to a convolutional layer is an image and the convolution operation extracts different features of the input. For example, the first convolution layer extracts low-level features like edges, lines, and corners and higher-level layers extract higher-level features.

Convolutional neural network has many strengths. First, feature extraction and classification are integrated into one structure (in traditional models for pattern recognition, feature extractors are hand designed). Moreover, it is relatively invariant to geometric, local distortions in the image, and have been shown to be invariant to pose, lighting, and surrounding clutter [196]. The improved network structures of CNNs lead to savings in memory requirements and computation complexity requirements and, at the same time, give better performance for applications where the input has local correlation (e.g., image and speech).

The successful application of CNN's to character recognition and facial recognition are covered in several studies[194]; however, character recognition and facial recognition are concerned with very controlled image input in to the system, compared to the data tat we collect to detect environmental fall hazards in this. As it is depicted in Fig. 4.3, real-life images have significantly more variety. Phung et al. [192] combined the concepts of image pyramids and local receptive fields, and proposed a new neural architecture -pyramidal neural network (PyraNet)- for classification of visual patterns (determining gender from a facial image). The hierarchical structure of PyraNet has two types of processing layers: 1) Nonlinear 2-D Pyramidal layers in which neurons are trained to perform both image feature extraction and dimensionality reductionand 2) one-dimensional (1-D) feedforward layers for classification 4.6.

A pyramidal layer consists of neurons arranged in a 2-D array; each neuron is connected

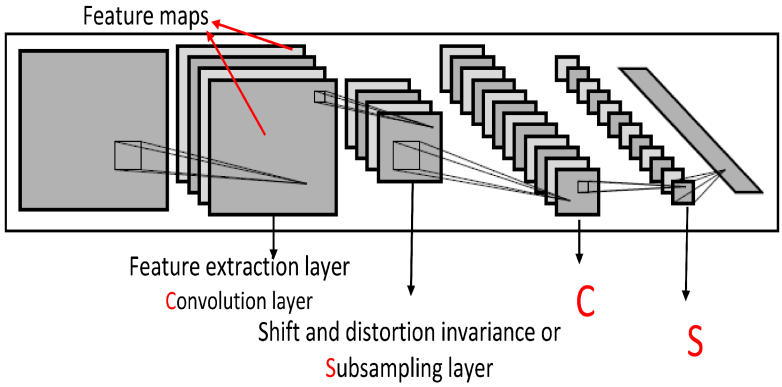

Figure 4.5: Layers of a Convolutional Neural Network

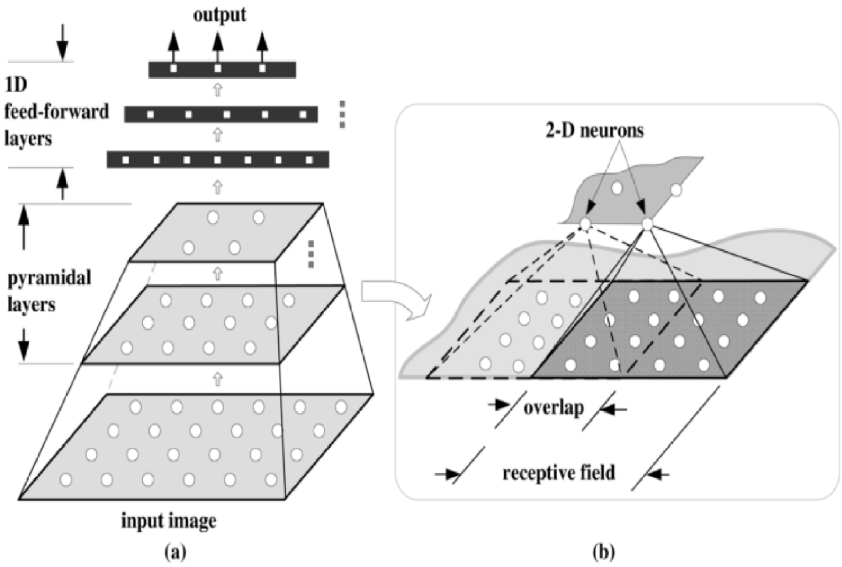

Figure 4.6: Structure of a Pyramidal Neural Network: (a) Layers, and (b) how the Receptive Fields overlap [192]

to a specific rectangular region (i.e., the receptive field) in the previous layer. The first pyramidal layer is connected to the input image, and it is followed by one or more pyramidal layers. The last pyramidal layer is connected to 1-D layers. A 2-D neuron computes a weighted sum of inputs from its receptive field, and then applies a nonlinear activation

function, e.g., sigmoid, to produce an output signal. The 1-D feedforward layers process the features produced by the pyramidal layers, and based on the training set and complexity of the images, several 1-D layers may be needed to form complex decision boundaries. The outputs of the last 1-D layer are the final network outputs, which determine the categories/class labels of input patterns. The use of pyramidal layers for 2-D feature extraction simplifies the role of 1-D layers for the task of feature classification.

In the present thesis, we develop a CNN model for detection of 12 different classes of environmental hazards (Table 4.1 using the PyraNet code by Phung e t al. [193][3]).

4.5 Computer vision-based results

4.5.1 Gabor barcode results

This first approach has two main steps: 1) extraction of binary features/Gabor Barcodes, 2) applying machine learning techniques and training classifiers, i.e., $k-$NN, Random forest, and Artificial neural networks, to classify and detect the environmental risk factors. There have been several studies in the literature reporting the optimal values for the parameters of the Gabor filter bank, i.e., spatial frequencies and number of orientations, in such a way that it mimics human visual system (HVS) as much as possible. Based on our primary investigations on the data/video. A Gabor filter bank (GFB) comprising of filters with $s = t = 11$ or 11×11 mask size, with $u = 5$ scales and $v = 8$ orientations resulted in a good accuracy. We applied the $GFB_{(5,8,11,11)}$ on 32×32 grayscale images in 2 different steps: 1) applying on the first data set 4.1 with 12 classes and 3669 images (after reducing the number of data points in a class with more than 7200 members), 2) applying the $GFB_{(5,8,11,11)}$ on 32×32 grayscale images and extracting GBCs from all three videos (V_{1+2+3}) simultaneously, resulting in 12382 binary features/Gabor Barcodes (with 17 classes) [189].

The required time for generation of GBCs from an image in our database is 0.0716

[3] "MATLAB library for convolutional neural network,", ICT Research Institute, Visual and Audio Signal Processing Laboratory, University of Wollongong.

seconds (Table 4.3) on average (applying GFB(5,8,11,11)), using Intel core i7-3.60GHz), which remarkably outperformed other image-processing-based methods for feature extraction like SIFT and SURF in terms of computational complexity. $k-$NN outperformed other methods, e.g., ANN and Rf.

For the $k-$NN method, 80% of data matrix $(12,382 \times N_{class}, N_{class} \in \{12,17\}$ of GBCs) was chosen randomly (using randperm in MATLAB) for training and 20% of data was randomly selected for testing the performance of the classifier. We also used our GBCs to train ANNs (MLP using 20, 30, 40 neurons in the hidden layer, 12 and 17 neurons in the output layer for the first and second database respectively, and Conjugate Gradient method for training). 70%, 15%, and 15% of data was randomly selected for training, validation, and testing of the network, respectively.

Tables 4.4 and 4.5 depict the mean accuracies after 10 times training, using random forest, $k-$NN, and ANN methods, for 12 classes (only video 1) and 17 classes (3 videos, V_{1+2+3}) respectively. n denotes the number of decision trees, closest neighbors, and neurons in the hidden layer, in RF_n, $k-NN_n$, and ANN_n respectively. Using GBCs and Hamming distance (Eq. 4.3) for identifying the class number for a test image, resulted in the highest accuracy.

Table 4.3: **Generation time and Barcode lengths for GBCs Using Intel core i7-3.60GHz**

Method	**Length of code**	**Extraction time**
GBC$_(8,15,23,23)$	8192	0.2114
GBC$_(8,12,23,23)$	6144	0.1618
GBC$_(5,12,23,23)$	3840	0.1034
GBC$_(5,20,23,23)$	6400	0.1678
GBC$_(5,8,23,23)$	2560	0.0715
GBC$_(5,16,23,23)$	5120	0.1352
GBC$_(5,8,27,27)$	2560	0.0795

Continued on next page

Table 4.3 – continued from previous page

Method	Length of code	Extraction time
$GBC_(10, 8, 23, 23)$	5120	0.1342
$GBC_(5, 8, 11, 11)$	2560	0.0716

Table 4.4: **Mean accuracies after 10 times training, using video1 database with 3669 data points and 12 classes**

KNN (K=1)	KNN (K=5)	KNN (K=15)	RF_{10}	RF_{20}	RF_{30}	ANN_{15}	ANN_{20}	ANN_{40}
95.82	92.86	81.01	88.32	92.67	93.07	91.92	92.72	93.89

Table 4.5: **Mean accuracies after 10 times training, using video$_{1+2+3}$ database with 12382 data points and 17 classes**

KNN (K=1)	KNN (K=5)	RF_{10}	RF_{20}	RF_{30}	ANN_{30}	ANN_{40}	ANN_{50}
88.51	78.97	78.08	79.81	81.29	79.25	82.26	82.45

While accuracy is our primary measure of classifier performance, it can yield misleading results if the data set is unbalanced. To evaluate performance more carefully, we consider confusion matrices.Confusion matrix is a specific table layout that allows visualization of the performance of an algorithm. This allows more detailed analysis than proportion of correct guesses (accuracy). The confusion matrices after applying ANN_{40} on V_1 and V_{1+2+3} are provided in Fig. 4.7 and 4.8 respectively.

4.5.2 Convolutional Neural Network results

To train the convolutional neural network based on the dataset provided in Table 4.1 ($32 \times 32 \times 3669$, 12 classes), we developed a network with 3 convolutional layers, 2 sub-sampling (max-pooling) layers, followed by a fully connected multilayer perceptron (FCMLP) with 12 neurons in the output (we have 12 classes so the target is a vector of size 12) [190].

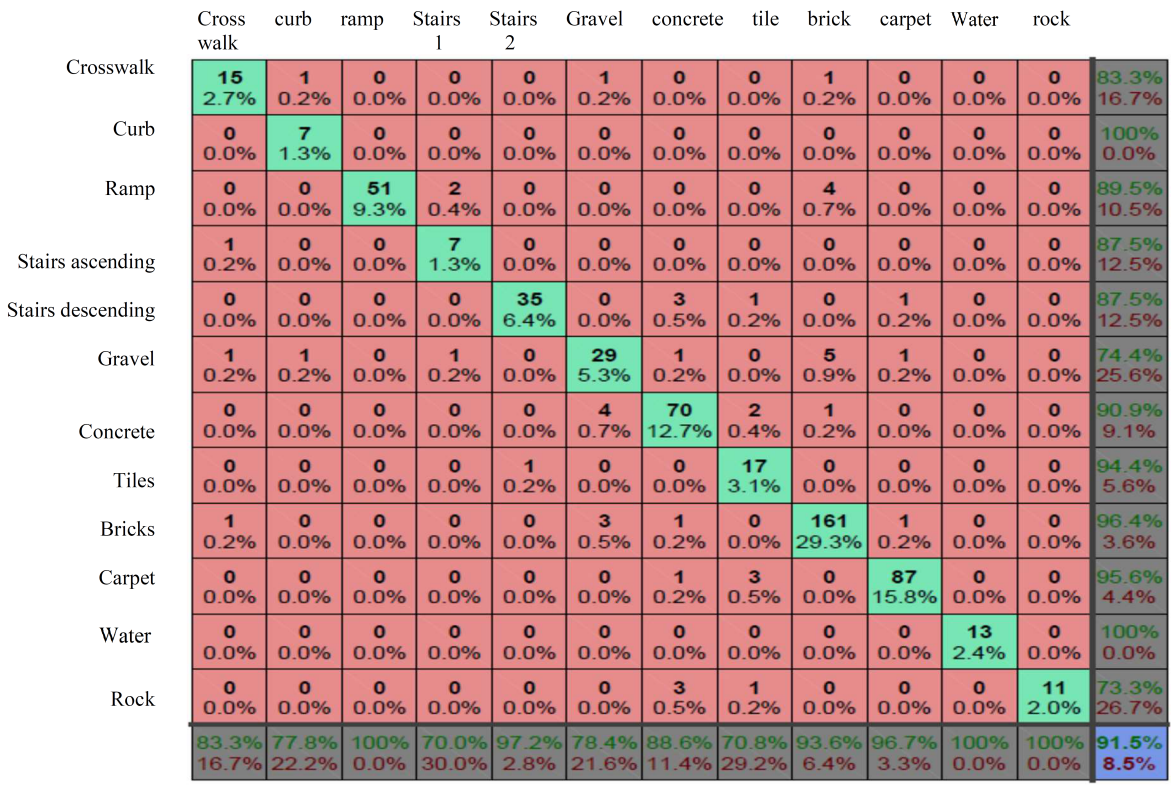

Figure 4.7: Confusion matrix for the ANN_{40} with 12 classes (70% training, 15% test, 15% validation)

The filter sizes are 5×5, 2×2, 3×3, 2×2, 6×6 for the C1, S2, C3, S4, C5 respectively. We employed 64, 32, and 16 features maps for the C1, C3, and C5 respectively and the connections between each feature map in convolution layer and its adjacent sub-sampling layer is one-to-one. There is full connection between F6 and C5 4.9 .

The activation functions for network layers are set as:

1. convolution layers C1, C3 and C5: tansig,
2. sub-sampling layers S2 and S4: purelin,
3. output layer F6: tansig.

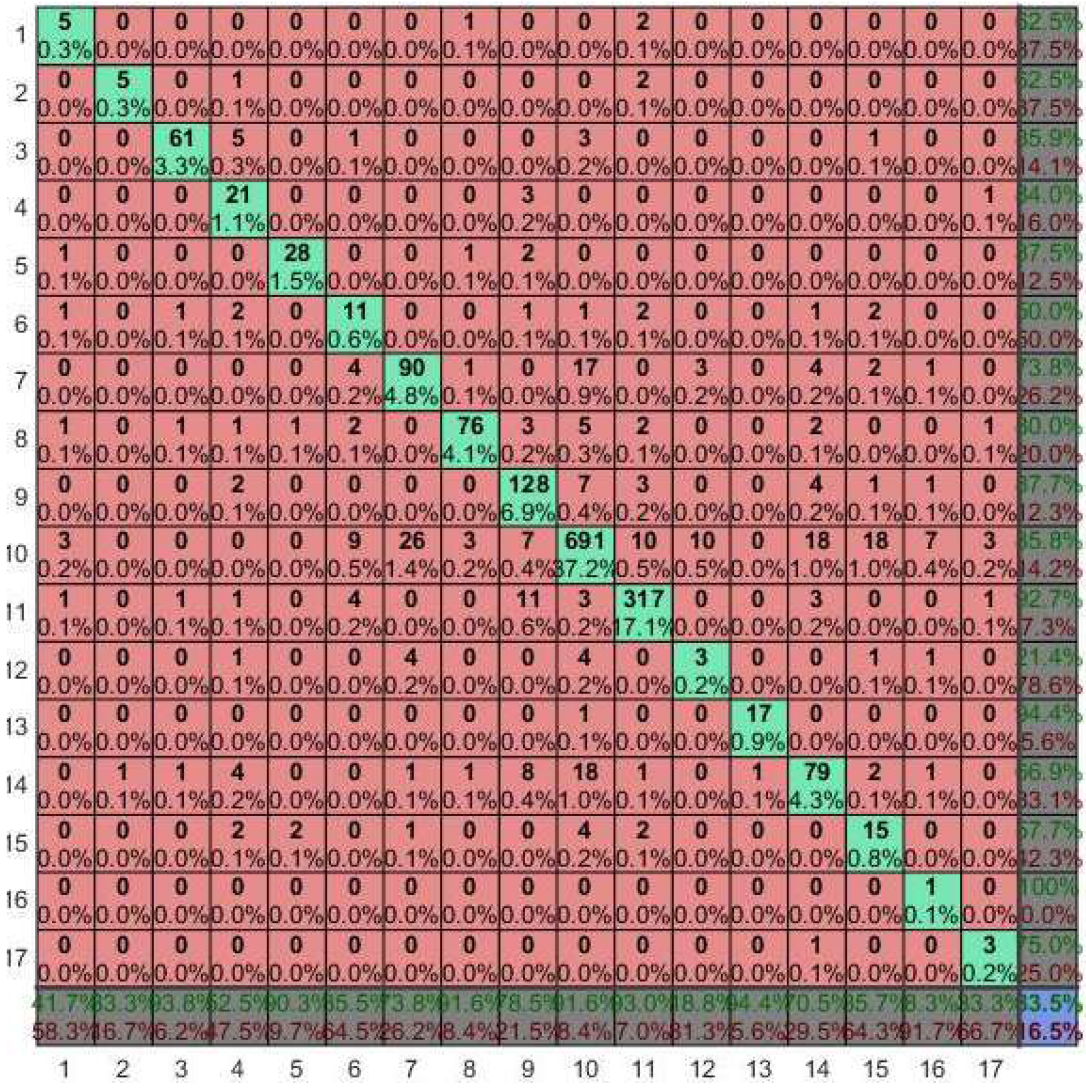

Figure 4.8: Confusion matrix for ANN_40 with 17 classes (70% training, 15% test, 15% validation): Crosswalk, 2: curbs, 3: ramp, 4: stairs (ascending), 5: stairs (descending), 6: gravel, 7: grass, 8: concrete, 9: tiles, 10: bricks, 11: carpets, 12: dirt, 13: water, 14: snow, 15: slush, 16: ice, 17: Rocks.)

The training method for the network is chosen to be RPROP (resilient backpropagation) which is one of the fastest among the first-order training algorithms. Weight update

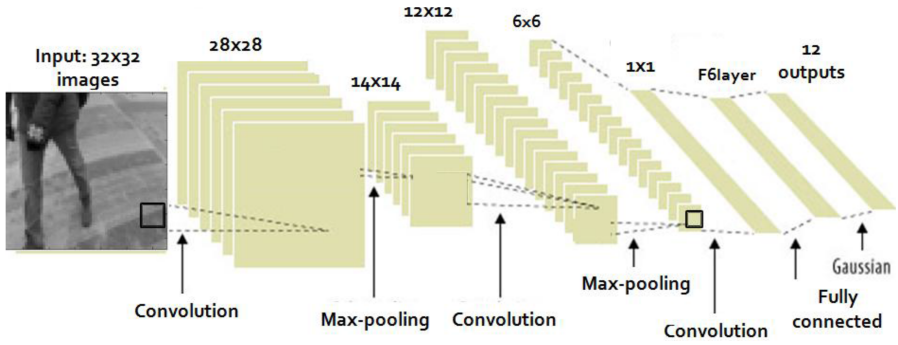

Figure 4.9: The developed CNN to detect fall-related environmental risks

depends only on the sign of the gradient.

$$\Delta w_i(t) = -sign\{\frac{\partial E}{\partial w_i} t \times \Delta_i(t)\} \tag{4.4}$$

$\Delta_i(t)$ is adaptive step specific to weight w_i defined as:

$$\Delta_i(t) = \begin{cases} \eta_{inc}\Delta_i(t-1), & \text{if} \frac{\partial E}{\partial w_i}(t) \times \frac{\partial E}{\partial w_i}(t-1) > 0 \\ \eta_{dec}\Delta_i(t-1), & \text{if} \frac{\partial E}{\partial w_i}(t) \times \frac{\partial E}{\partial w_i}(t-1) < 0 \\ \Delta_i(t-1), & \text{otherwise} \end{cases}$$

The goal is to minimize the mean square error (MSE) (Eq. 4.5) during the process of training. In Fig.4.10 there is a clear trend of decreasing training error (MSE) during 100 epochs. The MSE error clearly converges to ≈ 0.08, indicating the efficiency of the trained network in detection of objects/terrains.

$$E_{MSE} = \frac{1}{K \times N_L} \sum_{K-1}^{K} \sum_{n=1}^{N_L} |y_n^{L,k} - d_n^K k|^2 \tag{4.5}$$

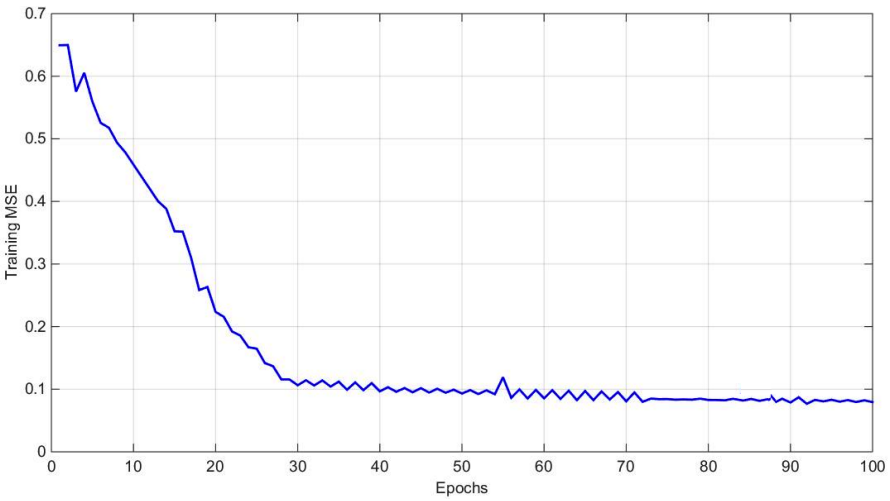

Figure 4.10: CNN Training Error for each Training of 12 Classes

4.6 Conclusion and future work

In this chapter, we incorporated imaging data captured by an egocentric mobile vision system to provide contextual information towards a novel FRA tool. We employed two different machine learning techniques, e.g., Gabor Barcodes and convolutional neural networks, to automatically detect 17 different classes of environmental risk factors. This data is promising step in identifying specific environmental conditions that pose unique challenges to a senior's balance control.

This research has generated many questions in need of further investigation. Further work needs to be done to establish whether the parameters that were selected for 1) cropping and resizing the frames, 2) the Gabor filter bank, and 3) CNN were optimal. Grey-scale images were used to train the machine learning models, which outperform RGB images in terms of lower processing time and complexity. However, using grayscale images may reduce the discriminative power of the system to distinguish environmental hazards that share similar texture, shape or color (e.g. bricks and tiles, or crosswalk and stairs). For the next steps, we aim to employ RGB images to increase the accuracy of the models.

Chapter 5

Validation of accuracy of the system during real-world activities

As it is mentioned in chapter 2, the majority of the current FRA methods that are widely used to assess seniors' mobility still lacking the capability to be generalized into everyday situations outside clinical settings. Therefore, we propose to develop new methods to address this limitation by employing WSSs. An important unanswered question is the extent to which our classification procedure and results will transfer to unexpected near-falls in real-life scenarios. In this chapter we aim to validate our methods for detection of CBRs and the associated environmental risk factors, which were discussed in chapters 3 and 4 respectively, with a new testing data set to better reflect usage conditions.

We asked participants to wear three IMUs as well as a mobile vision system (either the GoPro Hero Silver or GoPro Hero Session camera) (Fig. 5.1). The participants walked around the University of Waterloo campus and each was perturbed by lateral pushes to his/her right shoulder by a researcher walking alongside. We stimulated incidents of lateral CBRs (including sidestep or crossover strategies) in different situations, i.e., on carpet, brick, crosswalk, and pavement (concrete). The perturbations were exerted randomly and in a way to stimulate an involuntary reaction.

Figure 5.1: The validation process of the system. The subjects wore three SHIMMER sensors along with a GoPro Hero Silver camera and were perturbed in different settings, e.g., on crosswalk, pavement, and tiles.

5.1 Detection of lateral CBRs with IMU data

In this part, the data that was collected from 5 participants and was used in chapter 3 to develop machine learning models (SVMs and $k-$NN), is employed to train the pattern recognition system. Eight CBR trials, either CBR type 1 or CBR type 2, were collected and afterward, we applied segmentation methods and extracted 138 IMU features from each segment. The new testing dataset is a 8×138 matrix; however, as it was described in section 3.5.1, the dimension of the feature space can be reduced to increase the performance of the machine learning model. Therefore, we repeated the feature reduction step (P = 2,5,10 using PCA and KSPCA techniques) using the new dataset. Afterward, the SVMs and $K-$NN $k = 7$ methods were applied on the new $Data - Test_{p\times 8}$ ($p \in \{2, 5, 10\}$)

matrix. We achieved 100% accuracy in all of the cases, which indicates the efficiency and generalizability of our method in real-life situations. Figures 5.1 to 5.5 depict sample signals for 5 successive CBR incidents that happened during normal walking in a natural environment outside laboratory.

5.2 Detection of environmental risks

This section aims to identify the environment (and associated fall-related hazards), where each CBR happened. The videos were captured synchronously with the IMU data, while the participants were perturbed. The associated frame with each captured CBR was found in the videos and labeled with a number between 1 to 17 (developed in chapter 4). Two CBR incidents were captured on a crosswalk (Fig, 5.2), on bricks (Fig. 5.2), on pavement (concrete) (Fig. 5.2), and in an indoor environment covered with carpet (Fig. 5.9). The frames were cropped and resized (Algorithm 3) and their associated Gabor Barcodes were generated using Algorithm 4.

As it is clear in these figures, the captured frames contain many objects that pose an specific challenges on the process of automated environment detection. For instance, a vehicle appeared in the upper corner of the frame captured on a crosswalk (Fig. 5.2). Moreover, the lighting conditions, brightness and illumination considerably affect the videos and eventually may affect the performance of the detection system. For instance, the participant's shadow and the shadow of a building appeared in Figures 5.2 and 5.2 respectively, because the video was captured in a sunny day (in contrast to the initial data that was collected under cloudy, snowy conditions). The frames are considerably different from the initial dataset that was used in chapter 4; however, after extraction of Gabor Barcodes from these frames (results in a $Data_{8\times2560}$ matrix) and applying Hamming distance, 5 out of 8 frames were detected correctly.

For the future work, we aim to generate a more balanced data set to increase the performance of the machine learning system; and need to collect more data to increase the generalizabiliy of the risk factor detection system.

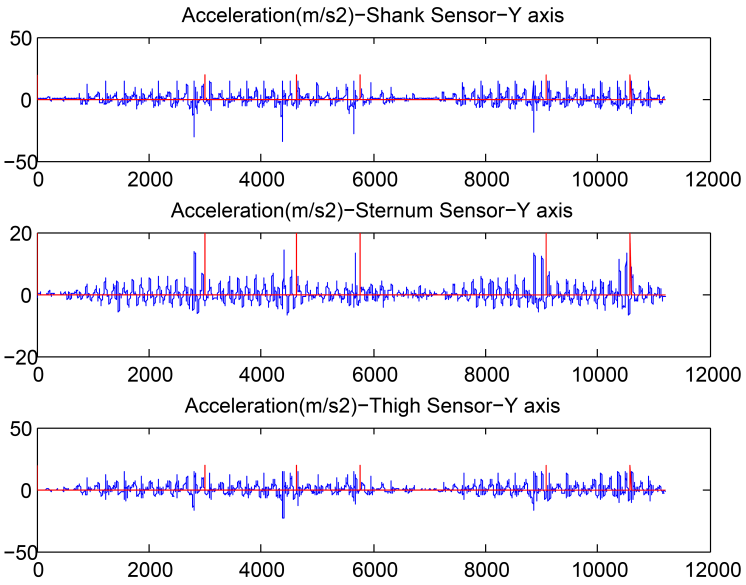

Figure 5.2: Sample acceleration signals in the y direction for 5 successive incidents of CBR captured from shank, sternum and thigh IMUs, while walking outdoor on tiles

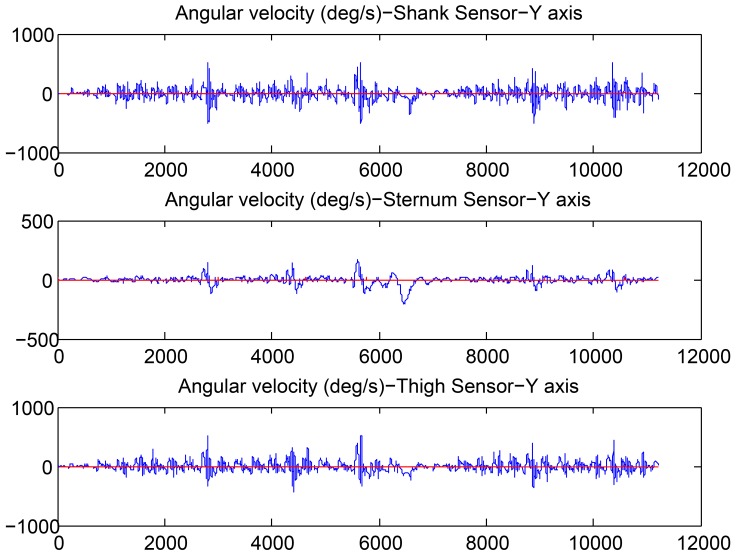

Figure 5.3: Sample angular velocity signals in the y direction for 5 successive incidents of CBR captured from shank, sternum and thigh IMUs, while walking outdoor on tiles

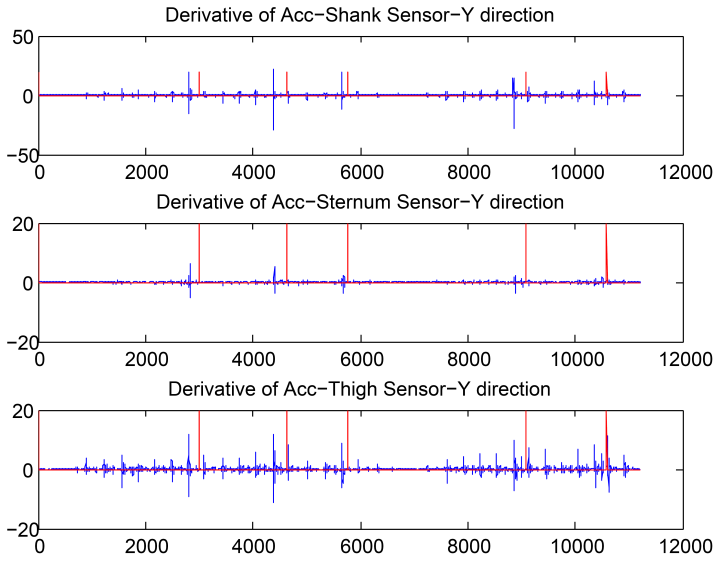

Figure 5.4: Sample derivative of acceleration signals in the y direction for 5 successive incidents of CBR captured from shank, sternum and thigh IMUs, while walking outdoor on tiles.

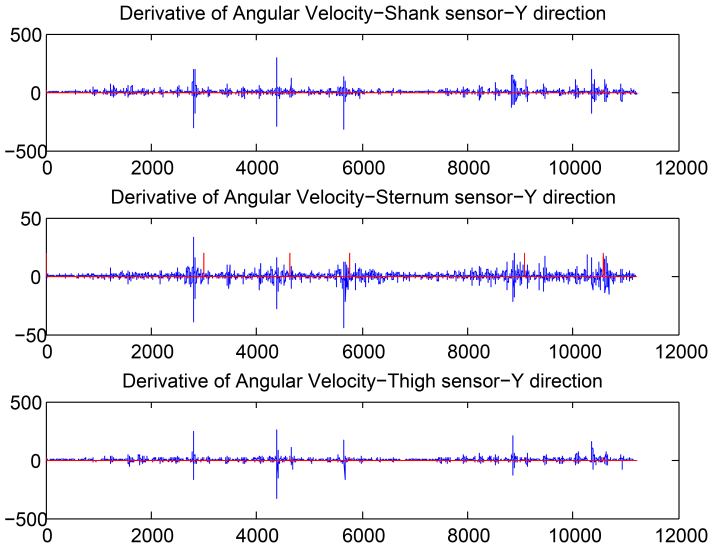

Figure 5.5: Sample derivative of angular velocity signals in the y direction for 5 successive incidents of CBR captured from shank, sternum and thigh IMUs, while walking outdoor on tiles.

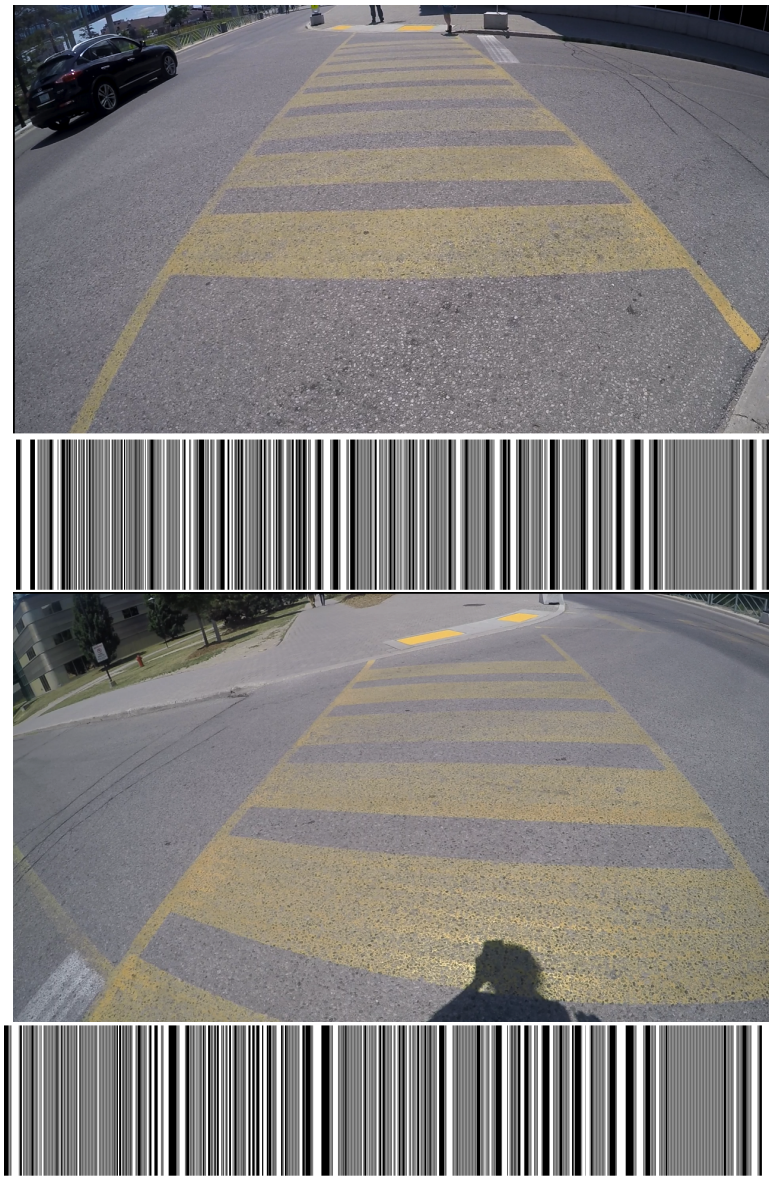

Figure 5.6: The captured frames by a GoPro Hero Silver camera and their associated Gabor Barcode, when the participant was perturbed on a crosswalk.

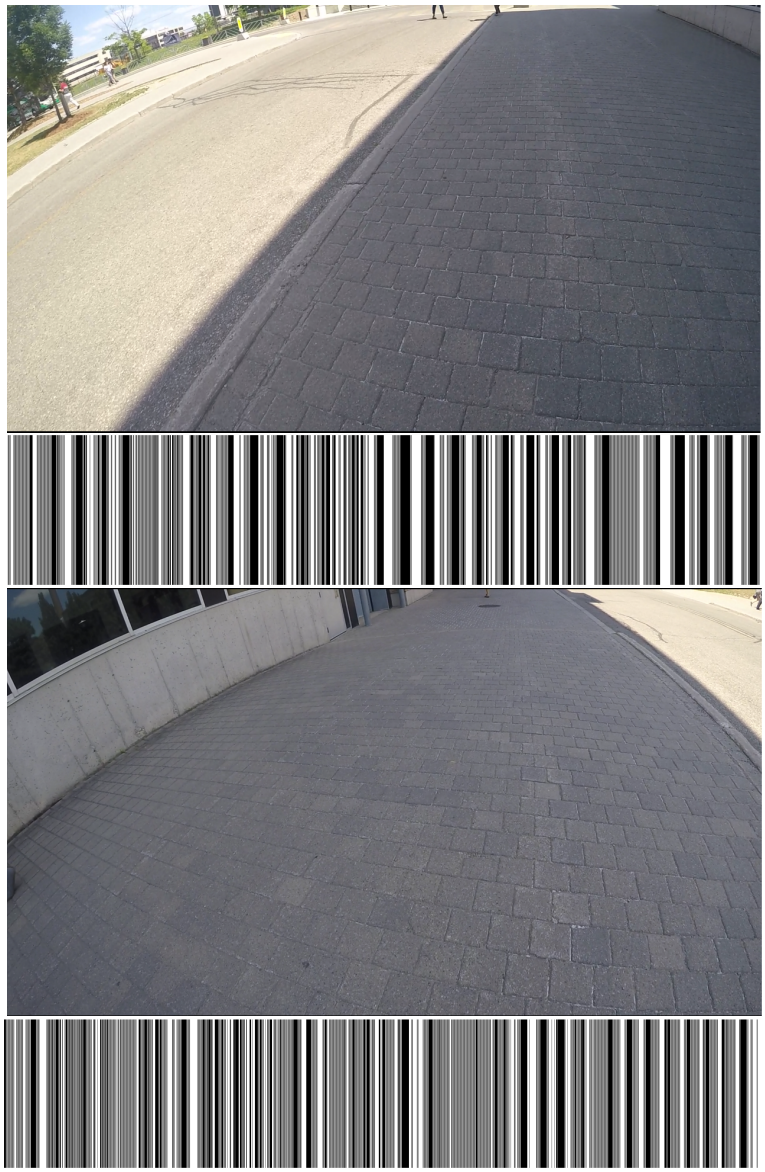

Figure 5.7: The captured frames by a GoPro Hero Silver camera and their associated Gabor Barcode, when the participant was perturbed on tiles.

Figure 5.8: The captured frames by a GoPro Hero Silver camera and their associated Gabor Barcode, when the participant was perturbed on pavement.

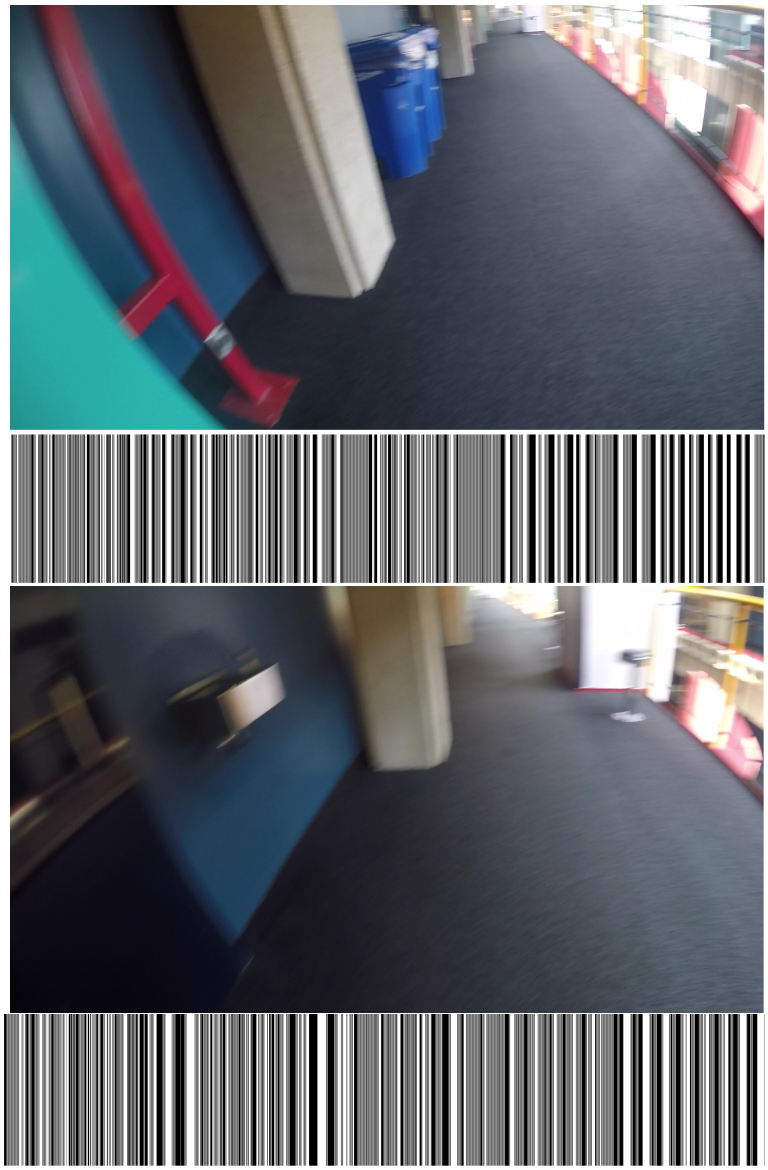

Figure 5.9: The validation process of the system. The subjects wore three SHIMMER sensors along with a GoPro Hero Silver camera and were perturbed in on carpet.

Chapter 6

Conclusion and Future Works

Insufficient recovery of balance after an unexpected perturbation such as a slip or trip is a key factor for falling in older adults. The present thesis demonstrates our initial step toward detection of CBRs for automatic and personalized risk of falling assessment in nonclinical settings. In conclusion, wearable sensors, combined with machine learning techniques, make the real-time detection of CBRs feasible. Although the CBRs in lateral direction are the most common type of CBRs, we need to take into consideration the CBRs in other directions, e.g., forward and backward. In collaboration with the the researchers at the University of Heidelberg, Germany [1], we aim to capture more trials of CBRs in different direction, using a perturbation-treadmill and different patient populations. This data collection has been conducted in a modern gait laboratory in Stuttgart, which is equipped with a perturbation-treadmill, motion tracking system (Vicon), force plates, and different wearable sensor systems for measuring human motion performance.

An important unanswered question is the extent to which our classification procedure and results will transfer to unexpected near-falls in real-life scenarios by older adults, including those with specific disease conditions or impairment (various patient populations (geriatric, orthopedic, neurologic, etc.). We aim to collect more data and increase the generalizability of our pattern recognition system and then examine the performance of

[1] www.nar.uni-heidelberg.de/en/youngscholars/jrg$_$schwenk/schwenk.html

the system on older adults in our future works.

Figure 6.1: Perturbation treadmill for a more systematic data collection

Additionally, further experiment and data collection would be of great help in increasing the generalizability of the CBR detection system and environmental risk factor identification system. Specifically, collection of videos in different lighting conditions, in different inclines (or field of views), and in different places and conditions is strongly recommended in order to increase the robustness of the proposed FRA system.

For a real-time detection of CBRs and associated environmental risk factors, we need to develop less computationally complicated methods. As it was discussed, the Gabor Barcodes are binary features and are already a memory-efficient way of texture-based feature extraction. Further research might explore the capabilities of the Radon-Barcodes and/or Radon-Gabor Barcodes that we have introduced recently [191], to achieve context awareness. The latter method is capable to harness the potentials of both Radon and Gabor transforms to extract shape-texture based binary features. It would be interesting to assess the effectiveness of these two methods in detection of fall-related environmental hazards, and compare their effectiveness with GBCs and CNN in terms of detection speed and development of real-time FRA methods.

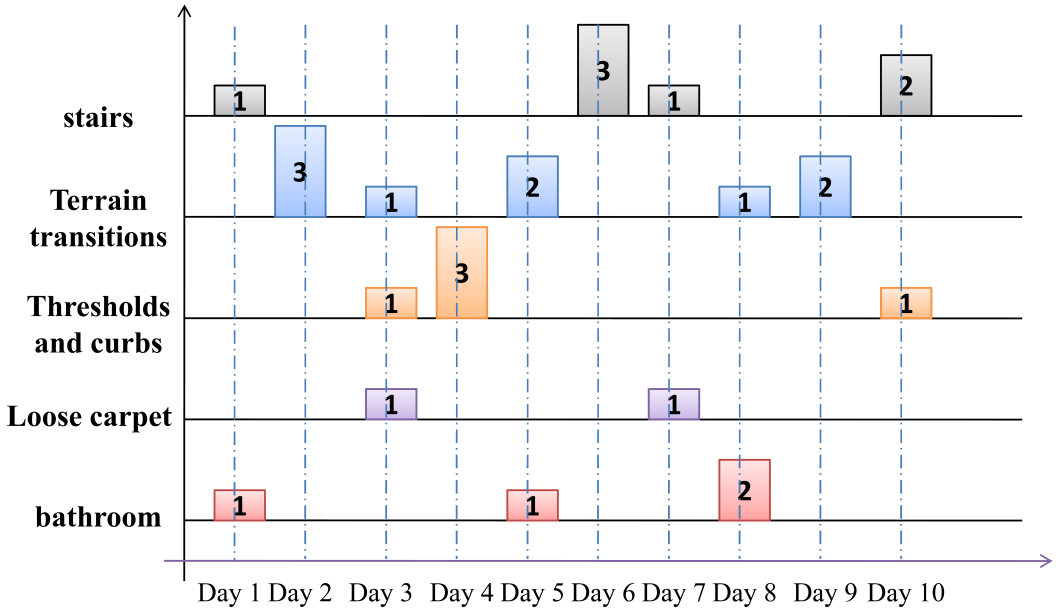

Figure 6.2: Frequency of CBRs per environmental risk factor

As it is depicted in Fig. 6.2, the long-term goal of this study is to develop a personalized FRA and fall prevention tool by automated detection of cause and frequency of CBRs per environmental risk factors (Fig. 6.2), over a specific time interval. Based on an ambulatory assessment of fall risk, interventions may be developed to deliver timely information. For example, it would be feasible to alert the older adult via a mobile application and subsequently protect the user from falling (Fig. 6.3) when an specific risk is detected (e.g., high number of recent CBRs).

Figure 6.3: Possible smart phone application for fall prevention and prediction

References

[1] World Health Organization. Ageing, & Life Course Unit. (2008). WHO global report on falls prevention in older age. World Health Organization.

[2] Hawley-Hague, H., Boulton, E., Hall, A., Pfeiffer, K., & Todd, C. (2014). Older adults' perceptions of technologies aimed at falls prevention, detection or monitoring: a systematic review. International journal of medical informatics, 83(6), 416-426.

[3] Tian, Yang, et al. "Exploring the system-wide costs of falls in older people in Torbay." London: The King's Fund (2013).

[4] Pfortmueller, C. A., Lindner, G., & Exadaktylos, A. K. (2014). Reducing fall risk in the elderly: risk factors and fall prevention, a systematic review. Minerva Med, 105(4), 275-81.

[5] smartrisK. the economic Burden of injury in canada. toronto, on: smartrisK; 2009. availablefrom:http://www.parachutecanada.org/research/item/economic-burden-of-injury-reports

[6] Hornbrook, M. C., Stevens, V. J., Wingfield, D. J., Hollis, J. F., Greenlick, M. R., & Ory, M. G. (1994). Preventing falls among community-dwelling older persons: results from a randomized trial. The Gerontologist, 34(1), 16-23.

[7] SMARTRISK, "The economic burden of unintentional injury in Canada," ed, 1998.

[8] Stevens, J. A., Corso, P. S., Finkelstein, E. A., & Miller, T. R. (2006). The costs of fatal and non-fatal falls among older adults. Injury prevention, 12(5), 290-295.

[9] M. Nikitovic, W. P. Wodchis, M. D. Krahn, and S. M. Cadarette, "Direct health- care costs attributed to hip fractures among seniors: a matched cohort study," Osteoporos Int, vol. 24, pp. 659-69, Feb 2013.

[10] Scott, V., L. Wagar, and S. Elliott. "Falls & related injuries among older Canadians: Fall-related hospitalizations & intervention initiatives. Prepared on behalf of the Public Health Agency of Canada, Division of Aging and Seniors. Victoria BC: Victoria Scott Consulting." Victoria, BC: Victoria Scott Consulting (2010).

[11] Scott, V., Wagar, B., Sum, A., Metcalfe, S., & Wagar, L. (2010). A public health approach to fall prevention among older persons in Canada. Clinics in geriatric medicine, 26(4), 705-718.

[12] http://www.statcan.gc.ca/2008/70000/ceb70000_000-eng.htm

[13] Section 3: Analysis of the results of the long-term projections. http://www.statcan.gc.ca/pub/91-520-x/2010001/part-partie3-eng.htm

[14] Perell, Karen L., et al. "Fall risk assessment measures an analytic review." The Journals of Gerontology Series A: Biological Sciences and Medical Sciences 56.12 (2001): M761-M766.

[15] Herman, M., E. Gallagher, and V. Scott. "The evolution of seniors' falls prevention in British Columbia." Victoria: British Columbia Ministry of Health (2006).

[16] Wiktorowicz ME, Goeree R, Papaioannou A, Adachi JD, Papadimitropoulos E: Economic implications of hip fracture: health service use, institutional care and cost in Canada. Osteoporos Int. 2001, 12 (4): 271-278. 10.1007/s001980170116.

[17] Braithwaite RS, Col NF, Wong JB: Estimating hip fracture morbidity, mortality and costs. J Am Geriatr Soc. 2003, 51 (3): 364-370. 10.1046/j.1532-5415.2003.51110.x.

[18] Cook, Wendy L., et al. "Post-discharge management following hip fracture-get you back to B4: A parallel group, randomized controlled trial study protocol." BMC geriatrics 11.1 (2011): 30.

[19] http:www.indiana.edu

[20] Hill, Keith, et al. "Falls among healthy, communitydwelling, older women: a prospective study of frequency, circumstances, consequences and prediction accuracy." Australian and New Zealand journal of public health 23.1 (1999): 41-48.

[21] S. Lehtola, P. Koistinen, and H. Luukinen, "Falls and injurious falls late in home-dwelling life," Arch Gerontol Geriatr, vol. 42, pp. 217-24, Mar-Apr 2006.

[22] J. B. Nadkarni, K. P. Iyengar, C. Dussa, S. Watwe, and K. Vishwanath, "Orthopaedic injuries following falls by hospital in-patients," Gerontology, vol. 51, pp. 329-33, Sep-Oct 2005.

[23] J. P. Empana, P. Dargent-Molina, G. Breart, and E. Group, "Effect of hip fracture on mortality in elderly women: the EPIDOS prospective study," J Am Geriatr Soc, vol. 52, pp. 685-90, May 2004.

[24] A. Ozcan, H. Donat, N. Gelecek, M. Ozdirenc, and D. Karadibak, "The relationship between risk factors for falling and the quality of life in older adults," BMC Public Health, vol. 5, p. 90, 2005.

[25] R. G. Cumming, G. Salkeld, M. Thomas, and G. Szonyi, "Prospective study of the impact of fear of falling on activities of daily living, SF-36 scores, and nursing home admission," J Gerontol A Biol Sci Med Sci, vol. 55, pp. M299-305, May 2000.

[26] A. Bergland and T. B. Wyller, "Risk factors for serious fall related injury in elderly women living at home," Inj Prev, vol. 10, pp. 308-13, Oct 2004.

[27] H. E. Meyer, A. Tverdal, J. A. Falch, and J. I. Pedersen, "Factors associated with mortality after hip fracture," Osteoporos Int, vol. 11, pp. 228-32, 2000.

[28] R. Norton, M. Butler, E. Robinson, T. Lee-Joe, and A. J. Campbell, "Declines in physical functioning attributable to hip fracture among older people: a follow-up study of case-control participants," Disabil Rehabil, vol. 22, pp. 345-51, May 20 2000.

[29] L. J. Melton, 3rd and S. R. Cummings, "Heterogeneity of age-related fractures: implications for epidemiology," Bone Miner, vol. 2, pp. 321-31, Jul 1987.

[30] J. C. Scott, "Osteoporosis and hip fractures," Rheum Dis Clin North Am, vol. 16, pp. 717-40, Aug 1990.

[31] "U.S. Department of Health and Human Services, Public Health Service, National Center for Health Statistics (1991). (unpublished data from the 1988 and 1991 National Hospital Discharge Survey.)."

[32] E. S. Fisher, J. A. Baron, D. J. Malenka, J. A. Barrett, W. D. Kniffin, F. S. Whaley, and T. A. Bubolz, "Hip fracture incidence and mortality in New England," Epidemiology, vol. 2, pp. 116-22, Mar 1991.

[33] Thompson, H. J., McCormick, W. C., & Kagan, S. H. (2006). Traumatic brain injury in older adults: epidemiology, outcomes, and future implications. Journal of the American Geriatrics Society, 54(10), 1590-1595.

[34] A. C. Mosenthal, R. F. Lavery, M. Addis, S. Kaul, S. Ross, R. Marburger, E. A. Deitch, and D. H. Livingston, "Isolated traumatic brain injury: age is an independent predictor of mortality and early outcome," J Trauma, vol. 52, pp. 907-11, May 2002.

[35] D. G. Vollmer and R. G. Dacey, Jr., "The management of mild and moderate head injuries," Neurosurg Clin N Am, vol. 2, pp. 437-55, Apr 1991.

[36] Agency for Healthcare Quality and Research [on-line] H-CUPnet, Healthcare cost and utilization project. [May 1, 2006]. Available at www.ahrq.gov/HCUPnet/

[37] http://www.cdc.gov/traumaticbraininjury/get_the_facts.html

[38] C. L. Curcio, F. Gomez, and C. A. Reyes-Ortiz, "Activity restriction related to fear of falling among older people in the Colombian Andes mountains: are functional or psychosocial risk factors more important?," J Aging Health, vol. 21, pp. 460- 79, Jun 2009.

[39] M. E. Tinetti and C. S. Williams, "The effect of falls and fall injuries on functioning in community-dwelling older persons," J Gerontol A Biol Sci Med Sci, vol. 53, pp. M112-9, Mar 1998.

[40] S. Franzoni, R. Rozzini, S. Boffelli, G. B. Frisoni, and M. Trabucchi, "Fear of falling in nursing home patients," Gerontology, vol. 40, pp. 38-44, 1994.

[41] M. E. Tinetti, W. L. Liu, and E. B. Claus, "Predictors and prognosis of inability to get up after falls among elderly persons," JAMA, vol. 269, pp. 65-70, Jan 6 1993.

[42] R. E. Roush, T. A. Teasdale, J. N. Murphy, and M. S. Kirk, "Impact of a personal emergency response system on hospital utilization by community-residing elders," South Med J, vol. 88, pp. 917-22, Sep 1995.

[43] Murphy S, Dubin J, Gill T. The development of fear of falling among community-living older women: predisposing factors and subsequent fall events. Journal of Gerontology. 2003;58A:9437.

[44] Soriano, Theresa A., Linda V. DeCherrie, and David C. Thomas. "Falls in the community-dwelling older adult: a review for primary-care providers." Clinical interventions in aging 2.4 (2007): 545.

[45] M. Nouredanesh and J. Tung, Machine learning based detection of compensatory balance responses to lateral perturbation using wearable sensors, pp. 14, 2015.

[46] Nouredanesh, Mina, Sunil Kukreja, and James Tung Detection of compensatory balance responses using wearable electromyography sensors for fall-risk assessment, To appear inproceedings of The 38th Annual International Conference of the IEEE Engineering in Medicine and Biology Society (IEEE-EMBC 2016), Aug 17-20, Orlando, USA.

[47] Who, WHO Global Report on Falls Prevention in Older Age., Community Health (Bristol)., p. 53, 2007.

[48] Rubenstein LV, Josephson KR, Osterweil D. Falls and fall prevention in the nursing home. Clin Geriatr Med. 1996;12:881903.

[49] King MB, Tinetti ME. A multifactorial approach to reducing injurious falls. Clin Geriatr Med. 1996;12:745759.

[50] Fleming KC, Evans JM, Weber DC, Chutka DS. Practical functional assessment of elderly persons: a primary-care approach. Mayo ClinProc. 1995;70:890910.

[51] Wolf-Klein GP, Silverstone FA, Basavaraju N, Foley CJ, Pascaru A, Ma PH. Prevention of falls in the elderly population. Arch Phys MedRehabil. 1988;69:689691.

[52] Morse JM, Morse R, Tylko S. Development of a scale to identify the fall-prone patient. Can J Aging. 1989;8:366377.

[53] Oliver D, Britton M, Seed P, Martin FC, Happer AH. Development and evaluation of evidence based risk assessment tool (STRATIFY) to predict which elderly inpatients will fall, case-control and cohort studies. Br Med J. 1997;315:10491053.

[54] Morris JN, Nonemaker S, Murphy K, et al. Commitment to change: revision of HCFA's RAI. J Am Geriatr Soc. 1997;45:10111016.

[55] Hendrich A, Nyhuuis A, Kippenbrock T, Soja ME. Hospital falls, development of predictive model for clinical practice. Appl Nurs Res.1995;8:129139.

[56] Fife DD, Solomon P, Stanton M. A risk falls program: code orange for success. Nurs Manage. 1984;15:5053.

[57] Mercer L. Falling out of favour. Aust Nurs J. 1997;4:2729.

[58] Tinetti ME, Williams TF, Mayewski R. Fall risk index for elderly patients based on number of chronic disabilities. Am J Med. 1986;80:429434.

[59] Kenny, R. A., Scanaill, C. N., & McGrath, M. (2010). Falls Prevention in the Home: Challenges for New Technologies. Intelligent Technologies for Bridging the Grey Digital Divide, 46.

[60] Hendrich, Ann. "Fall Risk Assessment for Older Adults: The Hendrich II Fall Risk ModelTM." Try This: Best Practices to Nursing Care of Older Adults. New York University, The Hartford Institute for, Geriatric Nursing, 2013. 8.

[61] Berg, Robert L., and Joseph S. Cassells. "Falls in older persons: risk factors and prevention." (1992).

[62] Campbell AJ, Borrie MJ, Spears GF, Jackson SL, Brown JS, Fitzgerald JL. Circumstances and consequences of falls experienced by a community population 70 years and over during a prospective study.Age and Ageing 1990;19:13641.

[63] Luukinen H, Koski K, Laippala P, Kivela SL. Predictors for recurrent falls among the home-dwelling elderly.Scandinavian Journal of Primary Health Care 1995;13:2949

[64] Lord, S. R., Sherrington, C., Menz, H. B., & Close, J. C. (2007). Falls in older people: risk factors and strategies for prevention. Cambridge University Press.

[65] Rodriguez, J. G., Sattin, R. W., DeVito, C. A., and Wingo, P. A. Developing an environmental hazards assessment instrument for falls among the elderly. In: R. Weindruch, editor; and M. Ory, editor. (eds.), Frailty Reconsidered: Reducing Frailty and Fall-related Injuries in the Elderly. Springfield, Ill.: Charles C Thomas, in press.

[66] Kronfol, N. (2012). Biological, medical and behavioral risk factors on falls. World Health Organisation. http://www.who.int/ageing/project/falls_prevention_older_age/en/inded.html.

[67] Rawsky, E. (1998). Review of the literature on falls among the elderly. Image: The Journal of Nursing Scholarship, 30(1), 47-52.

[68] Rubenstein LZ, Josephson KR. Falls. In: Kenny RA, ed. Syncope in the Older Patient. London: Chapman & Hall; 1996:283297.

[69] American Geriatrics Society2001. Guidelines for prevention of falls in older persons. J Am Geriatr Soc.49:664-672.

[70] Rubenstein, L. Z., Robbins, A. S., Schulman, B. L., Rosado, J., Osterweil, D., and Josephson, K. R. Falls and instability in the elderly. Journal of the American Geriatric Society 1988; 36(3):266-278.

[71] Stalenhoef, Paul A., et al. "Incidence, risk factors and consequences of falls among elderly subjects living in the community." The European Journal of Public Health 7.3 (1997): 328-334.

[72] Connell BR, 1996. Role of the environment in falls prevention. Clin Geriatr Med.12:859-880

[73] Di Pilla, Steven. Slip and fall prevention: a practical handbook. CRC Press, 2004.

[74] Berg, K., Wood-Dauphine, S., Williams, J. I., & Gayton, D. (1989). Measuring balance in the elderly: preliminary development of an instrument. Physiotherapy Canada, 41(6), 304-311.

[75] Berg K, Norman KE. Functional assessment of balance and gait. ClinGeriatr Med. 1996;12:705723.

[76] Pajala, S., Era, P., Koskenvuo, M., Kaprio, J., Trmkangas, T., & Rantanen, T. (2008). Force platform balance measures as predictors of indoor and outdoor falls in community-dwelling women aged 6376 years. The Journals of Gerontology Series A: Biological Sciences and Medical Sciences, 63(2), 171-178.

[77] Duncan PW, Wiener DK, Chandler J, Studenski S. Functional reach: a new clinical measure of balance. J Gerontol Med Sci. 1990;45A:M192M197.

[78] Whitney SL, Hudak MT, Marchetti GF. The dynamic gait index relates to self-reported fall history in individuals with vestibular dysfunction. J Vestib Res. 2000;10:99105.

[79] Province MA, Hadley EC, Hornbrook MC, et al. The effects of exercise on falls in elderly patients: a preplanned meta-analysis of the FICSIT Trials. JAMA. 1995;273:13411347.

[80] Cwikel JG, Fried AV, Biderman A, Galinsky D. Validation of a fall-risk screening test, the Elderly Fall Screening Test (EFST), for community-dwelling elderly. Disabil Rehabil. 1998;20:161167.

[81] Shumway-Cook A, Brauer S, Woollacott MH. Predicting the probability for falls in community-dwelling older adults using the Timed Up & Go Test. Phys Ther. 2000;80:896903.

[82] Steffen, T. M., Hacker, T. A., & Mollinger, L. (2002). Age-and gender-related test performance in community-dwelling elderly people: Six-Minute Walk Test, Berg Balance Scale, Timed Up & Go Test, and gait speeds. Physical therapy, 82(2), 128-137.

[83] Vassallo, Michael, et al. "Fall risk-assessment tools compared with clinical judgment: an evaluation in a rehabilitation ward." Age and ageing 37.3 (2008): 277-281.

[84] 16. Hausdorff JM, Rios DA, Edelberg HK: Gait variability and fall risk in community-living older adults: a 1-year prospective study. Arch Phys Med Rehabil. 2001, 82: 1050-1056. 10.1053/apmr.2001.24893.

[85] Laessoe, Uffe, Hans C. Hoeck, Ole Simonsen, Thomas Sinkjaer, and Michael Voigt. "Fall risk in an active elderly populationcan it be assessed?." Journal of negative results in biomedicine 6, no. 1 (2007): 1.

[86] Nyberg, Lars, Lillemor Lundin-Olsson, Bjrn Sondell, Anders Backman, Kenneth Holmlund, Staffan Eriksson, Michael Stenvall, Erik Rosendahl, Marcus Maxhall, and Gustaf Bucht. "Using a Virtual Reality System to Study Balance and Walking in a Virtual Outdoor Environment: APilot Study." Cyberpsychology & behavior 9, no. 4 (2006): 388-395.

[87] Duque, Gustavo, Derek Boersma, Griselda Loza-Diaz, Sanobar Hassan, Hamlet Suarez, Dario Geisinger, Pushpa Suriyaarachchi, Anita Sharma, and Oddom Demontiero. "Effects of balance training using a virtual-reality system in older fallers." Clin Interv Aging 8 (2013): 257-263.

[88] Singh, Devinder KA, Bala S. Rajaratnam, Vijayakumar Palaniswamy, Hannah Pearson, Vimal P. Raman, and Pei Sien Bong. "Participating in a virtual reality balance exercise program can reduce risk and fear of falls." Maturitas 73, no. 3 (2012): 239-243.

[89] Mirelman, Anat, Lynn Rochester, Miriam Reelick, Freek Nieuwhof, Elisa Pelosin, Giovanni Abbruzzese, Kim Dockx, Alice Nieuwboer, and Jeffrey M. Hausdorff. "V-TIME: a treadmill training program augmented by virtual reality to decrease fall risk in older adults: study design of a randomized controlled trial." BMC neurology 13, no. 1 (2013): 15.

[90] http:www.orthobalancept.com

[91] http://www.vicon.com/what-is-motion-capture

[92] Walsh, L., Greene, B. R., McGrath, D., Burns, A., & Caulfield, B. (2011, August). Development and validation of a clinic based balance assessment technology. In Engineering in Medicine and Biology Society, EMBC, 2011 Annual International Conference of the IEEE (pp. 1327-1330). IEEE.

[93] Howcroft, Jennifer, Jonathan Kofman, and Edward D. Lemaire. "Review of fall risk assessment in geriatric populations using inertial sensors." Journal of neuroengineering and rehabilitation 10.1 (2013): 1.

[94] Marschollek, M., Rehwald, A., Wolf, K. H., Gietzelt, M., Nemitz, G., Meyer Zu Schwabedissen, H., & Haux, R. (2011). Sensor-based fall risk assessment-an expert'to go'. Methods of information in medicine, 50(5), 420.

[95] Menz, H. B., Lord, S. R., & Fitzpatrick, R. C. (2003). Acceleration patterns of the head and pelvis when walking are associated with risk of falling in community-dwelling

older people. The Journals of Gerontology Series A: Biological Sciences and Medical Sciences, 58(5), M446-M452.

[96] Menz, H. B., Lord, S. R., & Fitzpatrick, R. C. (2003). Agerelated differences in walking stability. Age and ageing, 32(2), 137-142.

[97] Nelson-Wong, Erika, Ryan Appell, Mike McKay, Hannah Nawaz, Joanna Roth, Robert Sigler, Jacqueline Third, and Mark Walker. "Increased fall risk is associated with elevated co-contraction about the ankle during static balance challenges in older adults." European journal of applied physiology 112, no. 4 (2012): 1379-1389.

[98] Ceseracciu, Elena, Zimi Sawacha, and Claudio Cobelli. "Comparison of markerless and marker-based motion capture technologies through simultaneous data collection during gait: proof of concept." PloS one 9.3 (2014): e87640.

[99] Staranowicz, Aaron, Garrett R. Brown, and Gian-Luca Mariottini. "Evaluating the accuracy of a mobile Kinect-based gait-monitoring system for fall prediction." Proceedings of the 6th International Conference on PErvasive Technologies Related to Assistive Environments. ACM, 2013.

[100] J. Stone, Erik E., and Marjorie Skubic. "Evaluation of an inexpensive depth camera for passive in-home fall risk assessment." Pervasive Computing Technologies for Healthcare (PervasiveHealth), 2011 5th International Conference on. IEEE, 2011.

[101] Stone, Erik E., and Marjorie Skubic. "Unobtrusive, continuous, in-home gait measurement using the Microsoft Kinect." Biomedical Engineering, IEEE Transactions on 60.10 (2013): 2925-2932.

[102] Tinetti, Mary E., Mark Speechley, and Sandra F. Ginter. "Risk factors for falls among elderly persons living in the community." New England journal of medicine 319.26 (1988): 1701-1707.

[103] Rantz, Marilyn, et al. "Automated in-home fall risk assessment and detection sensor system for elders." The Gerontologist 55.Suppl 1 (2015): S78-S87.

[104] Marschollek, M., et al. "Sensor-based fall risk assessment-an expert'to go'." Methods of information in medicine 50.5 (2011): 420..

[105] Yardibi, T., Cuddihy, P., Genc, S., Bufi, C., Skubic, M., Rantz, M., ... & Phillips, C. (2011, March). Gait characterization via pulse-Doppler radar. In Pervasive Computing and Communications Workshops (PERCOM Workshops), 2011 IEEE International Conference on (pp. 662-667). IEEE.

[106] Hagler, Stuart, Daniel Austin, Tamara L. Hayes, Jeffrey Kaye, and Misha Pavel. "Unobtrusive and ubiquitous in-home monitoring: a methodology for continuous assessment of gait velocity in elders." Biomedical Engineering, IEEE Transactions on 57, no. 4 (2010): 813-820.

[107] Gabel, Moshe, Ran Gilad-Bachrach, Erin Renshaw, and Assaf Schuster. "Full body gait analysis with Kinect." In Engineering in Medicine and Biology Society (EMBC), 2012 Annual International Conference of the IEEE, pp. 1964-1967. IEEE, 2012.

[108] Cuddihy, Paul E., Tarik Yardibi, Zachary J. Legenzoff, Liang Liu, Calvin E. Phillips, Carmen Abbott, Colleen Galambos et al. "Radar walking speed measurements of seniors in their apartments: Technology for fall prevention." In Engineering in Medicine and Biology Society (EMBC), 2012 Annual International Conference of the IEEE, pp. 260-263. IEEE, 2012.

[109] Kaye, Jeffrey, Nora Mattek, Hiroko Dodge, Teresa Buracchio, Daniel Austin, Stuart Hagler, Michael Pavel, and Tamara Hayes. "One walk a year to 1000 within a year: Continuous in-home unobtrusive gait assessment of older adults." Gait & posture 35, no. 2 (2012): 197-202.

[110] Ranasinghe, D. C., Shinmoto Torres, R. L., Sample, A. P., Smith, J. R., Hill, K., & Visvanathan, R. (2012, August). Towards falls prevention: a wearable wireless and battery-less sensing and automatic identification tag for real time monitoring of human movements. In Engineering in Medicine and Biology Society (EMBC), 2012 Annual International Conference of the IEEE (pp. 6402-6405). IEEE.

[111] Robinovitch, Stephen N., Fabio Feldman, Yijian Yang, Rebecca Schonnop, Pet Ming Leung, Thiago Sarraf, Joanie Sims-Gould, and Marie Loughin. "Video capture of the circumstances of falls in elderly people residing in long-term care: an observational study." The Lancet 381, no. 9860 (2013): 47-54.

[112] Boissy, Patrick, et al. "User-based motion sensing and fuzzy logic for automated fall detection in older adults." Telemedicine and e-Health 13.6 (2007): 683-694.

[113] Wang, F., Skubic, M., Abbott, C., & Keller, J. M. (2010, August). Body sway measurement for fall risk assessment using inexpensive webcams. In Engineering in Medicine and Biology Society (EMBC), 2010 Annual International Conference of the IEEE (pp. 2225-2229). IEEE.

[114] Cardinaux, F., Bhowmik, D., Abhayaratne, C., & Hawley, M. S. (2011). Video based technology for ambient assisted living: A review of the literature. Journal of Ambient Intelligence and Smart Environments, 3(3), 253-269.

[115] Pannurat, Natthapon, Surapa Thiemjarus, and Ekawit Nantajeewarawat. "Automatic fall monitoring: a review." Sensors 14, no. 7 (2014): 12900-12936.

[116] Culhane, K. M., O'Connor, M., Lyons, D., & Lyons, G. M. (2005). Accelerometers in rehabilitation medicine for older adults. Age and ageing, 34(6), 556-560.

[117] Culhane, K.M., Lyons, G.M., Hilton, D., Grace, P.A. and Lyons, D., 2004. Long-term mobility monitoring of older adults using accelerometers in a clinical environment. Clinical rehabilitation, 18(3), pp.335-343.

[118] Najafi, B., Aminian, K., Paraschiv-Ionescu, A., Loew, F., Bla, C. J., & Robert, P. (2003). Ambulatory system for human motion analysis using a kinematic sensor: monitoring of daily physical activity in the elderly. Biomedical Engineering, IEEE Transactions on, 50(6), 711-723.

[119] Aziz, Omar, Edward J. Park, Greg Mori, and Stephen N. Robinovitch. "Distinguishing the causes of falls in humans using an array of wearable tri-axial accelerometers." Gait & posture 39, no. 1 (2014): 506-512.

[120] Howcroft, Jennifer, Edward D. Lemaire, and Jonathan Kofman. "Wearable-sensor-based classification models of faller status in older adults." PLoS one 11, no. 4 (2016): e0153240.

[121] Del Din, S., Godfrey, A., Galna, B., Lord, S., & Rochester, L. (2016). Free-living gait characteristics in ageing and Parkinson's disease: impact of environment and ambulatory bout length. Journal of neuroengineering and rehabilitation, 13(1), 1.

[122] Brodie, M. A., Wang, K., Delbaere, K., Persiani, M., Lovell, N. H., Redmond, S. J., ... & Lord, S. R. (2015). New methods to monitor stair ascents using a wearable pendant device reveal how behavior, fear, and frailty influence falls in octogenarians. Biomedical Engineering, IEEE Transactions on, 62(11), 2595-2601.

[123] Brodie, Matthew AD, Milou JM Coppens, Stephen R. Lord, Nigel H. Lovell, Yves J. Gschwind, Stephen J. Redmond, Michael Benjamin Del Rosario et al. "Wearable pendant device monitoring using new wavelet-based methods shows daily life and laboratory gaits are different." Medical & Biological Engineering & Computing (2015): 1-12.

[124] Brodie, M. A., Lord, S. R., Coppens, M. J., Annegarn, J., & Delbaere, K. (2015). Eight-Week Remote Monitoring Using a Freely Worn Device Reveals Unstable Gait Patterns in Older Fallers. Biomedical Engineering, IEEE Transactions on, 62(11), 2588-2594.

[125] Weiss A, Herman T, Giladi N, Hausdorff JM. Objective assessment of fall risk in Parkinson's disease using a body-fixed sensor worn for 3 days. PLoS One. 2014;9:e96675.

[126] Weiss, Aner, et al. "Does the evaluation of gait quality during daily life provide insight into fall risk? A novel approach using 3-day accelerometer recordings." Neurorehabilitation and neural repair 27.8 (2013): 742-752.

[127] van Schooten KS, Rispens SM, Elders PJ, Lips P, van Dieen JH, Pijnappels M. Assessing physical activity in older adults: required days of trunk accelerometer measurements for reliable estimation. J Aging Phys Act. 2015;23:917.

[128] de Bruin ED, Najafi B, Murer K, Uebelhart D, Aminian K. Quantification of everyday motor function in a geriatric population. J Rehabil Res Dev. 2007;44:41728.

[129] K. Aminian, B. Najafi, C. B ula, P. F. Leyvraz, and P. Robert, Spatio-temporal parameters of gait measured by an ambulatory system using miniature gyroscopes,J. Biomech., vol. 35, no. 5, pp. 689699, 2002

[130] Brach, J. S., Studenski, S. A., Perera, S., VanSwearingen, J. M., & Newman, A. B. (2007). Gait variability and the risk of incident mobility disability in community-dwelling older adults. The Journals of Gerontology Series A: Biological Sciences and Medical Sciences, 62(9), 983-988.

[131] Owings, Tammy M., and Mark D. Grabiner. "Step width variability, but not step length variability or step time variability, discriminates gait of healthy young and older adults during treadmill locomotion." Journal of biomechanics 37.6 (2004): 935-938.

[132] Blazkiewicz, et al., "Comparison of four methods of calculating the symmetry of spatial-temporal parameters of gait." Acta of Bioengineering and Biomechanics 16.1 (2014): 29-35.

[133] Feasel, J., Whitton, M. C., Kassler, L., Brooks, F. P., & Lewek, M. D. (2011). The integrated virtual environment rehabilitation treadmill system. IEEE Transactions on Neural Systems and Rehabilitation Engineering, 19(3), 290-297.

[134] Xu, Wenyao, Ming-Chun Huang, Navid Amini, Jason J. Liu, Lei He, and Majid Sarrafzadeh. "Smart insole: a wearable system for gait analysis." In Proceedings of the 5th International Conference on PErvasive Technologies Related to Assistive Environments, p. 18. ACM, 2012.

[135] Bamberg, Stacy J. Morris, Ari Y. Benbasat, Donna Moxley Scarborough, David E. Krebs, and Joseph A. Paradiso. "Gait analysis using a shoe-integrated wireless sensor system." Information Technology in Biomedicine, IEEE Transactions on 12, no. 4 (2008): 413-423.

[136] Dyer, Philip S., and Stacy J. Morris Bamberg. "Instrumented insole vs. force plate: A comparison of center of plantar pressure." Engineering in Medicine and Biology Society, EMBC, 2011 Annual International Conference of the IEEE. IEEE, 2011.

[137] Redd, Christian B., and Stacy J. Morris Bamberg. "A wireless sensory feedback device for real-time gait feedback and training." Mechatronics, IEEE/ASME Transactions on 17.3 (2012): 425-433.

[138] Rouhani, H., Favre, J., Crevoisier, X., & Aminian, K. (2011). Ambulatory measurement of ankle kinetics for clinical applications. Journal of biomechanics, 44(15), 2712-2718.

[139] Otis, M. J. D., & Menelas, B. A. J. (2012, October). Toward an augmented shoe for preventing falls related to physical conditions of the soil. In Systems, Man, and Cybernetics (SMC), 2012 IEEE International Conference on (pp. 3281-3285). IEEE.

[140] van Schooten, Kimberley S., et al. "Ambulatory fall-risk assessment: amount and quality of daily-life gait predict falls in older adults." The Journals of Gerontology Series A: Biological Sciences and Medical Sciences 70.5 (2015): 608-615.

[141] Patterson, Matthew R., et al. "Does external walking environment affect gait patterns?." Engineering in Medicine and Biology Society (EMBC), 2014 36th Annual International Conference of the IEEE. IEEE, 2014.

[142] Reginatto, Brenda, et al. "Context aware falls risk assessment: A case study comparison." 2015 37th Annual International Conference of the IEEE Engineering in Medicine and Biology Society (EMBC). IEEE, 2015.

[143] Taylor, Kenneth, et al. "Context focused older adult mobility and gait assessment." 2015 37th Annual International Conference of the IEEE Engineering in Medicine and Biology Society (EMBC). IEEE, 2015.

[144] King, Rachel Christina, et al. "Elderly risk assessment of falls with BSN." Body Sensor Networks (BSN), 2010 International Conference on. IEEE, 2010..

[145] Mellone, S., et al. "Smartphone-based solutions for fall detection and prevention: the FARSEEING approach." Zeitschrift fr Gerontologie und Geriatrie 45.8 (2012): 722-727.

[146] Guimares, Vania, et al. "A smartphone-based fall risk assessment tool: Testing Ankle Flexibility, Gait and Voluntary Stepping." Medical Measurements and Applications (MeMeA), 2014 IEEE International Symposium on. IEEE, 2014.

[147] Guimaraes, V., Ribeiro, D., & Rosado, L. (2013, October). A smartphone-based fall risk assessment tool: Measuring One Leg Standing, Sit to Stand and Falls Efficacy Scale. In e-Health Networking, Applications & Services (Healthcom), 2013 IEEE 15th International Conference on (pp. 529-533). IEEE.

[148] Greene, Barry R., et al. "Quantitative falls risk assessment using the timed up and go test." Biomedical Engineering, IEEE Transactions on 57.12 (2010): 2918-2926.

[149] Habib, Mohammad Ashfak, et al. "Smartphone-based solutions for fall detection and prevention: challenges and open issues." Sensors 14.4 (2014): 7181-7208.

[150] Luque, Rafael, et al. "Comparison and characterization of android-based fall detection systems." Sensors 14.10 (2014): 18543-18574.

[151] Majumder, Akm Jahangir Alam, Ishmat Zerin, Miftah Uddin, Sheikh I. Ahamed, and Roger O. Smith. "SmartPrediction: A real-time smartphone-based fall risk prediction and prevention system." In Proceedings of the 2013 Research in Adaptive and Convergent Systems, pp. 434-439. ACM, 2013.

[152] Aziz, Omar. Design and Validation of a Fall Event Detection System using Wearable Sensors: A Machine Learning Approach. Diss. Applied Sciences:, 2015.

[153] Mansfield, Avril, et al. "Effect of a perturbation-based balance training program on compensatory stepping and grasping reactions in older adults: a randomized controlled trial." Physical therapy 90.4 (2010): 476-491.

[154] Maki, Brian E., and William E. McIlroy. "Control of rapid limb movements for balance recovery: age-related changes and implications for fall prevention." Age and ageing 35.suppl 2 (2006): ii12-ii18.

[155] Maki, Brian E., and William E. Mcilroy. "Control of compensatory stepping reactions: age-related impairment and the potential for remedial intervention." Physiotherapy theory and practice 15.2 (1999): 69-90.

[156] Hof, A. L., and Jaak Duysens. "Responses of human hip abductor muscles to lateral balance perturbations during walking." Experimental brain research 230.3 (2013): 301-310.

[157] Schulz, Brian W., James A. Ashton-Miller, and Neil B. Alexander. "Can initial and additional compensatory steps be predicted in young, older, and balance-impaired older females in response to anterior and posterior waist pulls while standing?." Journal of biomechanics 39.8 (2006): 1444-1453.

[158] Maidan, I., T. Freedman, R. Tzemah, N. Giladi, A. Mirelman, and J. M. Hausdorff. "Introducing a new definition of a near fall: Intra-rater and inter-rater reliability." Gait and posture 39, no. 1 (2014): 645-647.

[159] Weiss, A., Shimkin, I., Giladi, N., and Hausdorff, J. M. (2010). Automated detection of near falls: algorithm development and preliminary results. BMC research notes, 3(1), 62.

[160] Mille, M. L., Johnson, M. E., Martinez, K. M., and Rogers, M. W. (2005). Age-dependent differences in lateral balance recovery through protective stepping. Clinical Biomechanics, 20(6), 607-616.

[161] Hof, A. L., S. M. Vermerris, and W. A. Gjaltema. "Balance responses to lateral perturbations in human treadmill walking." The Journal of experimental biology 213.15 (2010): 2655-2664.

[162] Hof, A. L. (2007). The equations of motion for a standing human reveal three mechanisms for balance. Journal of biomechanics, 40(2), 451-457.

[163] Aziz, Omar, et al. "Distinguishing near-falls from daily activities with wearable accelerometers and gyroscopes using Support Vector Machines." Engineering in Medicine and Biology Society (EMBC), 2012 Annual International Conference of the IEEE. IEEE, 2012.

[164] Aziz, Omar, Edward J. Park, Greg Mori, and Stephen N. Robinovitch. "Distinguishing the causes of falls in humans using an array of wearable tri-axial accelerometers." Gait & posture 39, no. 1 (2014): 506-512.

[165] Dinh, Anh, Yang Shi, Daniel Teng, Amitoz Ralhan, Li Chen, Vanina Dal Bello-Haas, Jenny Basran, Seok-Bum Ko, and Carl McCrowsky. "A fall and near-fall assessment and evaluation system." The open biomedical engineering journal 3 (2009): 1.

[166] Aziz, Omar, and Stephen N. Robinovitch. "An analysis of the accuracy of wearable sensors for classifying the causes of falls in humans." Neural Systems and Rehabilitation Engineering, IEEE Transactions on 19.6 (2011): 670-676.

[167] Ozdemir, A. T., and Barshan, B. (2014). Detecting falls with wearable sensors using machine learning techniques. Sensors, 14(6), 10691- 10708.

[168] Barshan, E., Ghodsi, A., Azimifar, Z., and Jahromi, M. Z. (2011). Supervised principal component analysis: Visualization, classification and regression on subspaces and submanifolds. Pattern Recognition, 44(7), 1357-1371.

[169] Phinyomark, Angkoon, Chusak Limsakul, and Pornchai Phukpattaranont. "A novel feature extraction for robust EMG pattern recognition." Journal of Computing, vol. 1, pp71-80, 2009.

[170] Hermens, Hermie J., Bart Freriks, Roberto Merletti, Dick Stegeman, Joleen Blok, Gunter Rau, Cathy Disselhorst-Klug, and Goran Hagg. "European recommendations for surface electromyography." Roessingh Research and Development 8, vol. 2, pp. 13-54, 1999.

[171] De Luca, Carlo J., et al. "Filtering the surface EMG signal: Movement artifact and baseline noise contamination." Journal of Biomechanics,vol. 43, pp. 1573-1579, 2010.

[172] Tizhoosh, H.R., Barcode Annotations for Medical Image Retrieval: A Preliminary Investigation, IEEE International Conference on Image Processing, pp. 818–822, DOI: 10.1109/ICIP.2015.7350913, 2015.

[173] Ko, Byoung Chul, Seong Hoon Kim, and Jae-Yeal Nam. "X-ray image classification using random forests with local wavelet-based CS-local binary patterns." Journal of digital imaging 24.6 (2011): 1141-1151.

[174] Cross, G.R., and Anil K. Jain. "Markov random field texture models" Pattern Analysis and Machine Intelligence, IEEE Transactions on 1 (1983): 25-39.

[175] Li, Shutao, Taylor, J.S., 2005. Comparison and fusion of multiresolution features for texture classification. Pattern Recognition Lett. 26, 633638.

[176] Wu, P., et al. "A texture descriptor for image retrieval and browsing." Content-Based Access of Image and Video Libraries, 1999.(CBAIVL'99) Proceedings. IEEE Workshop on. IEEE, 1999.

[177] Dunn, D. and W.E. Higgins. "Optimal Gabor filters for texture segmentation. IEEE Transactions on Image Processing, 4.7,pp. 947-964, 1995.

[178] Jain, Anil K., and Farshid Farrokhnia. "Unsupervised texture segmentation using Gabor filters." Systems, Man and Cybernetics, 1990. Conference Proceedings., IEEE International Conference on. IEEE, 1990.

[179] Andrysiak, Tomasz, and Micha? ChoraS. "Image retrieval based on hierarchical Gabor filters." International Journal of Applied Mathematics and Computer Science 15.4 (2005): 471.

[180] Zhang, Dengsheng, et al. "Content-based image retrieval using Gabor texture features." IEEE Pacific-Rim Conference on Multimedia, University of Sydney, Australia. 2000.

[181] Sastry, Challa S., et al. "A modified Gabor function for content based image retrieval." Pattern Recognition Letters 28.2 (2007): 293-300.

[182] Han, Ju, and Kai-Kuang Ma. "Rotation-invariant and scale-invariant Gabor features for texture image retrieval." Image and vision computing 25.9 (2007): 1474-1481.

[183] Jain, Anil K., Nalini K. Ratha, and Sridhar Lakshmanan. "Object detection using Gabor filters." Pattern Recognition 30.2 (1997): 295-309.

[184] Haghighat, Mohammad, SamanZonouz, and Mohamed Abdel-Mottaleb. "CloudID: Trustworthy cloud-based and cross-enterprise biometric identification." Expert Systems with Applications 42.21 (2015): 7905-7916.

[185] Kamarainen, Joni-Kristian, Ville Kyrki, and HeikkiKlviinen. "Invariance properties of Gabor filter-based features-overview and applications." Image Processing, IEEE Transactions on 15.5 (2006): 1088-1099.

[186] Chen, Lianping, Guojun Lu, and Dengsheng Zhang. "Effects of different gabor filter parameters on image retrieval by texture." null. IEEE, 2004.

[187] Mathie, M. J. B. J. and B. G. Celler. A system for monitoring posture and physical activity using accelerometers. In: Proceedings of the 23rd Annual International Conference of the IEEE Engineering in Medicine and Biology Society, vol. 4, pp. 36543657, 2001.

[188] Nouredanesh, Mina, Hamid R. Tizhoosh, and Ershad Banijamali. "Gabor Barcodes for Medical Image Retrieval." arXiv preprint arXiv:1605.04478 (2016).

[189] Nouredanesh, M., McCormick, A., Kukreja, S. L., & Tung, J. (2016, June). Wearable vision detection of environmental fall risk using Gabor Barcodes. In 2016 6th IEEE International Conference on Biomedical Robotics and Biomechatronics (BioRob) (pp. 956-956). IEEE.

[190] Nouredanesh, M., McCormick, A., Kukreja, S. L., & Tung, J. Wearable Vision Detection of Environmental Fall Risks using Convolutional Neural Network, To appear in proceedings of The 38th Annual International Conference of the IEEE Engineering in Medicine and Biology Society (IEEE-EMBC 2016), Aug 17-20, Orlando, USA.

[191] Nouredanesh, Mina, Hamid R. Tizhoosh, and Ershad Banijamali. "Gabor-Radon Barcodes for Medical Image Retrieval. To be appeared in the proceedings of ICPR conference (2016).

[192] Phung, Son Lam, and Abdesselam Bouzerdoum. "A pyramidal neural network for visual pattern recognition." IEEE Transactions on Neural Networks 18, no. 2 (2007): 329-343.

[193] S. L. Phung and A. Bouzerdoum, "MATLAB library for convolutional neural network," Technical Report, ICT Research Institute, Visual and Audio Signal Processing Laboratory, University of Wollongong. Available at:http://www.uow.edu.au/ phung.

[194] C. Nebauer, Evaluation of convolutional neural networks for visual recognition., IEEE Trans. Neural Netw., vol. 9, no. 4, pp. 685696, 1998.

[195] Y. LeCun, L. Bottou, Y. Bengio, and P. Haffner, Gradient-based learning applied to document recognition, Proc. IEEE, vol. 86, no. 11, pp. 22782323, 1998.

[196] S. Ji, M. Yang, and K. Yu, 3D Convolutional Neural Networks for Human Action Recognition., IEEE Trans. Pattern Anal. Mach. Intell., vol. 35, no. 1, pp. 22131, 2013.

[197] Mou, Wei, and Alexander Kleiner. "Online learning terrain classification for adaptive velocity control." Safety Security and Rescue Robotics (SSRR), 2010 IEEE International Workshop on. IEEE, 2010.

[198] Laible, Stefan, et al. "3d lidar-and camera-based terrain classification under different lighting conditions." Autonomous Mobile Systems 2012. Springer Berlin Heidelberg, 2012. 21-29.

[199] Zenker, Steffen, et al. "Visual terrain classification for selecting energy efficient gaits of a hexapod robot." Advanced Intelligent Mechatronics (AIM), 2013 IEEE/ASME International Conference on. IEEE, 2013.

[200] Lu, Xiaoye, and Roberto Manduchi. "Detection and localization of curbs and stairways using stereo vision." ICRA. Vol. 5. 2005.

[201] Wang, Shuihua, et al. "RGB-D image-based detection of stairs, pedestrian crosswalks and traffic signs." Journal of Visual Communication and Image Representation 25.2 (2014): 263-272.

APPENDICES

Appendix A.
Classic risk of falling assessment methods

Table 6.1: Clinical methods for fall risk assessment

Fall risk assessment methods	**Description**
Activities specific balance confidence scale (ABC)	Is a 16-item self-report measure (Paper survey) in which patients rate their balance confidence for performing activities (length of Test: 06 to 30 Minutes).
Berg balance scale [74]	Is a 14-item (scores range from 0-4, max =56) objective measure designed to assess static balance and fall risk in adult populations with impairment in balance function by assessing the performance of functional tasks.
STRATIFY score [53]	Is a scale for assessment of 2 month fall history, mental alteration, frequent toileting, visual impairment, psychotropic medication use, and mobility issues. Score of < 2 indicates increased fall risk.
Continued on next page	

Table 6.1 – continued from previous page

Fall risk assessment methods	**Description**
Single leg stance (SLS)	Is a test that measure the time during which a person can stand on one leg without upper extremity support; and without bracing the suspended leg against the stance leg. A time exceeding 30s indicates low fall risk and less than 5 s indicates high fall risk.
Five times sit to stand	Is a test for functional mobility assessment of lower limb muscle strength, in which patient sits with arms folded across chest and with back against the chair and is asked to stand up and sit down 5 times as quickly as he can.
Community Balance and Mobility Scale	Is a test that is used to identify the patients with high level of balance and mobility deficits based on 13 challenging tasks that are commonly encountered in community environments (length of Test: 31 to 60 minutes). Assessment type: performance measure.
Physiological Profile Assessment (PPA)	Is performed to assess vision, muscle force, peripheral sensation, reaction time, and postural sway.
Tinetti Assessment Tool	Is a method for dynamic balance and gait evaluation, and consists of 10 balance components and 8 gait components.

Appendix B.
List of the IMU-based features

1. Max-Peak-ACC-X-Shank
2. Max-Peak-ACC-Y-Shank
3. Max-Peak-ACC-Z-Shank
4. Max-Peak-ACC-X-Sternum
5. Max-Peak-ACC-Y-Sternum
6. Max-Peak-ACC-Z-Sternum
7. Max-Peak-ACC-X-Thigh
8. Max-Peak-ACC-Y-Thigh
9. Max-Peak-ACC-Z-Thigh
10. Max-SVA-Shank-Total
11. Max-SVA-Sternum-Total
12. Max-SVA-Thigh-Total
13. RMS-ACC-X-Shank
14. RMS-ACC-Y-Shank
15. RMS-ACC-Z-Shank
16. RMS-ACC-X-Sternum
17. RMS-ACC-Y-Sternum
18. RMS-ACC-Z-Sternum
19. RMS-ACC-X-Thigh
20. RMS-ACC-Y-Thigh
21. RMS-ACC-Z-Thigh
22. Mean-ACC-X-Shank
23. Mean-ACC-Y-Shank
24. Mean-ACC-Z-Shank
25. Mean-ACC-X-Sternum
26. Mean-ACC-Y-Sternum
27. Mean-ACC-Z-Sternum

28. Mean-ACC-X-Thigh
29. Mean-ACC-Y-Thigh
30. Mean-ACC-Z-Thigh
31. Var-ACC-X-Shank
32. Var-ACC-Y-Shank
33. Var-ACC-Z-Shank
34. Var-ACC-X-Sternum
35. Var-ACC-Y-Sternum
36. Var-ACC-Z-Sternum
37. Var-ACC-X-Thigh
38. Var-ACC-Y-Thigh
39. Var-ACC-Z-Thigh
40. Skewness-ACC-X-Shank
41. Skewness-ACC-Y-Shank
42. Skewness-ACC-Z-Shank
43. Skewness-ACC-X-Sternum
44. Skewness-ACC-Y-Sternum
45. Skewness-ACC-Z-Sternum
46. Skewness-ACC-X-Thigh
47. Skewness-ACC-Y-Thigh
48. Skewness-ACC-Z-Thigh
49. Kurtosis-ACC-X-Shank
50. Kurtosis-ACC-Y-Shank
51. Kurtosis-ACC-Z-Shank
52. Kurtosis-ACC-X-Sternum
53. Kurtosis-ACC-Y-Sternum
54. Kurtosis-ACC-Z-Sternum
55. Kurtosis-ACC-X-Thigh
56. Kurtosis-ACC-Y-Thigh
57. Kurtosis-ACC-Z-Thigh

58. Max-Peak-Diff-ACC-X-Shank
59. Max-Peak-Diff-ACC-Y-Shank
60. Max-Peak-Diff-ACC-Z-Shank
61. Max-Peak-Diff-ACC-X-Sternum
62. Max-Peak-Diff-ACC-Y-Sternum
63. Max-Peak-Diff-ACC-Z-Sternum
64. Max-Peak-Diff-ACC-X-Thigh
65. Max-Peak-Diff-ACC-Y-Thigh
66. Max-Peak-Diff-ACC-Z-Thigh
67. Mean-Diff-ACC-X-Shank
68. Mean-Diff-ACC-Y-Shank
69. Mean-Diff-ACC-Z-Shank
70. Mean-Diff-ACC-X-Sternum
71. Mean-Diff-ACC-Y-Sternum
72. Mean-Diff-ACC-Z-Sternum
73. Mean-Diff-ACC-X-Thigh
74. Mean-Diff-ACC-Y-Thigh
75. Mean-Diff-ACC-Z-Thigh
76. Var-Diff-ACC-X-Shank
77. Var-Diff-ACC-Y-Shank
78. Var-Diff-ACC-Z-Shank
79. Var-Diff-ACC-X-Sternum
80. Var-Diff-ACC-Y-Sternum
81. Var-Diff-ACC-Z-Sternum
82. Var-Diff-ACC-X-Thigh
83. Var-Diff-ACC-Y-Thigh
84. Var-Diff-ACC-Z-Thigh
85. Max-Peak-Gyro-X-Shank
86. Max-Peak-Gyro-Y-Shank
87. Max-Peak-Gyro-Z-Shank

88. Max-Peak-Gyro-X-Sternum
89. Max-Peak-Gyro-Y-Sternum
90. Max-Peak-Gyro-Z-Sternum
91. Max-Peak-Gyro-X-Thigh
92. Max-Peak-Gyro-Y-Thigh
93. Max-Peak-Gyro-Z-Thigh
94. Mean-Gyro-X-Shank
95. Mean-Gyro-Y-Shank
96. Mean-Gyro-Z-Shank
97. Mean-Gyro-X-Sternum
98. Mean-Gyro-Y-Sternum
99. Mean-Gyro-Z-Sternum
100. Mean-Gyro-X-Thigh
101. Mean-Gyro-Y-Thigh
102. Mean-Gyro-Z-Thigh
103. Var-Gyro-X-Shank
104. Var-Gyro-Y-Shank
105. Var-Gyro-Z-Shank
106. Var-Gyro-X-Sternum
107. Var-Gyro-Y-Sternum
108. Var-Gyro-Z-Sternum
109. Var-Gyro-X-Thigh
110. Var-Gyro-Y-Thigh
111. Var-Gyro-Z-Thigh
112. Max-Peak-Diff-Gyro-X-Shank
113. Max-Peak-Diff-Gyro-Y-Shank
114. Max-Peak-Diff-Gyro-Z-Shank
115. Max-Peak-Diff-Gyro-X-Sternum
116. Max-Peak-Diff-Gyro-Y-Sternum
117. Max-Peak-Diff-Gyro-Z-Sternum

118. Max-Peak-Diff-Gyro-X-Thigh
119. Max-Peak-Diff-Gyro-Y-Thigh
120. Max-Peak-Diff-Gyro-Z-Thigh
121. Mean-Diff-Gyro-X-Shank
122. Mean-Diff-Gyro-Y-Shank
123. Mean-Diff-Gyro-Z-Shank
124. Mean-Diff-Gyro-X-Sternum
125. Mean-Diff-Gyro-Y-Sternum
126. Mean-Diff-Gyro-Z-Sternum
127. Mean-Diff-Gyro-X-Thigh
128. Mean-Diff-Gyro-Y-Thigh
129. Mean-Diff-Gyro-Z-Thigh
130. Var-Diff-Gyro-X-Shank
131. Var-Diff-Gyro-Y-Shank
132. Var-Diff-Gyro-Z-Shank
133. Var-Diff-Gyro-X-Sternum
134. Var-Diff-Gyro-Y-Sternum
135. Var-Diff-Gyro-Z-Sternum
136. Var-Diff-Gyro-X-Thigh
137. Var-Diff-Gyro-Y-Thigh
138. Var-Diff-Gyro-Z-Thigh